Agglomeration, adsorption and polymerization of hydrolysate components

A Thesis Presented to the

Faculty of Graduate Studies of

Lakehead University

by

Haosong Zhao

Submitted in partial fulfillment of requirements

for the degree of Master of Science in Environmental Engineering

Dedications

To my parents, and my friends for all of their love, support, patience and encouragement.

Acknowledgments

I would first like to thank my Supervisor, Dr. Pedram Fatehi, whose guidance and suggestions were invaluable for me. He spent a lot of his precious time on me and encouraged me throughout my research. I also appreciate your patience and kindness.

I would like to extend my sincere thanks to my committee members, Dr. Baoqiang Liao, Dr. Leila Pakzad, Dr. Ehsan Behzadfar for their valuable input in preparing this thesis.

I am grateful to all lab members for your excellent cooperation. It was a pleasure to work with you in my master program. A special gratitude goes to Weijue Gao and Dmitry Tarasov for the tremendous help in my experiment.

I would like to give special thanks to my friend, Duowei Lu, Yichen Liao and Cong Gao. You made my time at Lakehead university positive and enjoyable.

In addition, I would like to thank my parents for providing me moral and emotional support in my life. Without your support, I cannot keep doing my research.

Abstract

Biomass utilization has been drawn attention of governments and industries, as it is renewable resource. Pulp and paper industry depend on woody biomass utilization system to get multiple products. However, it is also featured by large energy consumption and low efficiency of using raw material. It is crucial to integrate biorefinery concept into pulp mill to create a long-term sustainable pathway. This research work trends to investigate the performance of autohydrolysis of spruce wood at various parameters such as temperature, residence time, liquid to solid ratio. The performance of self-aggregation of hydrolysates with different conditions and deposition of hydrolysates on stainless steel surface were also studied. The hydrostats were characterized by gel permeation chromatography (GPC), nuclear magnetic resonance (NMR) spectroscopy, zeta potential analyzer, scanning electron microscopy (SEM), particle charge detector, quartz crystal microbalance with dissipation (QCM-D), dynamic light scattering (DLS). It was noticed that the hydrolysate with higher hydrophilicity and surface tension possessed higher affinity for adsorption of its lignocelluloses on stainless steel. The image analysis and QCM results revealed that the formation of agglomerates in hydrolysate and their deposition on stainless steel surface. The results of this thesis provided insights into the fundamental knowledge on the autohydrolysis, self-assembly behavior of hydrolysates which have great influence for producing lignocellulose-based coproducts.

In this thesis, the hydrolysates generated via autohydrolysis of spruce wood chips were directly used as feedstock for producing coagulant. In-situ polymerization of acrylamide (AM) and lignocellulose (LC) of hydrolysates in an aqueous solution in the presence of $K_2S_2O_8$ as an initiator was successfully conducted, and the reaction was optimized to generate LC-AM with the highest molecular weight and charge density. In order to confirm the grafting of acrylamide on LC NMR spectroscopy confirmed the grafting of acrylamide on LC. Other properties of product were characterized by elemental analyzer, zeta potential analyzer, gel permeation chromatography (GPC) and particle charge detector (PCD). The applications of the resultant copolymer as a coagulant in dye suspensions were systematically assessed. LC-AM was combined with cationic polyacrylamide and anionic polyacrylamide in dual-coagulant systems. These results confirmed that the dual system of LC-AM and APAM led to a similar dye removal as the singular system of APAM, which was due to the multibranch structure of LC-AM favoring bridging. In addition to its reliable dye removal efficiency, other advantages of LC-AM were its biodegradable,

environmentally friendly, and inexpensive production costs compared with other oil-based coagulants used in industry.

Table of Contents

List of figures

List of tables

Chapter 1: Introduction

1.1 Overview

Biomass has been considered as one of the most promising candidate raw material for biofuels due to low cost, biodegradable, most abundant sources and their renewable feature in nature. The utilization of these biomass could help ease society's dependence on fossil fuels and, in the process, reduce net greenhouse gas (GHG) emissions (Pu et al., 2013). In reality, biomass is not fully utilized in the most pulp and paper industry. For example, the pre-hydrolysis liquor (PHL) from the prehydrolysis stage in the kraft-based dissolving pulp production process is either mixed with black liquor and burned in the recovery boiler of the mill, or discharged for wastewater treatment plant (Wu, 2016). It is not economically feasible to incinerate lignin since lignin is only worth 0.18 US $/kg as a fuel source. The conservative estimation of the value of lignin is 1.08 US $/kg when it is served as a feedstock for value added products (Macfarlanea et al., 2009). The Biorefinery concept is to integrate biomass conversion process in a more efficient manner by the means of environment friendly approaches. It aims at the production of biofuels, power, heat, and value-added chemicals from biomass. Recently, the application of biorefinery concept was concentrated on pulping technologies, fractionation and more effective utilization of biomass as byproduct (Krutov et al., 2015). Using the biorefinery concept, the hemicellulose and lignin remaining in the hydrolysis liquor can be recovery. They can be used as flocculants for wastewater treatment via proper modification such as grafting copolymerization reaction. Pulp and paper is one of the most water intensive industries because water is used throughout the whole manufacturing process, such as, cooking, pulp washing, bleaching process. Pulp and paper mill can consume up to 60 m^3 of freshwater per tonne of final product depending on the nature of the feedstock (Wong et al., 2006). Therefore, it is importance for the industries follow the biorefinery concept which can not only reduce the burden for enviornment but also improve the profitability for the industries.

Autohydrolysis is mostly used as a pretreatment to partially remove hemicellulose and lignin in order to high purity cellulose for other applications (Alvarez et al., 2016). The delignification after autohydrolysis has been associated with with the cleavage of aryl-ether bonds, leading in lignin depolymerisation and the formation of new phenolic hydroxyl groups (Rauhala et al., 2011; Song, 2013). The disollution of hemiculloses leads in the formation of oligosaccharides which is further degraded to monosacharides at higher autohydrolysis intensity (Saeed et al., 2012). The The

dedrivatives of hemicellulose such as furfural yielded from pentose, hydroxymethylfurfural (HMF) from hexose via dehydration (Testova et al., 2011).

The self-assembly technology receives a great number of interest in various disciplines, such as such as chemistry, physics, medicine, material science, and food science. Self-assembly is usually an irreversible process which can be induced by heating or acidification (Linden & Venema, 2007; Salentinig & Schubert, 2017). However, the aggregates can be dissassociated or decomposed with the help of salt or ultrasonication. It was found that lignins tend to self-assembly in most solvents, and this aggregation hinders the extraction of lignins from plants, as well as the systhesis of lignin-based advanced materials (Ratnaweera et al., 2015). In anther study, xylan fractions formed agglomerates by self-assembly in water and the flocs size was increased with addition of lignin (Westbye et al., 2007).

In recent years, the adsorption of lignocellulosic on a number of substrate was extensivly studied. It was reported that the seperation efficency of lignocellulosic matters from beech wood hydrolysate can be improved by appling ploymeric resin and zeolites adsorbents. (Nitzsche et al., 2019). The effect of adsorbed lignin and a cationic polyelectrolyte (PDADMAC) on cellulose fibres at neutral pH has been studied. It was stated neither PDADMAC nor lignin alone can improve the strength of pulp sheets significantly. However, the bonding between fibers were strengthened with presence of both PDADMAC and Lignin. In this study, the adsorption of hydrolysate from spruce wood on stainless steel was comprehensively investigated.

To increase the profitability of forest industry and diminish the environmental pollution, hydrolysate can be used as a feedstock to generate some value-added products (Wu et al., 2008; Saini et al., 2015). The applications of these value-added product include, but not limited to food additives, flocculant and adsorbent. Due to degradability of the biomass, hydrolysate has been considered as a promising material for the production of flocculant/coagulant. In one paper, hemicellulose extracted from corn husk was modified into cationic hemicelluloses using 2,3-epoxypropyltrimethylammonium chloride. The results show cationic hemicellulose obtained higher removal efficiency than those of commercial polyacrylamide (Landim et al., 2013). The production of lignin-based product has been reported as well, such as lignin-acrylamide, lignin-acrylic acid and so on (Kong et al., 2015; Ibrahim et al., 2005). In this study, the copolymerization of hydrolysate consititunent with acrylamide was conducted to be a coagulant for dye waste water.

In this MSc thesis, the aggolermation and adsorption behavior of hydrolysate component was in-depth investigated. An optimal operating condition was developed to synthesize lignocellulose-based coagulant for dye dispersion. The application of coagulant was inspected in singular and dual coagulant systems.

Chapter 1 presents a brief summary of the subsequent chapters and the objectives of this research.

Chapter 2 introduces the background information in the literature related to the present work. In the fisrt section, some fundalmental knowledge regarding hydrolysis, hydrodynamic size, copolymerization, coagulation is explained. The second section states different analytical methods and some advanced technologies.

Chapter 3 provides a statistical analysis about the effects of temperature, residenct time, L/S ratio on the yield of hydrolysates in autohydrolysis process. To understand the self-assembly behavior of hydrolysates, hydrodynamic sizes of hydrolyssates were assesed under different temparture, salt concentration, pH, ultrasonication duration using a dynamic light scattering. Lastly, the adsoprtion of hydrolysate on stainless steel was investigated using a Quartz crystal microbalance with dissipation monitoring (QCM-D).

Chapter 4 disccuses the in-situ copolymerization of hydrolysate consititunents with acrylamide to produce a lignocellulose-based coagulant. The reactions were carried out at different reaction temperature, reaction time, pH, initiator concentration, and monomer concentrations to find the optimal conditions. The products were evaluated in terms of yield, grafting ratio, molecular weight and charge density. Further more, products and conventional coagulants (anionic acrylamide and cationic acrylamide) were utilized in dye waste water containing ethyl violet (EV)

Chapter 5 states the overall conclusions and recommendations for future work.

1.2 Objectives

The key objectives of this study included:

1. Examining the effect of operating conditions, such as temperature, residence time and L/S ratio, on the production of hydrolysates in the autohydrolysis of spruce wood following Taguchi orthogonal design method

2. Discovering how temperature, salt concentration, pH, ultrasonication, time impact the hydrodynamic size of hydrolysates
3. Understanding the deposition behavior of hydrolysates on stainless steel surface.
4. Synthesizing the grafting polymerization of lignocellulose (LC) in hydrolysis liquor with acrylamide (AM)
5. Testing coagulation efficiency of the produced polymer, LC-AM, as coagulant for waste water containing ethyl violet (EV) along with commercial charged polyacrylamides.

1.3 Novelty

1. Studying the agglomeration of hydrolysate components from the autohydrolysis of spruce using dynamic light scattering
2. Investigating the adsorption of hydrolysate on stainless-steel surface quantitatively using quartz crystal microbalance
3. Conducting the in-situ polymerization of hydrolysate constituents with acrylamide
4. Utilizing LC-AM as a coagulant for the dye removal in singular and dual coagulant systems.

1.4 References

Alvarez, C., Reyes-Sosa, F. M., & Diez, B. (2016). Enzymatic hydrolysis of biomass from wood. *Microbial Biotechnology, 6*(2), 149-156.

Ibrahim, N. A., Abu-Ilaiwi, F., Rahman, M. Z., MansorB.Ahmad, Dahlan, K. Z., & Yunus, W. M. (2005). Graft Copolymerization of Acrylamide onto Oil Palm Empty Fruit Bunch (OPEFB) Fiber. *Journal of Polymer Research, 12*, 173-179.

Kong, F., Wang, S., Price, J. T., Kondurib, M. K., & Fatehi, P. (2015). Water soluble kraft lignin–acrylic acid copolymer: synthesis and characterization. *Green Chem, 17*, 4355–4366.

Krutov, S. M., Evtuguin, D. V., Ipatova, E. V., Santos, S. A., & Sazanov, Y. N. (2015). Modification of acid hydrolysis lignin for value-added applications by micronization followed by hydrothermal alkaline treatment. *Holzforschung, 69*(6), 761–768.

Landim, A. S., Filho, G. R., Sousa, R. M., Ribeiro, E. A., Souza, F. R., Vieira, J. G., . . . Cerqueira, D. A. (2013). Application of cationic hemicelluloses produced from corn husk as polyelectrolytes in sewage treatment. *Polímeros, 23*(4), 468-472.

Linden, E. d., & Venema, P. (2007). Self-assembly and aggregation of proteins. *Current Opinion in Colloid & Interface Science, 12*(4-5), 158-165.

Macfarlanea, A., Prestidge, R., Farida, M., & Chen, J. (2009). Dissolved air flotation: A novel approach to recovery of organosolv lignin. *Chemical Engineering Journal, 148*, 15-19.

Nitzsche, R., Gröngröft, A., & Kraume, M. (2019). Separation of lignin from beech wood hydrolysate using polymeric resins and zeolites – Determination and application of adsorption isotherms. *Separation and Purification Technology, 209*, 491–502.

Pu, Y., Treasure, T., Gonzalez, R., Venditti, R. A., & Jameel, H. (2013). Autohydrolysis Pretreatment of Mixed Softwood to Produce Value Prior to Combustion. *Bioenergy Research, 6*, 1094–1103.

Ratnaweera, D. R., Saha, D., Pingali, S. V., Labbé, N., A. K., & Dadmun, M. (2015). The impact of lignin source on its self-assembly in solution. *RSC Adv., 5*, 67258–67266.

Rauhala, T., King, A. W., Zuckerstätter, G., Suuronen, S., & Sixta, H. (2011). Effect of autohydrolysis on the lignin structure and the kinetics of delignification of birch wood. *Nordic Pulp and Paper Research Journal, 26*(4), 386-391.

Saeed, A., Jahan, M. S., Li, H., Liu, Z., Ni, Y., & Adriaan, v. H. (2012). Mass balances of components dissolved in the pre-hydrolysis liquor of kraft-based dissolving pulp production process from. *Biomass and Bioenergy, 39*, 14-19.

Saini, J. K., Saini, R., & Tewari, L. (2015). Lignocellulosic agriculture wastes as biomass feedstocks for second-generation bioethanol production: concepts and recent developments. *3 Biotech, 5*(4), 337–353.

Salentinig, S., & Schubert, M. (2017). Softwood Lignin Self-Assembly for Nanomaterial Design. *Biomacromolecules, 17*, 2649−2653.

Song, T. (2013). *Extraction of polymeric galactoglucomannans from spruce wood by pressurised hot water (Academic Dissertation).* Turku: Abo Akademi.

Testova, L., Chong, S.-L., & Sixta, M. T. (2011). Autohydrolysis of birch wood. *Holzforschung, 65*, 535–542,.

Westbye, P., Köhnke, T., Glasser, W., & Gatenholm, P. (2007). The influence of lignin on the self-assembly behaviour of xylan rich fractions from birch (Betula pendula). *Cellulose, 14*(6), 603–613.

Wong, S., Teng, T., Ahmada, A., Zuhairi, A., & Najafpour, G. (2006). Treatment of pulp and paper mill wastewater by polyacrylamide (PAM) in polymer induced flocculation. *Journal of Hazardous Materials*, 378–388.

Wu, C. (2016). The Potential of Pre-Hydrolysis Liquor from the Dissolving Pulp Process as Recovery Source of Xylooligosaccharide - A Mini-Review. *BioResources 11(3)*, 7917-7927.

Wu, Y., Zhang, S., Guo, X., & Huang, H. (2008). Adsorption of chromium(III) on lignin. *Bioresource Technology, 99*, 7709-7715.

Chapter 2: Literature review

2.1 Introduction

This chapter provides a brief overview of the literature regarding the fundamental knowledge related to the research topic in the MSc studies. Different hydrolysis treatments and the parameters that may affect hydrolysis were discussed. The self-assembly and adsorption behavior of hydrolysis liquor constituents were also addressed. Then, the information about copolymerization of hydrolysates and its application in dyeing water treatment were provided. A number of characterization techniques, such as gel permeation chromatography (GPC), nuclear magnetic resonance (NMR) spectroscopy, zeta potential analyzer, scanning electron microscopy (SEM), particle charge detector, quartz crystal microbalance with dissipation (QCM-D), dynamic light scattering (DLS) used in this study were introduced.

2.2 Autohydrolysis

Autohydrolysis, also known as hot water extraction or autocatalytic, is a technology in which woody biomass is treated with water or stream at elevated temperature and pressure (Testova et al., 2011; Pu et al., 2013). Hemicellulose can be partially extracted through autohydrolysis at sever condition. A large porportion of the lignin dissolved in the course of autohydrolysis is refered as acid suluble lignin. The klason lignin is mostly insoluble in the autohydrolysis liquor or hydrolyzate and only a tiny amount of the klason lignin can be dissoved (Leschinsky et al., 2009). Autohydrolysis has been widely used in the biorefinery, bioenergy and pulping insdustry. The application of autohydrolysis includes: as a prehydrolysis stage in the kraft-based dissolving grade pulp process, defibration for firbreboard production, and as a pretreatment for the enzyhdrolysis of biomass for sythesis of ethanol and other value-added products (Wu, 2016; Garrote et al., 1999).

The advantage of autohydrolysis approch is that no additional chemicals (catalyst) requsted, limited corrosion to apparatus (pulping digestor), lower capital costs for the recovery of hydrolysis liquor, good cellulose digestiblity, and limited inhibitors for sequantial process (Yang & Wyman, 2008; Hou et al., 2014).

Autohydrolysis is initiated by the catalytic species and hydronium ions, which are generated from water autoionization, and then the acetic acid is released by the cleavage acetyl groups which is catalyzed by hydronium ions from water autoionization.The autoionization of acetic acid supplies more hydronium ions to improve the hydrolysis reaction kinetics (Garrote et al., 2001; Garrote &

Parajo, 2002).With the advent of an increasing number of hydroniums ions, the pH of hydrolysis liquor is decresed which will facilitate the hemicellulose removal (Liu & Wyman, 2005; Alfaro, et al., 2009). The disollution of hemicellulose leads in the formation of oligosaccharides, and with higher autohydrolysis intensity, sugar fractions is further degraded to monosacharides. However, the yield of sugars vareis primaily depending on the wood species and prehydrolysis factor (P-factor) of the fracnation treatment (Saeed et al., 2012). Afterwards sugars manily decompose to form furan dedrivates such as furfural principally from pentose, hydroxymethylfurfural (HMF) from hexose via dehydration raction. The HMF can be further hydrolyzed into formic acid and levulinic acid (Testova et al., 2011).

Autohydrolysis has a broad range of applications, including: (1) pulp and paper industry where the hemicellulose is fractionated with selectivity towards cellulose degradation, (2) defibration for fibreboard manufacturer, in processes using high pressure steam, and (3) as a pretreatment for the enzymatic hydrolysis of cellulose for the production of biofuel and other value-added products (Garrote et al., 1999).

2.2.1 Influencing factors in hydrolysis

Autohydrolysis technology can be performed using both liquid water and steam. The operating parameters such as liquid to solid ratio, temperature, residence time, flow rate can be tuned to optimize the kinetic severity and the selectivity of the desired product. It also can impede the formation of undesired by-products (Galia et al., 2015).

2.2.1.1 Liquid to solid ratio

Liquid to solid ratio (LSR) is an important factor that can impact the dissolution of the lignocellulose in the course of hydrolysis. It is generally used to quantify the solid concentration in hydrolysis. LSR can vary from 2 to 100 on weight basis and is limited by the setup of the equipment because only large continuous flow through reactor can handle enormous amount of water (Vallejos et al., 2012).

LSR is able to alter the hydrolysis performance through two pathway: 1) reducing the LSR facilitates the removal rate of acetyle groups from hemicellulose. Acetic acid is considered a catalyst spice and a source of hydronium ions. The concentration of the acetic acid increses due to the decrease of LSR, which favors the hydrolysis of the hemicellulose. 2) The buffer capacity of lignocellulose and water mixture at a neutral pH is intensified by lowering the LSR. This

phenomenon is assosiated with ash content of woody biomass and slow down the hydrolysis rate (Carvalheiro et al., 2008). Many researchers recently investigated LSR along with temperature and residence time to build up a kinetic model for a certain sugar and decomposition product.

According to Yadav et al. (2017), LSR also affects the formation of furfural in hydrolysis of pea pod. The experiment was conducted at 130 ^{0}C at 6 wt.% acid at different LSR. As LSR increased, the maximum concentration of furfural throughout the hydrolysis decreased. This is primarily due to the increment in total reaction volume while the limiting reactant, pentose, remaining constant. It was also observed that the conversion rate and degradation rate of furfural were increased with an increase in LSR.

In another study, eucalyptus globulus was used in both autohydrolysis and acid hydrolysis to explore yield of sugars and lignin at different LSR at 150 ºC for 100 min. The extraction yield of sugars decreased with increasing LSR no matter autohydrolysis or acid hydrolysis initially. The extraction yield of sugars became stable during autohydrolysis and acid hydrolysis when increasing LSR up to 10 and 20, respectively. On the contrary, the dissolution rate of lignin slightly increased with increasing LSR (Tunc M. S., 2014). However, a group of researchers stated that higher LSR would result in an improvement in mass transfer as well as the solubility for both hemicellulose and lignin when they investigated the fracnation of sugarcane bagasse by hot water extraction (Vallejos et al., 2015).

The benefit of optimazing LSR is to reduce the amount of processing water and lower the energy cost as much as possible while the concentration of product is ensured. Although LSR plays a significant role in every type of hydrolysis and pulping, such as, enzymatic hydrolysis, diulte acid hydrolysis and ethanol pulping, the consequences of varing LSR is still unresolved (Ares-Peón et al., 2011; Requejo et al., 2012; Vallejos et al., 2015).

2.2.1.2 Digestor configuration and flow rate

Basically, there are four types of hydrolysis reactor configurations: co-current, countercurrent, flow through and batch. Co-current digestor operates from 140 to 180 ℃, while coutercurrent and flow through digestor have simlar operating temperature range which is 180 to 220 ℃ (Mosier et al., 2005). However, the maximum hemicellulose yeild is approximately 65 % when an autohydrolysis conducted in batch system without interior flow. It is stated that just by passing water in a flow through reactor, not only the hemicellulose sugars yield can greatly enhance up to

90%, but also the theoretical cellulose digestibility is reached. Additionally, autohydrolysis in a batch reactor can remove 30% or less lignin, whereas flow through pretreatment can extract 75% of lignin at high flow rate (Yang & Wyman, 2008; Liu & Wyman, 2003).

The increasing flow rate is able to signficantly improve the subulization of hemicellulose and ligin in autohydrolysis or dilute sulfuric acid hydroylsis at high temperature. Hemicellulose hydrolysis is always accompanied by delignification reaction. The increment for removal rate of hemicellulose and lignin with high flow rate is prominent in the early hydrolysis stage (Liu & Wyman, 2004). Liu & Wyman (2003) proposed that increasing flow rate alters physical processes, for example, reducing the thickness of a liquid film over the fibre particles, thus accelarating mass transefer of catalytic speice (hydronium ions) onto the hydrophobic

surface in order to convert hemicellulose to short chain oligosaccharides. The disadvantage of flow through reactor in pulp and paper industry is that the comsumption of water especially at high flow rate is massive, which also causes high energy demand (Liu & Wyman, 2005).

2.2.1.3 Operating temperature

Temperature is considered as the most critical operating parameter. Temperature can alter the concentration of all the species during the autohydrolysis. Xylan is dissolved as oligosugar in the course of autohydrolysis of hardwood at 150 °C. Xylan initiates to depolymerize monomeric xyloase at prolonged residence time. There is scarcely detectable amount of furfural presented at 150 °C (Tunc & Van Heiningen, 2008). Mannose is the most important monomer for softwood followed by xylose, glucose, galactose and arabinose. Most of mannose is present as O-acetyl-galactoglucomannan. A small amount of galactoglucomannan (GGM) can be extracted from spruce wood by hot water at temperatures below 100 °C. It was also confirmed that at elevated temperatures above 170 °C or an extended extraction time at 170 °C, the yield of GGM from Southern pine increased drastically and accounted for more than half of the total dissolved lignocellulosic material. Autohydrolysis at 180 °C caused clearly decline in pH than autohydrolysis at 170 °C or 160 °C. This is an evident that significant amount of acetic acid liberated at 180 °C (Song et al., 2008). The concentration of polysugar reached its maximum value at 180 °C, whereas in more harsh conditions it dropped gradually. At high temperature, the polysugar depolymerized into monomeric sugars then further converted to furfural derivatives and acid, which may rationalize the decreased concentration of polysugar after 180 °C. (Khazraie et

al., 2017). A significant lignin isolation in the temperature range of 160–180 °C was also reported (Song, 2013).

2.2.1.4 Intensity of hydrolysis

P-factor was introduced to describe the intensity of autohydrolysis of woody biomass. It is an Arrhenius type function combining both residence time and temperature. The activation energy for the cleavage of glycosidic bonds of the sugars was resolved to be 125.6 kJ/mol, which is close to the activation energy of 124 kJ/mol in kraft cooking (Gütsch et al., 2012; Tunc & Van Heiningen, 2009). The p-factor is expressed as (Sixta, 2006):

$$P - factor = \int_0^t \frac{k(T)}{k_{100℃}} dt = \int_0^t e^{40.48 - \frac{15106}{T}} dt \quad [2.1]$$

where t is residence time (hr), T is temperature (K), and k is the rate constant.

According to Overend & Chornet (1987), the severity factor is an alternative term that qualifies the intensity of hydrothermal treatment. The assumptions for this approach is that the overall conversion is primarily due to the hydrolytic reactions whose kinetics follow first order and rate costant can be fitted into arrhenius equation. 100 °C is usually selected as a reference temperature in the calculation of severity factor (Hundt et al., 2014). The severity factor is defined as following:

$$R_o = te^{\frac{T[℃]-100}{14.75}} \quad [2.2]$$

where t is residence time (min), and T is temperature °C.

There are a variety of possibilities for modification of the severity factor or p-factor when the acid or enzyme is introduced in hydrolysis treatment (Hundt et al., 2014). However, these modifications are beyond the scope of this study, the intensity with respect to other hydrothermal treatments will not be discussed.

Wood yield in autohydrolysis treatment decreases drastically with increasing treatment intensity because acid soluble lignin and the majority of the hemicellulose become soluble in the hydrolysate. Klason lignin (KL) in solid residue does not decline with increasing treatment intensity. Klason lignin is independent from any operating conditions even though it is enzymatically hydrolyzed. In reality, it was discovered that the klason lignin content showed a slightly reduction after autohydrolysis (Gütsch et al., 2012).

In a study, an autohydrolysis of a mixture of southern hardwood was conducted at various intensities. It was found that xylan is the major component in hydrolysis liquor after P-factor exceeded 200 hrs. At a P-factor of 600 hrs, there was significant amount of furfural produced from dehydration of xylose. The maximum dissolution rate of xylan occurred at P-factor of 800 hrs and started to decline gradually. At P-factor of about 1000 hrs, the dissolution rate of xylan leveled off significantly and xylooligomer degradated to xylose remarkably. Approximately 70% of hemicelluloses in original southern hardwood were removed during autohydrolysis. There were 70 and 85% of initial acetyl groups and uronic acid groups extracted during autohydrolysis respectively (Tunc & Van Heiningen, 2009).

2.2.1.5 The effect of intensity of autohydrolysis on pH

This empirical equation is derived from the hydrothermal dissolution profile of a hardwood mixture during autohydrolysis. The pH of the hydrolysis liquor decreases from 5.5 to 3.6 over P-factor between 30 and 980 hrs. The concentration of hydronium has linear relationship with p-factor up to 400 hrs (Tunc & Van Heiningen, 2009). During the autohydrolysis acetyl groups are hydrolytically cleaved from hemicellulose and the acetic acid formed acts as a catalyst for the autohydrolysis. The concentration of free acetic acid increased dramatically at higher auhydrolysis intensity or severity (Gütsch et al., 2012). In one study, the autohydrolysis treatment of spruce was carried out at 170, 180 ,190 ^{0}C for 15 min or 45 min at liquid to solid ratio of 8. The pH of hydrolysis liquor was varied from 3.2 to 3.6 when the hydrolysis liquor was cooled down to room temperature (Khazraie et al., 2017). If auhydrolysis treatment was carried out at high liquid to solid ratio, the pH of the hydrolysis liquor after the treament would have increase accordingly.

$$pH = 7.59\ (P - factor)^{-0.11} \qquad [2.3]$$

2.3 Acid hydrolysis

Acid hydrolysis is generally of two types: dilute acid hydrolysis and concentrated acid hydrolysis. Hydrolysis mechanism is similar to autohydrolysis, but acid hydrolysis makes cellulose more accecsible than autohydrolysis so that glucose can be yielded from cellulose (Kumar et al., 2015; Kumar et al., 2009). Sulphuric and hydrochloric acids are the most commonly used catalysts for acid hydrolysis of woody biomass. (Lenihan et al., 2010). The dilute acid hydrolysis generally procceses at high temperature (160 to 230 °C) and high pressure. The concentrated acid hydrolysis operates at lower temperature (<50 °C) and atmospheric pressure. The acid concentration for diulte

acid hydrolysis is in the rang of 2 to 5% and that for concentrated acid hydrolysis is in the scope of 10 to 30% (Iranmahboob et al., 2002; Kumar et al., 2009). In contrast to dilute acid hydrolysis, the advantages of concentrated acid hydrolysis, other than lower operating temperature and pressure, are higher sugar yield (90% of theoretical yield for both cellulose and xylan) and lower inhibitor formation which are in favor of fermentation process for bioethanol production (Kanchanalai et al., 2016; Wijaya et al., 2014). However, concentrated acid hydrolysis requires the reactor/digestor that has resisitant to corrosion and high energy comsuption to recover all the acid after hydrolysis. High capital cost and mainetanence cost are main constraints for the application of concentrated acid (Taherzadeh & Karimi, 2007). Dicarboxylic acids such as oxalic, fumaric and maleic acids have been investigated as alternative acids for concentrated acid hydrolysis to overcome these disadvantages (Lim & Lee, 2013)

2.4 Enzymatic hydrolysis

The typical process currently employed for the production of fermented sugars and bioethanol consists of four steps: pretreatment, enzymatic hydrolysis, fermentation and separation. The enzymatic hydrolysis of untreated lignocellulose material has low efficiency due to the high lignin content and crystalline structure of cellulose (Li et al., 2016). Therefore, the pretreatment process, which aims at deconstructing the biomass matrix, must be applied prior to enzymatic hydrolysis. An efficient pretreatment results in reducing the enzyme loading, maximizing enzyme accessibility in enzymatic hydrolysis and minimizing the fermentation step inhibitor products (Barbanera et al., 2017). The typical inhibitors that hamper microbial fermentations are furfural and 5-hydroxymethylfurfural (HMF). An optimized pretreatment must have a threshold regarding the concentration of inhibitors, which is 1mg/mL generally; otherwise, the fermentation process will be significantly affected (Mosier et al., 2005). Pretreatments can produce pretreatment liquors below this threshold. Additionally, the maximal exposure of lignocellulosic material to enzyme contributes to reduction of energy input and sugar recovery enhancement (Vegi & Shastri, 2017). Hardwood consists of rich glucuronoxylan and xyloglucan content, therefore xylanase, beta-xylosidase and xyloglucanase are the desired hemicelluloses for the decomposition of the hemicellulose chains. On the other hand, galactoglucomannans and glucomannans are dominant in softwood, therefore the main hemicelluloses required are mannanases and beta-mannosidases. Thus, it is crucial to select the proper enzyme in saccharification to obtain target sugars. Generally, softwood species have much stronger recalcitrance to enzymes comparing to hardwood species

(Alvarez et al., 2016). The performce of enzymatic hydrolysis can be significantly affected by biomass dosage, enzyme dosage and incubation duration (Cotana et al., 2015). As the viscosity of the biomass increases rapidly at higher loadings, the high solid content operation may encounter inadequately uniform mixing and constrain mass transfer of the enzymes. However, at the lower biomass loading, enzymatic hydrolysis yields sugar in the hydrolysate at low concentration, prompting low productivity and high operation cost. The optimization of biomass loading still needs further research. However, enzymatic hydrolysis at the expanded biomass loading is a key to scale up the production at industrial level (Ioelovich & Morag, 2012).

2.5 Hydrolysate

Woody biomass can be separated by autohydrolysis in two fractions: hydrolysis liquor or hydrolysate, which is a mixture of oligosaccharides (mainly), monosacchrides, acetic acid and furan derivatives such as furfural (2-furaldehyde) and hydroxymethylfurfural (5-hydroxymethyl-2-furaldehyde, HMF), and a residual solid comprising of cellulose, lignin and hemicellulose remainings (Carvalheiro et al., 2008; Garrote et al., 2003).

2.5.1 Cellulose

The majority of lignocellulosic material is cellulose followed by hemicellulose and lignin. It is a linear homopolymer consisting of D-glucose units bounded by a β-(1,4)-glyosidic linkage and the repeating unit of cellulose backbone is cellobiose (Pu et al., 2013). The long-chain cellulose polymers are integrated by hydrogen bond and van der Waals bonds, making the bundles of cellulose packed into microfibrils. Cellulose has both crystalline and amorphous forms. In the microfibrils, crystalline cellulose, which is highly ordered regions, is substituted with amorphous cellulose that is presented in less ordered regions (da silva Morais et al., 2016). The bulk part of cellulose is in crystalline form. Due to its crystalline form, chemical compositions and structure, cellulose is insoluble in water and the most organic solvent. During the hydrolysis of biomass, cellulose undergoes depolymerization reaction by random cleavage of the glyosidic bonds. Nonetheless, the yield of cellulose in the solid residue after autohydrolysis has no significant change at moderate intensity due to the highly ordered structure (Tunc and van Heiningen, 2008). Cellulose is also resistant to hydrolysis by mineral acids or enzymes because it is highly recalcitrant. Cellulose with amorphous form tends to be more susceptible to enzymatic degradation (Kumar et al., 2009; Mosier et al., 2005).

2.5.2 Hemicellulose

Hemicelluloses, branched by short chains containing various sugars, have been studied for several decades as a promising raw material for value-added and sugar-based products. As hemicellulose has a lower molecular weight than cellulose due to short branches, hemicelluloses are more hydrolysable than cellulose. Hemicellulose may have large side groups substituting for the hydroxyls on the C2, C3 and C6 positions, which give hemicellulose the potential for different kinds of modification. The monosaccharides in the hemicellulose branches can be classified as: pentoses (five carbon sugars: xylose, rhamnose, and arabinose), hexoses (six carbon sugars: glucose, mannose, and galactose) and uronic acids (Sarip et al., 2016). Softwood hemicelluloses contain mainly glucomannan, while Xylan dominates hardwood hemicelluloses. The age of the wood also can influence hemicellulose compositions, there is more mannan and less xylan in latewood than in earlywood. Softwoods have a high proportion of mannose units, more galactose units and lignin than hardwoods, and hardwoods have a high proportion of xylose units and more acetyl groups than softwood. In terms of the degree of polymerization (DP), normally the polysaccharide from hardwood hemicellulose varies approximately from 70 to 250. It is in the range of 100 to 200 for that of softwood hemicellulose (Matsagar & Dhepe, 2015).

Hemicelluloses can be employed as the feedstock for the production of some industrially common chemicals such as furfural, 5-hydroxymethylfurfural (HMF), sugar alcohol (sweetener) and hemicellulose-based products, serving as strength additives for papermaking industry (Liu et al., 2011).

2.5.3 Lignin

Lignin is the second most abundant biopolymer in the world after cellulose and its content varies from 18 to 40 wt.% in woody biomass depending on wood species (Zhao et al., 2014). More than 50 million tons of lignin has been produced by the pulp and paper industries all over the world (Cheung et al., 2007). It is a primary structural material presented in the outer layer of the cellular wall, providing strength, impermeability and resistibility against microbial attack and oxidative stress. The plants containing higher lignin constituent show a tendency to have more resistant to ultraviolet light and frost (Hendriks & Zeeman, 2009; Dohertya et al., 2011). Lignin is a cross-linked macromolecular containing 3-dimentional amorphorus polymers and variety of functional groups, for instance, phenolics, aliphatic alcohols, methoxyls, ketones, aldehydes, and ethers. The

basic structural units for composing lignin are p-coumaryl alcohol (P), coniferyl alcohol(G), and sinapyl alcohol(S) (da Silva Morais et al., 2016; Kumar et al., 2015). The vast majority of the structural unit for softwood lignin is coniferyl alcohol (more than 95%); whereas, that of hardwood lignin is composed of p-coumaryl alcohol and sinapyl alcohol (Shen et al., 2015).

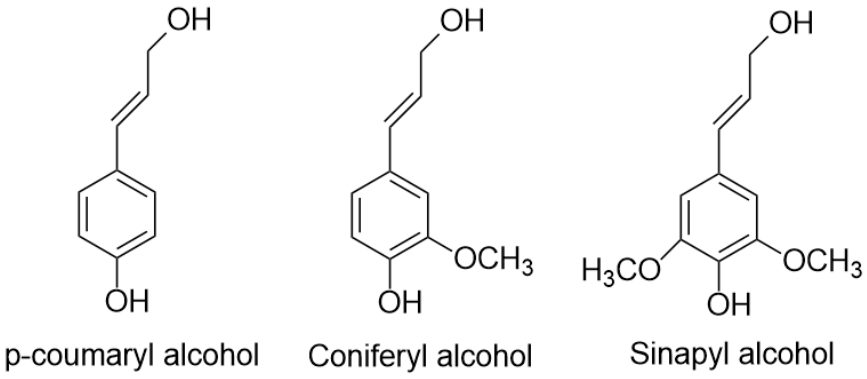

Figure 2.1. Different structures of lignin

2.5.3.1 Klason lignin and acid soluble lignin

In the early 1900's, the sulfuric acid method for lignin content determination was proposed. Peter Klason stated that the concentrated sulfuric acid was critical to determine the acid insoluble lignin (AIL). In 1932, 72% sulfuric acid method was published, which has been the most commonly used lignin determination procedure until now (Nicholson et al., 2014). This method isolates lignin as an insoluble material by depolymerization of cellulose and hemicellulose in 72% sulfuric acid and then followed by hydrolysis of the dissolved polysaccharides in boiling 3% sulfuric acid. In this stage, depolymerized polysaccharides are converted to soluble monosaccharides. However, part of the lignin is dissolved in the filtrate as so-called acid-soluble lignin (ASL), while the solid residues covered by filtration after hydrolysis are regarded as acid insoluble lignin or Klason lignin (KL) (Yasuda et al., 2001).

2.5.4 Furfural

The global production of furfural is approximately 200,000 to 210,000 tonnes per annum. It can be converted to a variety of value-added products through chemical and biochemical pathways and has very widely range of applications. 60% of furfural is used to produce furfuryl alcohol as a raw material. The rest of furfural serves as an important chemical intermediate in the commercial

production of hexamethylene diamine and adipic acid, which are the main constituents for the synthesis of nylon (Yadav et al., 2017; Liu et al., 2015; Mamman et al., 2008; Testova et al., 2011). Pentose sugars are dissovled during the course of the hydrolysis of biomass. Then, furfural is yielded under acid conditons when pentose sugars undergo dehydration, lossing three molecules of water. In the autohydrolysis, a detailed model for the production of the furfural was propsed: sequential degradation of xylan into high molecular weight oligosccahrides (XO_H), then low molecular weight oligosaccharide (XO_L), further hydrolyzed to monoric sugar xylose (X), and eventually furfural (F) formed through irreversibe first-order, pseudohomogenous reactions (Garrote & Parajo, 2002). However furfural yield/selectivity is limited due to serveral side reactions. The side reactions would be more vigorous under high acid concentration and ealevated temperature. The side reactions include fragmentation side reaction which is the degradation of furfural to formic acid, condensation reation of furfural, resinification side reactions between furfural and xylose or phenolic compounds related to lignin (Liu et al., 2014).

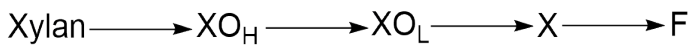

Figure 2.2. The formation of furfural from xylan

2.5.5 Acetic acid

Acetic acid in hydrolysis liquor is produced from the cleavage of acetyl group (around 5% in hardwood) mainly bounded to the hemicelluloses (Li et al., 2010). With more acetic acid liberated from acetyl group, the pH of hydrolysis liquor will decrease. By intensifying the severity of the hydrolysis treatment, the concentration of acetic acid can vary greatly. Acetic acid inhibits fermentation process; therefore, an effective recovery of acetic acid is crucial in some industry applications. It can sell as a commodity chemical and enhance the utilization of hemicellulose sugars in the downstream process. It was proposed that recovery of acetic acid can be achieved by adsorption onto resin and by reactive extraction process using trioctyl amine in octanol as a diluent (Ahsan et al., 2014).

2.6 Self-assembly of hydroysate

Self-assembly is a phenomena wherein a paricle is spontaneously assembled without the influence of external forces or interferences (Dommelen et al., 2018). Lignin and hemicellulose contain

many functional groups such as carboxylic acid, hydroxyl groups, and amine. These functional groups can interact with each other. The driving force for self-assembly consists of hydrogen bonding, van der Waals forces, electrostatic forces, and π–π interactions (Xiong et al., 2017). It was found that, the main driving force for adsorption is the formation of hydrogen bonds between xylan and the cellulose fibers and xylan adsorption on the fibers in the form of aggregates (Linder et al., 2003). It was also reported that, in aqueous solution, xylan chains interact via hydrogen bonds and hydrophobic interactions gernerating associated structures (Grigoray et al., 2014). In one study, lignin sample extracted from spruce forms aggregates in a dioxane-water (5:1) solvent system, with a hydrodynamic radius of 60 nm (Gilardi & Cass, 1993). Dynamic light scattering technique is suitable for studying the self-assembly behavior of the hydrolysate, since a growth in hydrodynamic size is the evidence of the self-assembly of the lignocelulosic matters.

2.7 Variables effect hydrodynamic size of hydrolysate

Generally, the hydrodynamic size of sample increased with an increasing sample concentration because unpredictable agglomeration happens in high concentrations unless with presence of some surfactants. Furthermore, high concentration can lead to multiple scattering effects and particle interactions, both of which causes some deviations in hydrodynamic size. On the other hand, using too dilute samples may not generate enough scattered light to be detected (Müller et al., 2014). Hydrodynamic size is also dependent on ionic strength and pH due to the ionization of the functional groups (Huang & Wu, 1999). Ionized group can alter the zeta potential and thus create electrostatic repulsion force. Temperature is another factor that can influence the hydrodynamic size. It may change the diffusivity of the solution and accelarate the Brownian motion. The hydrodynamic size aslo depends on the salt concentration of the suspending medium. Some electrolyte like NaCl and KCl can screen the double layer surrounding the paricle.

2.8 Copolymerization

2.8.1 Mechanism of lignin copolymerized with vinyl monomer

The reaction can be classified into three stages: initiation, chain propagation, and chain termination. During initiation stage, free radicals, which are essential for propagation, are created. Radicalized molecule interacts with a monomer in propagation rapidly. In the last stage, two radical copolymers are coupled with each other to form a single molecule (Mahdavi et al., 2011).

Figure 2.3 demonstrates the free radical copolymerization scheme of lignin and vinyl monomer initiated by potassium persulfate ($K_2S_2O_8$). The vinyl monomer has a functional group R, which can be either amide or carboxylic group representing acrylamide and acrylic acid respectively. In the initiation stage, the formation of free radical can be the radical formation for the initiation reaction, occurring either on the polymer backbone or on the monomer to be grafted (Bhattacharyaa & Misra, 2004). In reaction (a), the sulfate radical is produced from the decomposition of the initiator ($K_2S_2O_8$) when subjected to heat. The sulfate radical can take the unstable hydrogen from phenol group to form phenoxyl radical, which serves as reaction site on the lignin backbone. Theoretically, the resonance forms of phenoxyl radicals could be C_5, C_1 and C_β radicals (b). The sulfate radicals can also initiate the side reaction, which is the homopolymerization of vinyl monomer (reaction (C)) (Wang et al., 2016). In propagation stage, all the resonance structures are involved with copolymerization (reaction (d)). In termination stage, lignin polymer can be further coupled with a propagating vinyl monomer or another lignin polymer (reaction (f)). In such case, lignin also works as a chain transfer agent (Kong et al., 2015).

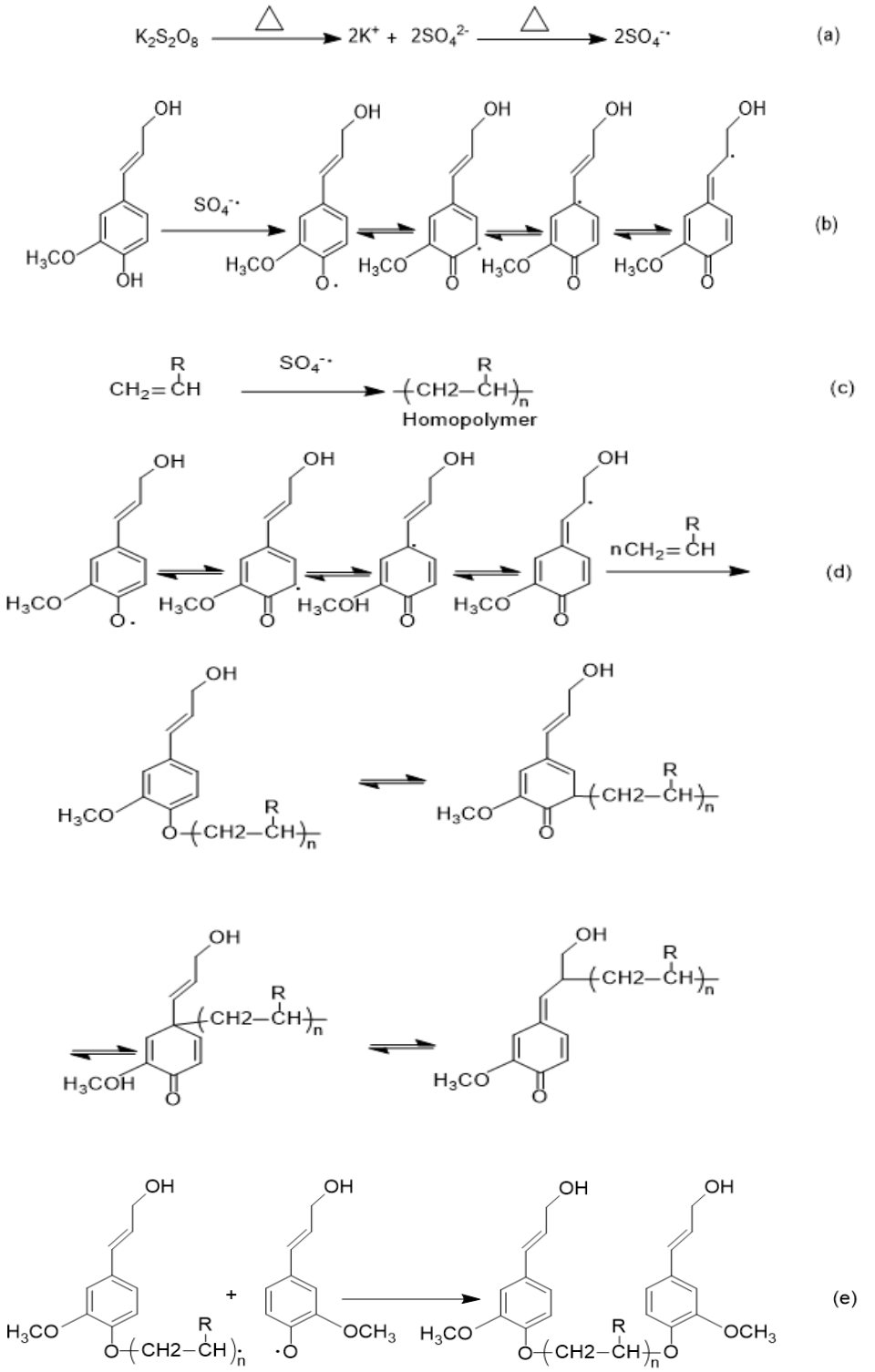

Figure 2.3. The reaction scheme of lignin copolymerized with vinyl monomer

2.8.2 The effect of phenolic hydroxyl group

The decreasing content of phenolic-OH after grafting copolymerization was mainly contributed to its function as active center. Another reason regarding the decreasing content of phenolic-OH is that phenolic-OH was oxidized to quinoid structure by initiator, as seen the resonance structures in reaction (b). The grafting efficiency, monomer conversion, and yield were also confirmed to be proportional to phenolic-OH in the first hour in the grafting copolymerization (Ye et al., 2013; 2014). Additionally, the lignin radicals are mostly derived from the phenolic hydroxyl groups rather than aliphatic group beause phenoxyl radicals have high stablility comparing to aliphatic alcohol radicals. Some researchers studies stated that: 1) acrylic acid is not able to graft onto lignin without phenolic hydroxyl group in lignin macromolecules. 2) the aliphatic hydroxyl groups indeed parcitipate in copolymerization but of kraft lignin can not enhance the grafting of acrylic acid on kraft lignin (Kong et al., 2015).

$$Y(\%) = \frac{W_2}{W_0+W_1} \times 100\% \quad [2.4]$$

where W_0 is the weight of lignin used in the reaction (g), W_1 is the weight of vinyl monomer used in the reaction (g), W_2 is the weight of the copolymer (g), and Y is yield (wt.%.).

Grafting ratio:

$$GR(\%) = \frac{71\times N_1}{14\times 100 - N_1\times 71} \times 100\% \quad [2.5]$$

where N_1 is the nitrogen content measured by elemental analysis (%), 71 is the molecular weight of acrylamide (g/mol), and 14 is the atomic weight of nitrogen (g/mol).

2.8.3 Initiator effect

Many efforts have been made to exam the efficiency of different kinds of initiator. Table 2.1 demonstrates the yield and intrinsic viscosity for copolymerization of enzymatic hydrolyzed lignin with acrylamide. Higher intrinsic viscosity of lignin/acrylamide copolymer's aqueous solution indicates large molecular weight of copolymer which favors flocculant performance in its application. Potassium persulfate based initiators have yield of 37.4 at least, which is higher than any other initiators. The binary-initiator, $K_2S_2O_8$ – $Na_2S_2O_3$ has the highest yield and intrinsic viscosity in this case. Copolymerization of lignin with vinyl monomer could also be induced by laccase enzymatically.

Table 2.1. The effect of initiators on yield and intrinsic viscosity (Fang et al., 2009)

Initiator	Yield (%)	Intrinsic viscosity
Fe^{2+} -H_2O_2	34.30	35.76
$(NH_4)_2Ce(NO_3)_6$	30.86	34.51
$K_2S_2O_8$	37.83	35.37
$(NH_4)S_2O_8$	34.55	37.15
$K_2S_2O_8$ – $NaHSO_3$	37.40	36.93
$K_2S_2O_8$ – $Na_2S_2O_3$	39.60	37.86

2.8.4 Time effect

The copolymerization reaction is signicantly affeacted by the reaction time. In one study, acrylic acid (AA) was grafted onto kraft lignin (KL) under alkaline aqueous conditions to produce a water soluble lignin-based copolymer. The copolymerization was conducted using $K_2S_2O_8$-$Na_2S_2O_3$ as the initiator. The grafting ratio and charge density of lignin-based copolymer dramtically increased with increasing reation time from 0.5 h to 2 h. As the reaction time was extented from 2h to 4h, the increasing rate of the grafting ratio and charge density was reduced. There were more free radicals and monomer presented in the solution with an increase in reation time, which resulted in the extention of the lignin-based copolymer chain (Kong et al., 2015). A similar effect of reation time was reported in another study in which soda lignin was copolymerized with acrylamide (AM). The coplymerization was carried out using $K_2S_2O_8$ as initiator in acid aqueous conditions. The yield and grafting ratio of copolymer increased rapidly as reaction time was increased up to 4h. When the reaction time was exceeded for 4h, the growth of yield and grafting became negligible (Wang et al., 2016). The formation of polymer on the surface of the lignin may delay the AM diffusion rate into lignin particle and the concentration of acrylamide and initiators declined with elapsed time, which caused the free radical grafting copolymerization rate become remarkable (Ibrahim et al., 2005).

2.8.5 Effect of monomer dosage on copolymerization

The monomer dosage is always described as mass/molar fraction between monomer and lignocellulose dry matter. Generally, the higher monomer concentration can accelerate the graft copolymerization reaction kinetic because lignocelluloses can contact with monomers readily in this case. When the monomer dosage reaches a certain level, the homopolymerization of monomer tends to take place more rapidly. This certain level is usually referred as optimal monomer dosage since the formation of monomer hampers the graft copolymerization. If the optimal monomer dosage is exceeded, the yield and grafting ratio start to decrease and homopolymerization becomes dominant. Additionally, the molecular weight of copolymer increases due to the chain of homopolymer grafted on the lignocellulose is extended (Fang et al., 2009).

2.8.6 Copolymerization of different lignin

Soda lignin (SL) is derived from soda pulping process. Unlike kraft lignin, soda lignin is sulphur free and its chemical content and structure are the same as natural lignin (Vishtal & Kraslawski, 2011). However, soda lignin only holds soluble under alkaline aqueous solution, therefore, its end-use applications is restricted. To expand the application of soda lignin, the copolymerization of SL-Arylamide was investigated in a paper. Acrylamide (AM) is a crystalline and relatively stable monomer, which is soluble in water and many organic solvents. Acrylamide is a polyfunctional molecule containing a vinylic carbon–carbon double bond and an amide group (Ahmada et al., 2007). During the copolymerization, the effect of the operating temperature, reaction time, imitator dosage and acrylamide to lignin molar ratio were taken into account. The optimal conditions for the copolymerization of SL and acrylamide were AM/SL molar ratio of 7.5, K2S2O8 at 3.0 wt.% based on lignin, 4 h reaction time, and 90 °C. Under the optimal conditions, the grafting copolymerization reaction had a yield and a grafting ratio of 80 % and 398 %, respectively (Wang et al., 2016).

Enzymatic hydrolyzed lignin (EH-lignin) is novel renewable natural polymer, which is the by-product of fuel ethanol industry. Comparing to traditional lignosulfonate or alkali lignin, EH-lignin exhibits some features: lower sugar content, less impurities and narrow molecular weight distribution. According to Fang et al. (2009), in order to obtain the highest yield and grafting ratio, the optimum conditions for the graft copolymerization of EH-lignin with acrylamide were as

follows: initiator $K_2S_2O_8$-$Na_2S_2O_3$ with a quantity 3 wt% of EH-lignin, mass ratio of AM to EH-lignin was 2~3, reaction time 4h and temperature at 50 ℃.

Kraft lignin (KL) is a by-product from traditionally dissolution of lignin technical process, kraft (soda) pulping. It is extracted from the black liquor of kraft pulping process via acidification. Since kraft lignin is only soluble in alkaline aqueous solution, it would limit its application in industry (Gellerstedt, 2015). Kraft lignin based copolymer was studied to resolve the difficulty in solubility in a paper. Kraft lignin (KL) was copolymerized with acrylic acid (AA) in an aqueous solution to produce a water-soluble lignin-based copolymer. The grafting copolymerization reaction was conducted in presence of $K_2S_2O_8$–$Na_2S_2O_3$ as the initiator under alkaline aqueous conditions. The optimal conditions were AA/KL ratio of 8.0 mol mol−1, 1.5 wt% initiator, 70 °C and 3 h. The optimal conditions caused the charge density and molecular weight of lignin copolymer reach 1.86 meq/g and 46421 g/mol, respectively. The solubility of lignin after modification improved from 1.80 g/L to 100 g/L at neutral pH. The analysis also confirmed that the kraft lignin-based copolymer was soluble in water at pH of 4 (Kong et al., 2015).

Additionally, the impact of lignin species on the grafting mechanism of lignosulfonate from eucalyptus (hardwood) and pine (softwood) with acrylic acid was elucidated. Phenolic group was portional to product yield and monomer conversion in the copolymerization. Although pine had higher initial content of phenolic group than hardwood, the copolymerization of softwood lignin with acrylic acid had lower prodct yield and monomer conversion compared to the copolymerizasiton of hardwood lignin with acrylic acid. This is due to the quinonoid structure which can be formed by the self-conjugated of phenoxy radical in guaiacyl unit. Therefore, it was recommened that hardwood lignin with higher phenolic group was more efficient in the copolymerzation with acrylic acid (Ye et al., 2014).

2.8.7 Mechanism of hemicellulose copolymerized with vinyl monomer

A variety of chemical modifications of hemicellulose has been investigated, including esterification, etherification, methacrylation, and graft copolymerization. Among these modification methods of polysaccharides, graft polymerization is the most commonly used and an effective way to modify hemicellulose and to alter performance for specific end-uses (Wan et al., 2007; Li et al., 2012; Dong et al., 2012). The mechanism of hemicellulose copolymerized with vinyl monomer is illstrated from reaction (f) to reaction (i). Its mechanism is similar to the

mechanism of lignin copolymerized with vinyl monomer. The sulfate radicals extract hydrogen from the hydroxyl groups of hemicellulose to form more active groups (macro-radicals). Then, the active centers on hemicellulose attract the vinyl monomer (AA or AM) to propagate a polymeric chain. The grafted monomer works as free radical donors to offer free radical to neighboring molecules in order to prolong the grafted chain (Ren et al., 2014). The mechanism of hemicellulose copolymerized with vinyl monomer differs from the machanism of lignin copolymerized with vinyl monomer in that there are no resonance forms of radicals.

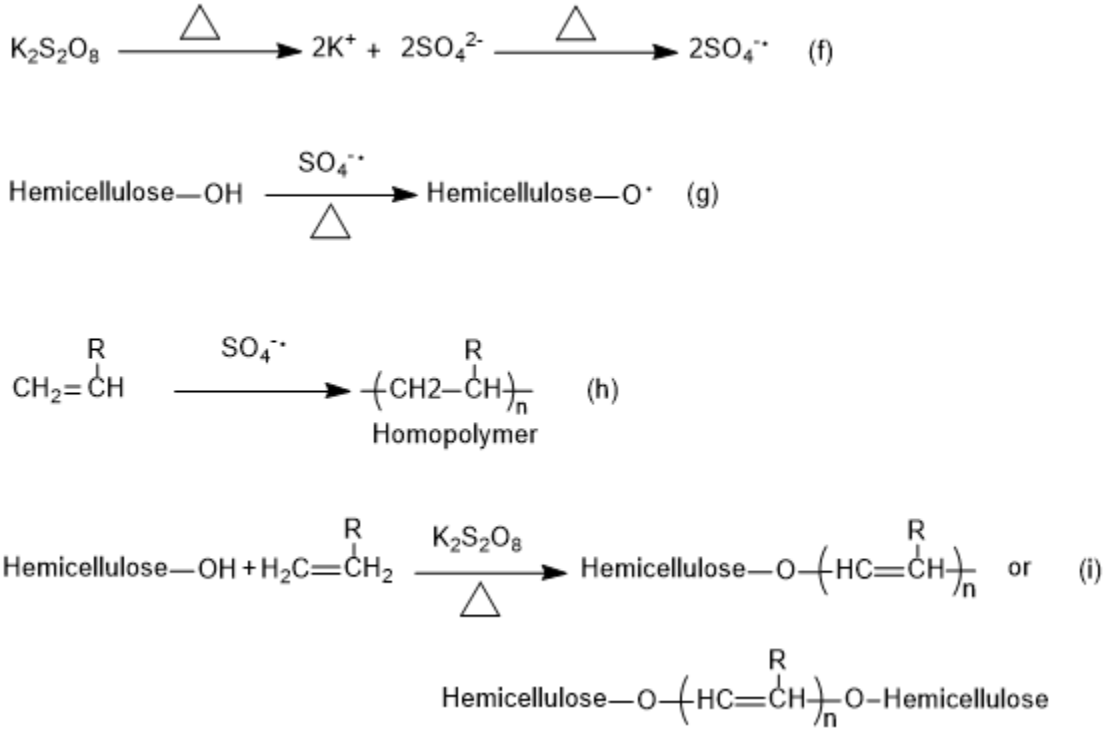

Figure 2.4. Reaction scheme of hemicellulose copolymerized with vinyl monomer

2.8.8 Copolymerization of hemicellulose with different monomers

In one paper, the main constituent of hemicellulose, L-arabino-4-O-methyl-D-glucurono-D-Xylan (wis-AGX), was extracted from corncobs by the ultrasound-assisted diluted alkali extraction method. However, poor water solubility of the hemicellulose was a barrier that can limit its applications. Hemicelluloses-g-polyacrylamide (PAM) was synthesized in diluted alkaline aqueous solution with the initiator of potassium persulfate $K_2S_2O_8$ and sodium thiosulfate $Na_2S_2O_3$.

The optimal condition was achieved when grafting percent and grafting efficiency reached its maximum values. The optimal condition occurred at initiator dosage of 3.89×10^{-3} mol/L and monomer concentrations of 1.41 mol/L, at 30 °C for 4h. The hemicellulose-based copolymer exhibited satisfying water solubility, which can expand the applications of hemicellulose-based copolymer as gels, films, adsorbents, coatings, or drug delivery systems (Li & Zhou, 2017).

Recently, there has been an increased attention in hemicellulose based hydrogels. Hydrogels are three-dimensional cross-linked networks of hydrophilic polymer, which are committed to absorb a large amount of water or biological fluids. In one study, hemicellulose was used to synthesize hydrogel separated from prehydrolysis liquor (PHL) of the kraft-based dissolving pulp production process. The hemicellulose was composed of 45.89% xylose, 41.10% glucose, 7.21% galactose, 5.29% mannose, 0.29% arabinose, and 0.23% rhamnose. In the polymerization, cross-linker could facilize the formation of the nodes of network and the cross-linker density, which enhances the performance of super-absorbent in absorbing and retaining fluid. Acrylic acid (AA) is an important monomer that is widely used for the preparation of functional hydrogels. By incorporating AA into the network, hydrogels can find important applications in water adsorption and selective removal of heavy metal ions or dyes. The mass ratio of monomers for the optimal conditions was m(AA): m(AM): m(hemicellulose)=15 : 3.5 : 1. The neutralization degree of AA was 75%, and weight ratio (to monomers) of the cross-linker and the initiator was 0.03% and 1.0%, respectively. Under the optimal conditions, the product obtained the best liquid absorbency of 1128 g/g in distilled water and 132 g/g in 0.9 wt % NaCl solution (Zhang et al., 2015).

2.9 Polyacrylamide (PAM)

Acrylamide is a crystalline and relatively stable monomer which is soluble in water and many organic solvents. Acrylamide is a polyfunctional molecule containing a vinylic carbon–carbon double bond and an amide group. Flocculation of suspended particles uasually take place on charged amide or carboxylic group (Ahmada et al., 2007). Figure 2.5 shows the chemical structure of PAM.

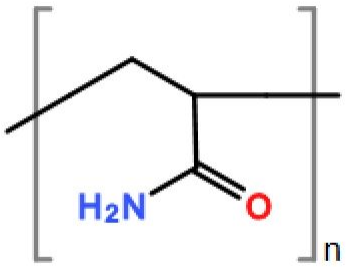

Figure 2.5. Chemical structure of PAM

Polyacrylamide (PAM) is the most commonly used polymeric flocculant for pulp and paper industry. The advantage of polymeric flocculants is their capability of producing large, dense, compact and stronger flocs with good settling characteristic compared to those obtained by coagulation. It can also contribute to the reduction of the sludge volume. Additionally, the flocculation efficiency is not affected extensively by pH (Wong et al., 2006).

Cationic polyacrylamide (C-PAM) and anionic polyacrylamide (A-PAM) are used more often than nonionic one in papermaking. Charged polymeric flocculant that has electrolyte group along the backbone is also known as polyelectrolyte. The primary driving force for charged polyacrylamide is the electrostatic attraction between the polyelectrolytes and oppositely charged particles. The majority of the colloids in the pulp and paper waste water are negatively charged, therefore synthetic cationic flocculant is favorable for the flocculation process due to charge neutralization (Wang, 2009).

2.10 Coagulation/flocculation treatment

Coagulation/flocculation is one of the most commonly applied techniques to achieve efficient solid-liquid separation in water treatment (Wei et al., 2018; Huang et al., 2015). The fundalmental concept in coagulation process is to destablize the paricle in wastewater by adding coagulants with opposite charges. Without electrical repulsion force, colloidals tend to aggregate and form large flocs eventually. This process is named as charge neutralization. To optimize the charge neutralization performance, the dosage of flocculant should reduce the zeta potential close to zero (isoelectric point). However, if flocculant is excess, a charge reversal can occur. The particles in

colloidal system gain charges and disperse again. The flocs formed from charge neutralization are fragile, packed loosely and settle down slowly.

In order to enhance the aggolomeration and settelling efficiency, the polymer with high molecular weight served in the wastewater as coagulant aid, which is also know as flocculant. The bridging effect is owing to long polymeric chain, flocculant can attract the paricles in waster water by forming a brige between them (Li et al., 2012). Bridging flocculation can sometimes be prevented or destroyed by adding surfactant in sufficient quantity to adsorb and cover all of the interfaces in a system, thus displacing the bridging molecules from at least one of each pair of interfaces (Schramm, 2014).

Electrostatic patch occures when a portion of the charged surface of the suspended particle is neutralized by adsorbing oppositively charged ions. The coagulation of the particles is induced by local contact between neutralized ‘‘patches’’ of surface. During the electrostatic patch, the overall surface charges of suspended particles are far from neutralized (Cheng et al., 2010; Zhou & Franks, 2006). It is critical that the polyelectrolytes should be short chain (low molecular weight), otherwise polyelectrolyte may cover all the surface area of the particles. In this case, the particles have no uncoated region that allows electrostatic patch to occur. Flocs produced in this way are not as strong as those formed by bridging, but stronger than flocs formed in the presence of metal salts or by simple charge neutralization (Lee et al., 2014). Besides charge density and molecular weight, chemical structure, functional group, and pH can potentially impact coagulant/flocculant performance (Hasan & Fatehi, 2019; Chen et al., 2010).

2.11 Analytical methods

2.11.1 Particle charge detector (PCD)

Particle charge detector is used to determine charge density of polymers. The hydrolysis liquor or the copolymer is titrated with a standard polymer solution of opposite charge. Since the hydrolysis liquor and copolymers are either weak anionic or anionic, the typical standard polymer solution for anionic polymer is polydiallyldimethylammonium chloride (PDADMAC).

2.11.2 Nuclear magnetic resonance spectroscopy (NMR)

Nuclear magnetic resonance spectroscopy, commonly referred to as NMR, is a powerful analytical tool to determine concentration of the components in hydrolysis liquor and the structure of

copolymers with relaxation delay time of 1.0 s. The concentration of furfural and acetic acid can be determined by ^{1}H-NMR. The preparation of the sample must be precise and careful. Since acetic acid and furfural are volatile and evaporate under high temperature, the samples should be dried at low temperature (60 ^{o}C). Then, 3-(trimethylsilyl) propionic-2,2,3,3-d4 acid sodium salt (TSP) in deuterium oxide (D_2O) is prepared with the concentration of 5 mg/ml. Approximately, 0.1g of dry sample with 1ml of D_2O and TSP solution are well mixed at 60 RPM in the NMR vials (Khazraie et al., 2017). The peak corresponding to acetic acid presented on ^{1}H-NMR spectrum is 2.08 ppm while that of furfural ^{1}H-NMR spectrum includes 6.78, 7.56, 7.85, and 9.49 ppm (Saeed et al., 2011). Protons in the methenyl attached to amide group in acrylamide were presented by the peaks at 1.665, 1.782, 2.220 and 2.349 ppm.

To investigate the structure of the copolymers, it is crucial to find the monomer peaks in the spectrum. The protons in the methenyl connected to amide group in acrylamide which can be proved by the peaks at 1.665 and 1.782 ppm, and 2.220 and 2.349 ppm (Dong et al., 2012). The peaks attributed to polyacrylic acid chain appears at 1.6 ppm, 2.2 ppm and 2.6 ppm (Kong et al., 2015). Comparing the ^{1}H-NMR spectrum of copolymer with that of original hydrolysis liquor, if the peaks of acrylamide or acrylic acid don't exist in the spectra of the original hydrolysis liquor, it well confirms that acrylamide or acrylic acid is successfully grafted onto the components in the hydrolysis liquor.

2.11.3 Molecular weight (GPC)

The most common technique to obtain the molecular weight of the solid content in hydrolysis liquor is Gel Permeation Chromatograph (GPC). This apparatus can specify the molecular weight of the solid content in hydrolysis liquor in terms of number average molecular weight (M_n), weight average molecular weight (M_w) and polydispersity index (D). Polydispersity index is the ratio of M_w to M_n indicating the molecular weight distribution of the polymers (Tolbert et al., 2014).

2.11.4 Sugar analysis

The concentration of the polysaccharide and monosaccharide were measured by ion chromatograph (IC). The hydrolysis liquor runs through a pressurized chromatographic column containing a stationary column constituents (adsorbent) where ions are adsorbed. When an ion extraction liquid, known as eluent, passes through the column, the components of the analyte will move down the column as well at different speeds. At the end of the column, a detector can convert

the retention time of different components in the hydrolysis liquor to a signal which is shown as a peak on the chromatogram. The concentration of sugars can be determined in parts-per-billion (ppb) range. IC is only capable of measuring the monosaccharide in the hydrolysis liquor. In order to calculate the oligomeric of hydrolysis liquor, an acid hydrolysis must be applied to convert oligosugars to monosugars. The hydrolysis liquor is pretreated with 4% sulfuric acid at 121 ^{0}C in a sealed autoclave or a reactor (Liu et al., 2014). After acid hydrolysis, the monosugars in hydrolysis liquor measured by IC is referred as total sugar. On the other hand, the monosugar concentration of hydrolysis liquor can be directly measured be IC without any pretreatment. The concentration of the polysaccharide can be determined by the difference between total sugar and monosaccharide (Khazraie et al., 2017).

2.11.5 Quartz crystal microbalance (QCM)

Quartz crystal microbalance with dissipation monitoring (QCM-D) has been considered as one of powerful equipment specializing in the study of adsorption/desorption process of polymers at solid/liquid interface (Andersson et al., 2005). The QCM sensor is made of a quartz crystal and sometimes coated with other material for the purpose of study the adsorption on a specific material. It is sandwiched between two electrodes which provide AC electric field causing shear oscillatory movement of the sensor. Once the external electric field is turned off, the resonance frequency (f) of the sensor and the energy dissipation (D) were plotted as a function of time. Based on the Sauerbrey Equation the mass of adsorption layer on the sensor or the is relevant to the frequency change (Salas et al., 2013). Alternatively, frequency change also can be related to the thickness of the adsorbed layer in order to investigate the formation of the adsorption layer.

$$\Delta m = -C\frac{\Delta f}{n} \qquad [2.6]$$

where Δm is the change of mass Δf is the change in frequency in (Hz), n is the overtone number, C is a mass sensitive constant, 17.7 ng cm2 s−1 at f= 5 MHz.

The energy dissipation factor provides the information on viscoelastic properties of bound mass on the sensor as well as variations in the density and viscosity of the solution. The higher dissipation value indicates more viscous adsorption layer formed on the sensor. D is the fraction of energy dissipated to the energy stored by the systems at the interface as interpreted by following equation:

$$D = \frac{E_{disspated}}{2\pi E_{stored}} \quad [2.7]$$

2.11.6 Dynamic light scattering (DLS)

Dynamic light scattering is an effective approach to determine the size distribution and Brownian motion. The velocity of Brownian motion is also known as translational diffusion coefficient. In this technique, a laser light is passing through a dispersion system and fluctuations in scattered light intensity due to Brownian motion offer diffusion using autocorrelation function. (Lusvarghi et al., 2018). The diffusion coefficient of nanoparticles inserts into the Stokes-Einstein equation which can provide the hydrodynamic radius (R_h) (Rahdar et al., 2019).

$$R_h = \frac{k_B T}{6\eta\pi D} \quad [2.8]$$

where k_B is Boltzmann's constant, T is the temperature in K, and η is the viscosity of continuous phase in mPa.s, D is the diffusion coefficient.

Hydrodynamic radius is the radius of the hypothetical hard sphere that diffuses at the same speed as the particles examined by DLS (Hawe et al., 2011). However, the geometry of the paricles that disperse in the colloidal system are not always spherical. Hence, the hyhrodynamic size provided by DLS is an indicative size rather than accurate size in reality.

2.11.7 Zeta potential

Figure 2.6 shows the electrical double layer of a negative charged particle in an aquous sytem. The formation of the electrical double layer on a particle is due the counter ions approaching the surface of the particle. Stern layer in which a particle is tightly bounded by oppositely charged ions is the first layer around the paritcle. Outer region is known as diffuse layer where ions are less firmly associated. The potential at boundary of stern layer and diffuse later reffers to zeta potential (Kaszuba et al., 2010). The potential decays exponentially as moving away from the particle surface. In colloidal syetem, zeta potential is an indicative term to evaluate the stability of the systerm. The higher the value of absolute zeta potential results stronger the repulsion and more stable the system. Zeta potential can be influenced by a number of parameters, including temperature, pH, ionic strength. Small changes in any of these parameters can potentially have dramatic effects on the zeta potential values (Smith et al., 2017). Zeta potential has been extensively used to assese the stability of the colloidal system in many industries, for instance,

waste water treatment, pharmaceuticals, pulp and paper and biomedical (Li et al., 2016; Valizadeh et al., 2011; Ge et al., 2011).

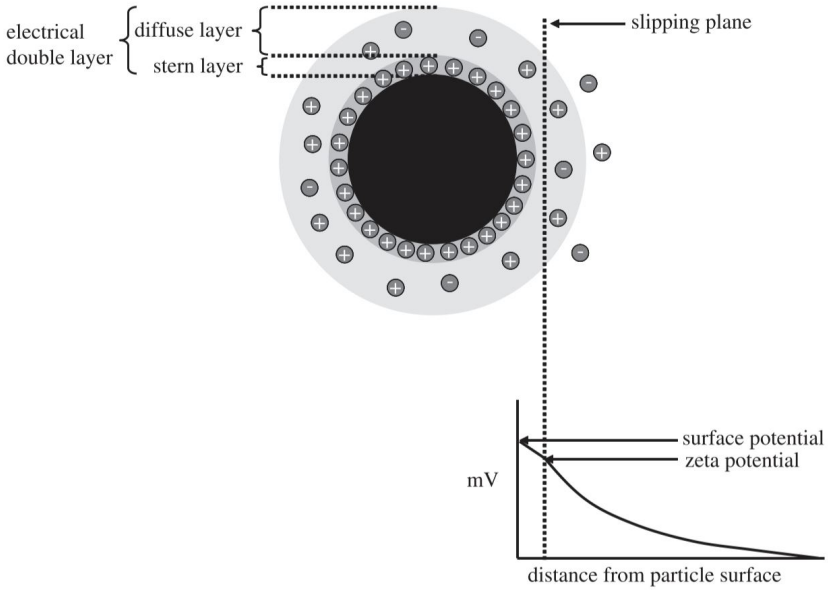

Figure 2.6. Schematic of the electrical double layer that surrounds a particle in an aqueous medium and the position of the slipping plane. The zeta potential is the electrical potential at the slipping plane (Kaszuba et al., 2010)

2.11.8 Contact angle

Tensiometer can be used to determine the wettability of polymers or solid surface by measuring the angle formed by the liquid of interest on a solid surface. Contact angle measurement usually applies sessile drop technique in which a liquid drop is placed on a surface and the contact angle is measured directly at the three phase (liquid/ solid/vapor) contact line of the formed drop (Alghunaim et al., 2016). If the cohesive forces between the liquid molecules are stronger than the adhesive forces between the solid and liquid molecules, then the liquid balls up to minimize contact with the surface. Contrarily, if the solid/liquid adhesion is dominant than the cohesion within the liquid molecules, then liquid spreads on the surface (Erbil, 2014). Generally, if the water contact angle is smaller than 90°, the solid surface is considered hydrophilic; whereas, the water contact angle is larger than 90°, the solid surface is considered hydrophobic.

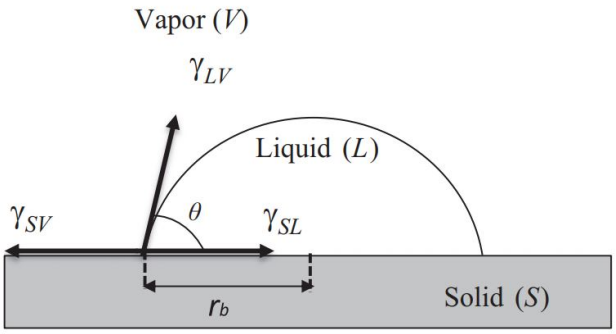

Figure 2.7. Profile of a drop of liquid on a solid surface. Contact angle, contact radius and three interfacial tensions, γ, between solid, liquid, vapor phases (Erbil, 2014).

2.11.9 Elemental analyzer

CHNS analysis is an important step in characterization of synthesized organic compounds as well as for quality control of the obtained organic compounds. Elemental analyzer can provide qualitative information about basic elements such as C, H, N, S, comprising the organic compounds (Eksperiandova et al., 2011). The combustion tube in elemental analyzer oxidizes samples in the presence of oxygen (O2) gas using tungsten oxide (WO3) as catalyst at high temperature. Carbon is converted to carbon dioxide; hydrogen to water; nitrogen to nitrogen gas, and sulphur to sulphur dioxide. Helium (He) gas serves as flushing and carrier purpose gas (Dhaliwal et al., 2014). The thermal conductivity detector (TCD) determines the desired measuring components cooperating with specific adsorption columns. The software converts electrical signal to percentages of elements in the sample.

2.12 References

Ahmada, A., Wong, S., Teng, T., & Zuhairi, A. (2007). Improvement of alum and PACl coagulation by polyacrylamides (PAMs) for the treatment of pulp and paper mill wastewater. *Chemical Engineering Journal*, 510-517.

Ahsan, L., Jahan, M. S., & Ni, Y. (2014). Recovering/concentrating of hemicellulosic sugars and acetic acid by nanofiltration and reverse osmosis from prehydrolysis liquor of kraft. *Bioresource Technology, 155*, 111-115.

Alfaro, A., Rivera, A., Pérez, A., Yáñez, R., García, J., & López, F. (2009). Integral valorization of two legumes by autohydrolysis and organosolv delignification. *Bioresource Technology, 100*, 440-445.

Alghunaim, A., Kirdponpattara, S., & Newby, B.-m. Z. (2016). Techniques for determining contact angle and wettability of powders. *Powder Technology, 287*, 201–215.

Alvarez, C., Reyes-Sosa, F. M., & Diez, B. (2016). Enzymatic hydrolysis of biomass from wood. *Microbial Biotechnology, 6*(2), 149-156.

Andersson, M., Andersson, J., Sellborn, A., Berglin, M., Nilsson, B., & Elwing, H. (2005). Quartz crystal microbalance-with dissipation monitoring (QCM-D) for real time measurements of blood coagulation density and immune complement activation on artificial surfaces. *Biosensors and Bioelectronics, 21*, 79-86.

Ares-Peón, I. A., Vila, C., Garrote, G., & Parajó, J. C. (2011). Enzymatic hydrolysis of autohydrolyzed barley husks. *J. Chem. Technol. Biotechnol., 86*, 251-260.

Barbanera, M., Lascaro, E., Foschini, D., Cotana, F., & Buratti, C. (2017). Optimization of bioethanol production from steam exploded hornbeam wood (Ostrya carpinifolia) by enzymatic hydrolysis. *Renewable Energy*.

Bhattacharyaa, A., & Misra, B. (2004). Grafting: a versatile means to modify polymers Techniques, factors and applications. *Progress in Polymer Science, 29*, 767–814.

Carvalheiro, F., Duarte, L. C., & Gírio, F. M. (2008). Hemicellulose biorefineries: a review on biomass pretreatments. *Journal of Scientific & Industrial Research, 67*, 849-864.

Chen, T., Gao, B., & Yue, Q. (2010). Effect of dosing method and pH on color removal performance and floc aggregation of polyferric chloride–polyamine dual-coagulant in synthetic dyeing wastewater treatment. *Colloids and Surfaces A: Physicochem. Eng. Aspects , 355*, 121-129.

Cheng, Y.-L., Wong, R.-J., Lin, J. C.-T., Huang, C., Lee, D.-J., & Mujumdar, A. S. (2010). Water coagulation using electrostatic patch coagulation (EPC) mechanism. *Drying Technology, 28*, 850–857.

Cheung, W., Szeto, Y., & McKay, G. (2007). Intraparticle diffusion processes during acid dye adsorption onto chitosan. *Bioresource Technology, 98*, 2897-2904.

Cotana, F., Buratti, C., Barbanera, M., & Lascaro, E. (2015). Optimization of the steam explosion and enzymatic hydrolysis for sugars production from oak woods. *Bioresource Technology, 198*, 470–477.

Dhaliwal, G. S., Gupta, N., Kukal, S. S., & Meetpal-Singh. (2014). Standardization of Automated Vario EL III CHNS Analyzer for Total Carbon and Nitrogen Determination in Plants. *Communications in Soil Science and Plant Analysis, 45*, 1316–1324.

Dohertya, W. O., Mousaviouna, P., & Fellows, C. M. (2011). Value-adding to cellulosic ethanol: Lignin polymers. *Industrial Crops and Products, 33*, 259-276.

Dommelen, R. v., Fanzio, P., & Sasso, L. (2018). Surface self-assembly ofcolloidal crystals for micro- and nano-patterning. *Advances in Colloid and Interface Science, 251*, 97-114.

Dong, L., Hu, H., Yang, S., & Cheng, F. (2012). Grafted Copolymerization Modification of Hemicellulose Directly in the Alkaline Peroxide Mechanical Pulping (APMP) Effluent and Its Surface Sizing Effects on Corrugated Paper. *Bioresource Technology, 118*, 204-209.

Eksperiandova, L., Fedorov, O., & Stepanenko, N. (2011). Estimation of metrological characteristics of the element analyzer EuroVector EA-3000 and its potential in the single-reactor CHNS mode. *Microchemical Journal, 99*, 235-238.

Erbil, H. Y. (2014). The debate on the dependence of apparent contact angles on drop contact area or three-phase contact line: A review. *Surface Science Reports, 69*, 325–365.

Fang, R., Cheng, X., Fu, J., & Zheng, Z. (2009). Research on the Graft Copolymerization of EH-lignin with acrylamide. *Natural Science, 1*, 17-22.

Galia, A., Schiavo, B., Antonetti, C., Galletti, A. M., Interrante, L., Lessi, M., & Valenti, O. S. (2015). Autohydrolysis pretreatment of Arundo donax: a comparison between microwave-assisted batch and fast heating rate flow-through reaction systems. *Biotechnol Biofuels, 8*, 218.

Garrote, G., & Parajo, J. C. (2002). Non-isothermal autohydrolysis of Eucalyptus wood. *Wood Science and Technology, 36*, 111-123.

Garrote, G., Cruz, J., Dominguez, H., & Parajo, J. (2003). Valorisation of waste fractions fromautohydrolysis of selected lignocellulosicmaterials. *Journal of Chemical Technology and Biotechnology, 78*, 392–398.

Garrote, G., Dominguez, H., & Parajo, J. C. (1999). Mild autohydrolysis: an environmentally friendly technology for xylooligosaccharide. *Journal of Chemical Technology and Biotechnology, 74*, 1101-1109.

Garrote, G., Dominguez, H., & Parajo, J. C. (2001). Generation of xylose solutions from Eucalyptus globulus wood by autohydrolysis±posthydrolysis processes: posthydrolysis kinetics. *Bioresource Technology, 79*, 155-164.

Ge, X., Leng, Y., Ren, F., & Lu, X. (2011). Integrity and zeta potential of fluoridated hydroxyapatite nanothick coatings for biomedical applications. *Journal of the Mechanical Behavior of Biomedical Materials, 4*(7), 1046-1056.

Gellerstedt, G. (2015). Softwood kraft lignin: Raw material for the future. *Industrial Crops and Products, 77*, 845-854.

Gilardi, G., & Cass, A. E. (1993). Associative and Colloidal Behavior of Lignin and Implications for Its Biodegradation in vitro. *Langmuir 1993*, 1721-1726.

Grigoray, O., Järnström, J., Heikkilä, E., Fardim, P., & Heinze, T. (2014). Modification of pine pulp during oxygen delignification by xylan self-assembly. *Carbohydrate Polymers, 112*, 308–315.

Gütsch, J. S., Nousiainen, T., & Sixta, H. (2012). Comparative evaluation of autohydrolysis and acid-catalyzed hydrolysis of Eucalyptus globulus wood. *Bioresource Technology, 109*, 77-85.

Gütsch, J. S., Nousiainen, T., & Sixta, H. (2012). Comparative evaluation of autohydrolysis and acid-catalyzed hydrolysis of Eucalyptus globulus wood. */Bioresource Technology, 109*, 77-85.

Hasan, A., & Fatehi, P. (2019). Cationic kraft lignin-acrylamide copolymer as a flocculant for clay suspensions: (2) Charge density effect. *Separation and Purification Technology, 210*, 963–972.

Hawe, A., Hulse, W. L., Jiskoot, W., & Forbes, R. T. (2011). Taylor Dispersion Analysis Compared to Dynamic Light Scattering for the Size Analysis of Therapeutic Peptides and Proteins and Their Aggregates. *Pharmaceutical Research, 28*, 2302-2310.

Hendriks, A., & Zeeman, G. (2009). Pretreatments to enhance the digestibility of lignocellulosic biomass. *Bioresource Technology, 100*, 10-18.

Hou, Q., Wang, Y., Liu, W., Liu, L., Xu, N., & Li, Y. (2014). An application study of autohydrolysis pretreatment prior to poplar chemi-thermomechanical pulping. *Bioresource Technology, 169*, 155-161.

Huang, J., & Wu, X. (1999). Effects of pH, Salt, Surfactant and Composition on PhaseTransition of Poly(NIPAm/MAA) Nanoparticles. *Journal of Polymer Science: Part A: Polymer Chemistry, 37*, 2667–2676.

Huang, X., Gao, B., Rong, H., Yue, Q., Zhang, Y., & Teng, P. (2015). Effect of using polydimethyldiallylammonium chloride as coagulation aid on polytitanium salt coagulation performance, floc properties and sludge reuse. *Separation and Purification Technology, 143*, 64-71.

Hundt, M., Engel, N., Schnitzlein, K., & Schnitzlein, M. G. (2014). Combining the effects of pulping severity and alkali concentration to optimize the lignocellulose-based AlkaPolP biorefinery concept. *Bioresource Technology , 166*, 411-419.

Ibrahim, N. A., Abu-Ilaiwi, F., Rahman, M. Z., MansorB.Ahmad, Dahlan, K. Z., & Yunus, W. M. (2005). Graft Copolymerization of Acrylamide onto Oil Palm Empty Fruit Bunch (OPEFB) Fiber. *Journal of Polymer Research, 12*, 173-179.

Ioelovich, M., & Morag, E. (2012). Study of enzymatic hydrolysis of pretreated biomass at increased solids loading. *BioResources, 7*(4), 4672-4682.

Iranmahboob, J., Nadima, F., & Monemi, S. (2002). Optimizing acid-hydrolysis: a critical step for production of ethanol from mixed wood chips. *Biomass and Bioenergy, 22*, 401-404.

Kanchanalai, P., Temani, G., Kawajiri, Y., & Realff, M. J. (2016). Reaction kinetics of concentrated-acid hydrolysis for cellulose and hemicellulose and effect of crystallinity. *BioResources, 11*(1), 1672-1689.

Kaszuba, M., Corbett, J. C., Watson, F. M., & Jones, A. (2010). High-concentration zeta potential measurements using light-scattering techniques. *Phil. Trans. R. Soc. A, 368*, 4439–4451.

Khazraie, T., Zhang, Y., Tarasov, D., Gao, W., Price, J., DeMartini, N., . . . Fatehi, P. (2017 10:47). A process for producing lignin and volatile compounds from hydrolysis liquor. *Biotechnol Biofuels*.

Kong, F., Wang, S., Price, J. T., Kondurib, M. K., & Fatehi, P. (2015). Water soluble kraft lignin–acrylic acid copolymer: synthesis and characterization. *Green Chem, 17*, 4355–4366.

Kumar, P., Barrett, D. M., Delwiche, M. J., & Stroeve, P. (2009). Methods for pretreatment of lignocellulosic biomass for efficient hydrolysis and biofuel production. *Ind. Eng. Chem. Res, 48*, 3713–3729.

Kumar, S., Dheeran, P., Singh, S. P., Mishra, I. M., & Adhikari, D. K. (2015). Kinetic studies of two-stage sulphuric acid hydrolysis of sugarcane bagasse. *Renewable Energy 83 (2015) 850e858, 83*, 850-858.

Lee, C. S., Robinson, J., & Chong, M. F. (2014). A review on application of flocculants in wastewater treatment. *Process Safety and Environmental Protection, 92*, 489–508.

Lenihan, P., Orozco, A., O'Neill, E., Ahmad, M., Rooney, D., & Walker, G. (2010). Dilute acid hydrolysis of lignocellulosic biomass. *Chemical Engineering Journal, 156*, 395–403.

Leschinsky, M., Sixta, H., & Patt, R. (2009). Detailed mass balances of the autohydrolysis of eucalyptus globulus at 170 °C. *BioResources 4(2), 687-703.*

Leschinsky, M., Zuckerstatter, G., Weber, H. K., & Sixta, R. P. (2008). Effect of autohydrolysis of Eucalyptus globulus wood on lignin structure. Part 1: Comparison of different lignin fractions formed during water prehydrolysis. *Holzforschung, 62*, 645-652.

Li, P., Liu, Y., Lu, J., Yang, R., & Wang, H. L. (2016). Structural Characterization and Effect on Enzymatic Hydrolysis of Milled Wood Lignin Isolated from Reed Straw and Corn Stover Pretreated with Liquid Hot Water. *BioResources, 11*(4), 8777-8790.

Li, Q., Ma, Z., Yue, Q., Gao, B., Li, W., & Xu, X. (2012). Synthesis, characterization and swelling behavior of superabsorbent wheat straw graft copolymers. *Bioresource Technology, 118*, 204-209.

Li, R., Gao, B., Sun, J., Qinyan Yue, Y. W., & Xu, X. (2016). Synthesis, characterization of a novel lignin-based polymer and its behavior as a coagulant aid in coagulation/ultrafiltration hybrid process. *International Biodeterioration & Biodegradation, 13*, 334-341.

Li, W., & Zhou, X. (2017). Modification of the water-insoluble hemicelluloses via free radical copolymerization in diluted alkali aqueous medium. *Journal of Wood Chemistry and Technology, 37*, 191-200.

Lim, W.-S., & Lee, J.-W. (2013). Effects of pretreatment factors on fermentable sugar production and enzymatic hydrolysis of mixed hardwood. *Bioresource Technology, 130*, 97-101.

Linden, E. d., & Venema, P. (2007). Self-assembly and aggregation of proteins. *Current Opinion in Colloid & Interface Science, 12*(4-5), 158-165.

Linder, Å., Bergman, R., Bodin, A., & Gatenholm, P. (2003). Mechanism of assembly of xylan onto cellulose surfaces. *Langmuir 2003, 19*, 5072-5077.

Liu, C., & Wyman, C. E. (2003). The effect of flow rate of compressed hot water on xylan, lignin, and total mass removal from corn stover. *Ind. Eng. Chem. Res. 42, 5409-5416*.

Liu, C., & Wyman, C. E. (2004). Impact of fluid velocity on hot water only pretreatment of corn stover in a flowthrough reactor. *Applied Biochemistry and Biotechnology, 115*(1-3), 977-987.

Liu, C., & Wyman, C. E. (2005). Partial flow of compressed-hot water through corn stover to enhance hemicellulose sugar recovery and enzymatic digestibility of cellulose. *Bioresource Technology, 96*, 1978-1985.

Liu, H., Hu, H., Baktash, M. M., Jahan, M. S., Ahsan, L., & Ni, Y. (2014). Kinetics of furfural production from pre-hydrolysis liquor (PHL) of a kraft-based hardwood dissolving. *Biomass and Bioenergy, 66*, 320-327.

Liu, H., Hu, H., Jahan, S., & Ni, Y. (2015). Improvement of furfural production from concentrated prehydrolysis liquor (PHL) of a kraft-based hardwood dissolving pulp production process. *Journal ofWood Chemistry and Technology, 35*, 260-269.

Liu, H., Hua, H., Baktash, M. M., Jahan, M. S., Ahsan, L., & Ni, Y. (2014). Kinetics of furfural production from pre-hydrolysis liquor (PHL) of a kraft-based hardwood dissolving. *Biomass and Bioenergy, 66*, 320-327.

Liu, Z., Pedram Fatehi, M. S., & Ni, Y. (2011). Separation of lignocellulosic materials by combined processes of pre-hydrolysis and ethanol extraction. *Bioresource Technology, 102*, 1264-1269.

Lusvarghi, S., Ghirlando, R., R. Davison, J., & A. Bewley, C. (2018). Chemical and biophysical approaches for complete characterization of lectin–carbohydrate interactions. *Methods in Enzymology, 598*, 3-35.

Mahdavi, M., Ahmad, M. B., Haron, M. J., & Fatehi, M. Z. (2011). Optimized conditions for graft copolymerization of poly(acrylamide) onto rubberwood fibre. *BioResources, 6*(4), 5110-5120.

Mamman, A. S., Lee, J.-M., Kim, Y.-C., Hwang, I. T., Park, N.-J., Hwang, Y. K., . . . Hwang, J.-S. (2008). Furfural: hemicellulose/xylose-derived biochemical. *Biofuels, Bioproducts and Biorefining, 2*, 438-454.

Matsagar, B. M., & Dhepe, P. L. (2015). Brönsted acidic ionic liquid-catalyzed conversion of hemicellulose into sugars. *Catalysis Science & Technology, 5*, 531-539.

Morais, A. P., Sansígolo, C. A., & Neto, M. d. (2016). Effects of autohydrolysis of Eucalyptus urograndis and Eucalyptus grandis on influence of chemical components and crystallinity index. *Bioresource Technology, 214*, 623–628.

Mosier, N. S., Hendrickson, R., Brewer, M., Ho, N., Sedlak, M., Dreshel, R., . . . Ladisch, M. R. (2005). Industrial scale-up of pH-controlled liquid hot water pretreatment of corn fiber for fuel ethanol production. *Applied Biochemistry and Biotechnology, 125*(2), 77-97.

Mosier, N., Wyman, C., Dale, B., Elander, R., Lee, Y., Holtzapple, M., & Ladisch, M. (2005). Features of promising technologies for pretreatment of lignocellulosic biomass. *Bioresource Technology, 96*, 673-686.

Müller, K. H., Motskin, M., Philpott, A. J., Routh, A. F., Shanahan, C. M., Duer, M. J., & Skeppera, J. N. (2014). The effect of particle agglomeration on the formation of a surface-connected compartment induced by hydroxyapatite nanoparticles in human monocyte-derived macrophages. *Biomaterials, 35*(3), 1074-1088.

Nicholson, D. J., Leavitt, A. T., & Francis, R. C. (2014). A three-stage klason method for more accurate determinations of hardwood lignin content. *Cellulose Chemistry and Technology, 48 (1-2)*, 53-59.

Overend, R. P., & Chornet, E. (1987). Fractionation of lignocellulosics by steam-aqueous pretreatments. *Philosophical Transactions of the Royal Society of London. Series A, 321*, 523-536.

Pu, Y., Treasure, T., Gonzalez, R., Venditti, R. A., & Jameel, H. (2013). Autohydrolysis Pretreatment of Mixed Softwood to Produce Value Prior to Combustion. *BioEnergy Research, 6*, 1094–1103.

Rahdar, A., Najafi-Ashtiani, H., & Sanchooli, E. (2019). Fluorescence and dynamics studies of dye-biomolecule interaction in the nano-colloidal systems. *Journal of Molecular Structure, 1175*, 821-827.

Ren, J., Kong, W., & Sun, R. (2014). Preparation of sugarcane bagasse/poly(acrylic acid-coacrylamide) hydrogels and their application. *BioResources, 9*(2), 3290-3303.

Requejo, A., Rodríguez, A., González, Z., Vargas, F., & Jiménez, L. (2012). Ethanol pulping as a stage in the bio-refinery of olive tree prunings. *BioResources, 7*(3), 3142-3159.

Saeed, A., Fatehi, P., Ni, Y., & Heiningen, A. v. (2011). Impact of furfural on the sugar analysis of prehydrolysis liquor of kraft-based dissolving pulp production process using the hpaec technique. *BioResources, 6*(2), 1707-1718.

Saeed, A., Jahan, M. S., Li, H., Liu, Z., Ni, Y., & Adriaan, v. H. (2012). Mass balances of components dissolved in the pre-hydrolysis liquor of kraft-based dissolving pulp production process from. *Biomass and Bioenergy, 39*, 14-19.

Salas, C., Rojas, O. J., Lucia, L. A., Hubbe, M. A., & Genzer, J. (2013). On the Surface interactions of proteins with lignin. *ACS Applied Materials & Interfaces, 5*, 199-206.

Sarip, H., Hossain, M. S., N, M. A., & Allaf, K. (2016). A Review of the thermal pretreatment of lignocellulosic biomass towards glucose production: autohydrolysis with DIC technology. *Bioresources, 11*(4).

Schramm, L. L. (2014). *Emulsions, Foams, Suspensions, and Aerosols: Microscience and Applications, Second Edition.* Wiley-VCH.

Shen, D., Liu, G., Zhao, J., Xue, J., Guan, S., & Xiao, R. (2015). Thermo-chemical conversion of lignin to aromatic compounds: Effect of lignin source and reaction temperature. *Journal of Analytical and Applied Pyrolysis, 112*, 56-65.

Sixta, H. (2006). *Handbook of Pulp (first edition).* Weinheim: Wiley-VCH.

Smith, M. C., Crist, R. M., & Clogston, J. D. (2017). Zeta potential: a case study of cationic, anionic, and neutral liposomes. *Anal Bioanal Chem, 409*, 5779–5787.

Song, T. (2013). *Extraction of polymeric galactoglucomannans from spruce wood by pressurised hot water (Academic Dissertation).* Turku: Abo Akademi.

Song, T., Pranovich, A., Sumerskiy, I., & Holmbom, B. (2008). Extraction of galactoglucomannan from spruce wood with pressurised hot water. *Holzforschung, 62*(6), 659–666.

Suzuki, M., & Hanabusa, K. (2010). Polymer organogelators that make supramolecular organogels through physical cross-linking and self-assembly. *Chem. Soc. Rev., 39*, 455–463.

Taherzadeh, M. J., & Karimi, K. (2007). Acid-based hydrolysis processes for ethanol from lignocellulosic materials: A review. *BioResources, 2*(3), 472-499.

Testova, L., Chong, S.-L., & Sixta, M. T. (2011). Autohydrolysis of birch wood. *Holzforschung, 65*, 535–542,.

Thakura, V. K., Thakurb, M. K., & Gupta, R. K. (2013). Development of functionalized cellulosic biopolymers by graft copolymerization. *International Journal of Biological Macromolecules, 61*, 44-51.

Tolbert, A., Akinosho, H., Khunsupat, R., Naskar, A. K., & Ragauskas, A. J. (2014). Characterization and analysis of the molecular weight of lignin for biorefining studies. *Biofuels, Bioprod. Bioref., 8*, 836–856.

Tunc, M. S. (2014). Effect of liquid to solid ratio on autohydrolysis of eucalyptus globulus wood meal. *BioResources 9(2), 3014-3024*.

Tunc, M. S., & Heiningen, A. R. (2008). Hemicellulose extraction of mixed southern hardwood with water at 150 °C: Effect of time. *Industial & Engineering Chemistry Research, 47*, 7031–7037.

Tunc, M. S., & Heiningen, A. R. (2009). Autohydrolysis of mixed southern hardwoods: Effect of P-factor. *Nordic Pulp and Paper Research Journal , 24 no. 1*, 42-47.

Valizadeh, H., Farajnia, A., & Zakeri-Milani, P. (2011). Formulation of cefuroxime axetil oral suspension and investigation of its pharmaceutical properties. *Advanced Pharmaceutical Bulletin, 1*(2), 93-96.

Vallejos, M. E., Zambon, M. D., Area, M. C., & Curvelo, A. A. (2015). Low liquid-solid ratio fractionation of sugarcane bagasse by hot water autohydrolysis and organosolv delignification. *Industrial Crops and Products, 65*, 349–353.

Vallejos, M. E., Zambon, M. D., Areaa, M. C., & Curvelo, A. A. (2012). Low liquid–solid ratio (LSR) hot water pretreatment of sugarcane bagasse. *Green Chemistry, 4*, 1982–1989.

Vegi, S., & Shastri, Y. (2017). Optimal control of dilute acid pretreatment and enzymatic hydrolysis for processing lignocellulosic feedstock. *Journal of Process Control, 56*, 100-111.

Vishtal, A., & Kraslawski, A. (2011). Challenges in industrial applications of technical lignins. *BioResources, 3*, 3547-3568.

wan, x., Li, Y., Wang, X., & Gu, X. (2007). Synthesis of cationic guar gum-graft-polyacrylamide at low temperature and its flocculating properties. *European Polymer Journal, 8*, 3655-3661.

Wang, S., Sun, Y., Kong, F., Yang, G., & Fatehi, P. (2016). Preparation and characterization of lignin-acrylamide copolymer as a paper strength additive. *BioResources, 11*(1), 1765-1783.

Wei, H., Gao, B., Ren, J., Li, A., & Yang, H. (2018). Coagulation/flocculation in dewatering of sludge: A review. *Water Research, 143*, 608-631.

Wijaya, Y. P., Putra, R. D., Widyaya, V. T., Ha, J.-M., Suh, D. J., & Kim, C. S. (2014). Comparative study on two-step concentrated acid hydrolysis for the extraction of sugars from lignocellulosic biomass. *Bioresource Technology, 164*, 221-231.

Wu, C. (2016). The Potential of pre-hydrolysis liquor from the dissolving pulp process as recovery source of xylooligosaccharide - A mini-review. *BioResources 11(3)*, 7917-7927.

Xiong, F., Han, Y., Wang, S., Li, G., Qin, T., Chen, Y., & Chu, F. (2017). Preparation and formation mechanism of renewable lignin hollow nanospheres with a single hole by self-assembly. *ACS Sustainable Chemistry & Engineering, 5*, 2273−2281.

Yadav, S. P., Ghosh, U. K., & Ray, A. K. (2017). Kinetic Studies on pisum sativum waste (pea pod) hydrolysis to furfural. *BioResources, 12*(2), 2326-2338.

Yang, B., & Wyman, C. E. (2008). Characterization of the degree of polymerization of xylooligomers produced by flowthrough hydrolysis of pure xylan. *Bioresource Technology, 99*, 5756-5762.

Yasuda, S., Fukushima, K., & Kakehi, A. (2001). Formation and chemical structures of acid-soluble lignin h sulfuric acid treatment time and acid-soluble lignin content of hardwood. *The Japan Wood Research Society, 46*, 69-72.

Ye, D. z., Jiang, L., Ma, C., Zhang, M.-h., & Zhang, X. (2014). The graft polymers from different species of lignin and acrylic acid: Synthesis and mechanism study. *International Journal of Biological Macromolecules, 63*, 43-48.

Ye, D. z., Zhang, M. h., Gan, L. l., Li, Q. l., & Zhang, X. (2013). The influence of hydrogen peroxide initiator concentration on the structure of eucalyptus lignosulfonate. *International Journal of Biological Macromolecules, 60*, 77-82.

Zhang, J., Xiao, H., Li, N., Ping, Q., & Zhang, Y. (2015). Synthesis and characterization of super-absorbent hydrogels based on hemicellulose. *Journal of Applied Polymer Science, 132*(34). doi:10.1002/APP.42441

Zhao, J., Xiuwen, W., Hu, J., Liu, Q., Shen, D., & Xiao, R. (2014). Thermal degradation of softwood lignin and hardwood lignin by TGFTIR and Py-GC/MS. *Polymer Degradation and Stability, 108*, 133-138.

Zhou, Y., & Franks, G. V. (2006). Flocculation mechanism induced by cationic polymers investigated by light scattering. *Langmuir*, Vol 22. 6775-6786.

Chapter 3: Hydrolysis component agglomeration and adsorption

3.1 Abstract

Autohydrolysis is vastly used in industry to extract hemicellulose from lignocellulosic biomass. Despite their promising potential end-use applications, lignocelluloses cannot be completely extracted as they may deposit on equipment. This study tends to investigate the physicochemical properties and adsorption behavior of the components of hydrolysates produced via autohydrolysis process. In this work, the autohydrolysis of softwood was conducted under different conditions to produce hydrolysates with different lignin and hemicellulose contents. Dynamic light scattering (DLS) was used for determining the hydrodynamic size of components dissolved in the hydrolysates under different conditions. The results provided evidence for aggregation of lignocelluloses under acidic conditions in hydrolysates. Furthermore, the deposition of lignocelluloses on stainless steel surface was studied by means of quartz crystal microbalance using hydrogen chloride and acetic acid buffer solutions. The results confirmed that the hydrolysate with higher hydrophilicity and lower surface tension possessed higher affinity for adsorption of its lignocelluloses on stainless steel. The reversibility of this deposition process depicts the weak interaction between the dissolved lignocelluloses and stainless steel. The image analysis also indirectly confirmed the formation of agglomerates in hydrolysate and their deposition on stainless steel surface.

3.2 Introduction

Woody biomass is one of the most abundant organic resources on earth. Since the fossil resources are limited, there is a growing interest in biomass utilization, which is considered as an alternative approach to generate energy and chemicals (Liu et al., 2012). Biorefining, which is the fractionation of biomass into varieties of products through a biological, biochemical, physical and thermal chemical treatment and separation, is well aligned with the production of sustainable product. The fractionation process of biomass may include dilute acid hydrolysis, alkaline hydrolysis, autohydrolysis and enzymatic hydrolysis. Among fractionation processes, autohydrolysis is the most environmentally friendly procedure to extract lignocelluloses from biomass. The efficiency of autohydrolysis can be adjusted by tuning operating parameters, such as temperature and residence time. Currently, the autohydrolysis of hardwood has received much attention. Recently, there has been a growing interest in the autohydrolysis process of softwood

for dissovling pulp production (Sixta et al., 2013; Li et al., 2012). However, the studies on the autohydrolysis of softwood are limted, especially in a flow through process.

The lignocellulosic materials dissolved in hydrolysates contain mainly hemicellulose and lignin (Pu et al., 2013). Hemicellulose is an amorphous carbohydrate that accounts for 15–30% of lignocellulosic materials. It has short chains consisting of five-carbon (xylose, rhamnose, and arabinose) and six-carbon (glucose, mannose, and galactose) sugars. It was used as a main feedstock for the production of ethanol, xylitol and lactic acid (Sarip et al., 2016). Lignin is a natrual polymer with a three dimentional structure that is the second most abundant biopolymer after cellulose (Zhao et al., 2014). Lignin's strcutre contains three major subuints of p-hydroxyphenyl (H), guaiacyl (G), and syringyl (S). Furfural also exsits in hydrolysates but only a small portion of hydrolysates. Furfural is a valuable derivative of hemicellulose generated via hemicellulose's decomposition, and has application in food, pharmaceutical and agricultural industries (López et al., 2014). Furfural has also been used to produce a wide range of chemicals, such as furan, tetrahydrofuran, and furfuryl alcohol.

In the past, the self-aggregation of lignin and hemicelluloses in native wood, and their aggregation in the hydrolysate of a hardwood was reported (Liu et al., 2013). There is still lack of comprehension of the driving forces to develop agglomorates of lignocelluloses and their deposition on surfaces. It is not clear if the deposition of lignocelluloses would occur via molecular adsoprtion or deposition of aggregated particles. The varied hydrodynmaic size of lignin at different pH was dependent on the pKa of its functional groups (Sipponen et al., 2018; Westbye et al., 2007). In addition, it was proposed that lignin tends to aggregate at high temperature or high ionic strength (Norgren et al., 2002). In one study, alkali lignin aggregation was controlled by $\pi - \pi$ interactions between the aromatic group. The $\pi - \pi$ interactions also induce the molecular aggregation of lignin chains due to Van der waals attraction (Deng et al., 2011). The self-assembly of xylan was correlated with hydrogen bonding development between linear portions of its polysaccharide backbone (Linder et al., 2003). In addition, the interactions between the hydrophobic groups of dissolved lignocelluloses can be another interpretation for their self-assembly in hydrolysates (Westbye et al., 2007).

There are some reports addressing the deposition of lignocelluloses on process equipment including digesters and membranes, which hampers the utilization of autohydrolysis for the

generation of lignin, hemicellulose and furfural for value-added production (Jansson et al., 2014; Hamaguchi et al., 2013). Recently, the adsorption behavior of lignin and hemicellulose has been studied on different surfaces, such as actiavated carbon, calcium carbonate, cellulose, gold or poly(diallyldimethylammonium chloride) (PDADMAC) (Fatehi et al., 2013; Qiu et al., 2014; Eronena et al., 2011). In a literature report, it was proposed that the mechanisms governing the adsorption of polysaccharide on talc surfaces included hydrophobic interaction, hydrogen bonding, chemical and electrostatic interactions (Liu et al., 2006). However, the interaction mechanism of lignocelluloses of hydrolysates has not been elucidated.

The objectives of this study were to (1) examine the effect of operating conditions, such as temperature, residence time and L/S ratio, on the production of hydrolysates in the autohydrolysis of spruce wood following Taguchi orthogonal design method, (2) discover how temperature, salt concentration, pH, ultrasonication, and time impact the hydrodynamic size of hydrolysates, and (3) understand the deposition behavior of hydrolysates on stainless steel surface. To the best of our knowledge, it is first time that the deposition of lignocelluloses of hydrolysates under different conditions was studied using advanced techniques, such as dynamic light scattering and quartz crystal microbalance.

3.3 Materials and methods

3.3.1 Materials

Ethanol (95 vol.%), acetone (98 wt.%), sulfuric acid (98 wt.%), sodium hydroxide powder (97 wt.%), potassium chloride and 3-(trimethylsilyl) propionic-2,2,3,3-d4 acid sodium salt (TSP) were purchased from Fisher Scientific. Deuterium oxide (D_2O) was purchased from Sigma-Aldrich. Decahydronaphthalene, mixture of cis and trans, cellulose acetate membrane tubes with a molecular weight cut-off of 10,000 g/mol were obtained from Wako Chemicals, Japan. Spruce wood chips with a 40% moisture content were received from a pulp and paper mill located in Northern Ontario, Canada. The wood chips were kept refrigerated in sealed plastic bags at 4 °C before use. The moisture content of wood chips was confirmed by drying in the oven at 104 °C for 24 hours.

3.3.2 Autohydrolysis

The spruce wood chips were hydrolyzed in a 2-L pulping digester (Greenwood Instruments, 2200, USA). The digester is a flow through pressurized vessel with self-circulation system. The wood

chips were fed into the digester first. Then, deionized water was added based on the different liquid to solid (L/S) weight ratios. When the vessel was completely sealed, the pulping digestor was programed to have a constant heating rate of 4.5 ℃/min. After hydrolysis, the vapor inside the digester was released. Hydrolysate was collected from the digester in beakers, while wood residues still remained in the vessels. In autohydrolysis experiment, 3 factors with 4 levels were considered: temperature (160 °C, 170 °C, 180 °C, 190 °C); residence time (15 min, 30 min, 45 min, 60 min) and liquid to solid (L/S) ratio (5, 10, 15, 20 wt./wt.). The L16 array of the Taguchi approach was applied to design the experimental plan of this study. Minitab 18 was used for interpreting and comparing the response of Taguchi experiment at different factor levels by means of analysis of variance (ANOVA).

3.3.3 Lignin and hemicellulose analysis

The lignin content of hydrolysate was determined following TAPPI UM 250 using UV/Vis spectrometric (GENESYS 10S UV–Vis, Thermo Scientific) at a wavelength of 205 nm (Liu et al., 2011). The hemicellulose content of hydrolysates was determined using an ion chromatography, Dionex, ICS 5000, Thermofisher Scientific, equipped with CarboPac™ SA10 column and an electrochemical detector (ED) (Dionex-300, Dionex Corporation, Canada). Hemicellulose may be in the form of mono or poly sugars in the hydrolysates, but the chromatography can only detect monosugars. Therefore, the hydrolysates were mixed with 4% sulfuric acid in sealed vials. In order to convert all the polysugars to monosugars, the vials were transferred to an autoclave for further acid hydrolysis at 120 °C for 1 hour. The analysis on the hydrolysate before this acid hydrolysate would show the monomeric sugars of hydrolysates; while, after acid hydrolysis it would depict the total sugars of the hydrolysates.

3.3.4 Acetic acid and furfural

The concentrations of acetic acid and furfural in the hydrolysates were determined by a proton nuclear magnetic resonance (NMR, Varian Unity Inova 500 MHz spectrometer). In this experiment, TSP served as an internal standard to quantify the concentration of acetic and furfural. First, 0.5 wt.% of TSP was mixed with deuterium oxide (D_2O). Then, approximately 0.1 g of dry hydrolysate was added to 1 g of D_2O in a small vial. After mixing, the samples were centrifuged at 100 rpm for 15 mins and then transferred to NMR tubes for analysis.

3.3.5 Dynamic light scattering (DLS) and sample preparation

The hydrodynamic radius of the hydrolysate's constituents was determined using a static light scattering instrument (BI-200SM Brookhaven Instruments Corp) at 90º with the power of 35 mW and a wavelength of 659 nm. There were two different hydrolysate samples that were tested by DLS. Sample 1 was the hydrolysate produced from hydrolysis experiment at 180 ℃ for 15 minutes with an L/S ratio of 10 wt./wt. Sample 1 had the lowest concentration of lignin and hemicellulose. The hydrolysis conditions for sample 2 were 190 ℃, 15 min and a L/S ratio of 5 wt./wt.

The concentration of samples for DLS measurement was 1.5 g/L. To prepare the samples for DLS measurement, hydrolysates were dried at 60 °C for 2 days. The dried hydrolysates were mixed with 10 mM of potassium chloride solution or water. The samples were then kept at room temperature for 2 days. Afterward, about 30 mL of the samples were centrifuged at 1500 rpm for 5 mins in order to settle large particles from the hydrolysate solutions. The supernatants of this test were filtered through a 0.45 µm syringe filter to remove undissolved impurities. In the ultrasonication assessment, the hydrolysate samples were treated with ultrasonic using ultrasonic bath (Fisher Scientific). Each sample was tested in triplicates by DLS, and the average hydrodynamic diameter (Dh) values were reported.

3.3.6 Quartz crystal microbalance (QCM)

Stainless steel is extensively used in manufacturing of equipment used in industry; likewise, the equipment used in the hydrolysis process and handling of hydrolysate (Chandrasekaran et al., 2013; Al-Hamarneha et al., 2012). Hydrolysate's constituents may adsorb on the surface of stainless steel duinrg its handling process. To resemble the adsoprtion of lignocelluloses on stainless steel, the adsorption performance of constituents of hydrolysates was studied by the means of quartz crystal microbalance with dissipation (QCM-D 401, E1, Q-Sense Inc. Gothenborg, Sweden). Once hydrolysate's constituents started to deposit on stainless steel coated sensors (SS2343 US 316, Biolin Scientific), the frequency and dissipation of the sensors were changed and evaluated by Q-tools software (Q-Sense, Gothenburg, Sweden) at different overtones (n = 1, 3, 5, 7, 9, 11 or 13). In this study, the 7th overtone was selected for investigating the adsorption performance of hydrolysate on stainless steel. The Voigt model for viscoelastic material was employed to calculate the adsorbed mass. The sensors were treated with a solution of fresh Mili-Q water/ammonium hydroxide/hydrogen peroxide at the ratio of 10/2/2 v/v/v for 5 min. Then, the sensors were dried

with nitrogen gas and cleaned in the UV/ozone oxidation cleaner (PSD Series, digital UV ozone system, NOVASCAN) for 10 min prior to use. In this set of experiments, hydrolysis liquor was analyzed by two different buffer solutions; hydrogen chloride and acetic acid solution. The buffer solutions were prepared by mixing the acids with Mili-Q water to reach pH 3.9 (the pH of hydrolysate). Afterwards, they were pumped through the QCM chamber until a stable baseline was obtained, then the hydrolysates were pumped through the QCM chamber at a constant flow rate of 0.15 mL/min and 20 ± 2 °C. After adsorption experiment, the sensors were washed with the buffer solution.

3.3.7 Scanning electron microscopy (SEM)

After QCM experiment, the treated sensors were air dried and transferred to a sealed glass container for SEM analysis. The images were obtained by a Hitachi SU-70 field emission SEM in tandem with Oxford Xmax energy dispersive X-ray spectroscopy at 5kV voltage with maximum of 10,000 magnification. ImageJ, Java-based image, processing program developed at the Nation Institutes of Health and Laboratory for Optical and Computational Instrumentation (LOCI, university of Wisconsin) was used for image analysis.

3.3.8 Contact angle and surface tension measurements

The static contact angles of hydrolysate samples were determined on stainless steel coated sensor using a Theta Lite Optical tensiometer, TL100 (Biolin Scientific, USA) equipped with USB2 digital camera and Attention software. The hydrolysate samples were directly injected on the sensor using a sessile drop method. The contact angle was calculated using Young's equation based on the average of three independent measurements.

The surface tension of hydrolysate samples was determined using a tensiometer (Biolin, model # Sigma 700) following Du Noüy ring method. First, a glass container was filled with 20 mL of hydrolysate samples. The ring was burned and washed with ethanol and deionized water prior to use. The experiment was conducted by immersing a platinum–iridium ring into the samples, and then the samples were slowly lifted the ring from the surface of the hydrolysate samples. All the measurements were repeated three times and the average values were reported.

3.4 Results and discussion

Table 3.1 lists the results of hydrolysis experiments. Lignin was the primary species in hydrolysates. The hemicellulose content varied from 2.14 wt.% to 8.21 wt.% based on the mass of

dried wood. Furfural and acetic acid had low concentrations. The hydrolysates produced at 160 ℃, 15 mins, L/S ratio of 20 wt./wt. and at 160 ℃, 30 mins and L/S ratio of 15 wt./wt. had no trace of furfural, because at low temperature and low acidity, the degradation of C5 sugar (almost exclusively from xylan/xylose) was reported to be limited (Liu et al., 2014). In one study, it was reported that an insignificant amount of furfural was produced in the autohydrolysis of mixed southern hardwood at 150 ℃, L/S ratio of 3.7/1 wt./wt., for 500 mins in a batch reactor (Tunc & Van Heiningen, 2009). The lowest yield of this experiment was 4.91 %, while the highest yield was 20.18 %. In this case, the highest yield was obtained at highest temperature and residence time of hydrolysis. In another research, the yield of hydrolysis of eucalyptus globulus dropped dramatically with increasing hydrolysis intensity (i.e., high temperature and long residence time), indicating that an extensive extraction of lignin and hemicellulose is associated with extensive hydrolysis intensity (Gütsch et al., 2012).

Table 3.1. Operating parameters and compositions of hydrolysate after autohydrolysis

Temperature (°C)	Time (min)	L/S (wt./wt.)	Lignin (wt.% dry wood)	Total sugars (wt.% dry wood)	Furfural (wt.% dry wood)	Acetic acid (wt.% dry wood)	Solid content (wt.% dry wood)
190	15	5	8.03	5.74	3.44	0.58	17.16
190	30	10	9.60	5.80	2.15	1.28	16.76
190	45	15	8.68	5.32	2.45	1.23	16.87
190	60	20	8.88	6.01	4.61	2.69	20.18
180	15	10	7.36	4.21	0.37	1.24	12.13
180	30	5	7.18	4.37	0.54	1.72	13.85
180	45	20	6.53	8.21	0.78	2.45	16.01
180	60	15	8.99	7.89	1.08	1.50	17.21
170	15	15	4.54	2.07	0.15	0.34	6.78
170	30	20	5.31	4.01	0.20	1.17	10.12
170	45	5	7.08	4.53	0.25	1.04	12.23
170	60	10	7.78	6.04	0.20	1.24	13.21
160	15	20	2.93	2.14	NA	0.81	4.91
160	30	15	5.30	3.25	NA	0.49	5.60
160	45	10	6.65	4.79	0.22	1.21	8.10
160	60	5	8.72	6.25	0.22	1.19	10.39

3.4.1 Influence of process variables on acetic acid

The primary effect of independent variables (temperature, time, L/S ratio) on acetic acid production was statistically assessed by ANOVA and the results of this analysis are listed in Table

3.2. It was observed that all of the tested variables were crutial to control the acetic acid production. Residence time was identified as the most significant variable followed by temperature and L/S ratio. Acetic acid was the primary cause of the variations in pH of hydrolysates (Liu et al., 2015). It was reported that the pH of the autohydrolysis liquor of spruce wood chips declined with prolonging the residence time (Song et al., 2008). Acetic acid was genreated from the cleavage of acetyl group mainly bound to the hemicelluloses (Shen et al., 2012). In Figure 3.1, the generation of acetic acid was plotted as a function of different variables. In this figure, dash line represents the average of acetic acid concentration in the samples. It was also observed that its acetic acid content increased by elevating temeprature to 180 °C. When the temperature was increased to 190 ℃, the yield of acetic acid generation dropped. As explained in the experimental section, piror to collecting hydrolysates from the digestor, the digestor was ventilated to depressurize the system. Therefore, the loss of acetic acid was probably due to acetic acid vaporation along with steam. When liquid to solid ratio increased from 10 to 15 wt./wt., the yield of acetic acid production decreased probably due to the pH drop caused by additonal water in the system. However, when liquid to solid ratio further increased to 20 wt./wt., the yield of acetic acid raised sharply. The hypothesis is that excess water improved water penetration through the wood chips, which can hydrolyze more acetyl group from wood chips for inducing acetic acid.

Table 3.2. Statistically analysis for the influence of operating parameter on acetic acid concentration of hydrolysate

Source	DF	Adj SS	Adj MS	F-Value	P-Value
Temperature	3	1.8508	0.61694	8.66	0.013
Time	3	1.9328	0.64428	9.04	0.012
L/S	3	1.6931	0.56437	7.92	0.017
Error	6	0.4276	0.07126	-	-
Total	15	5.9043	-	-	-

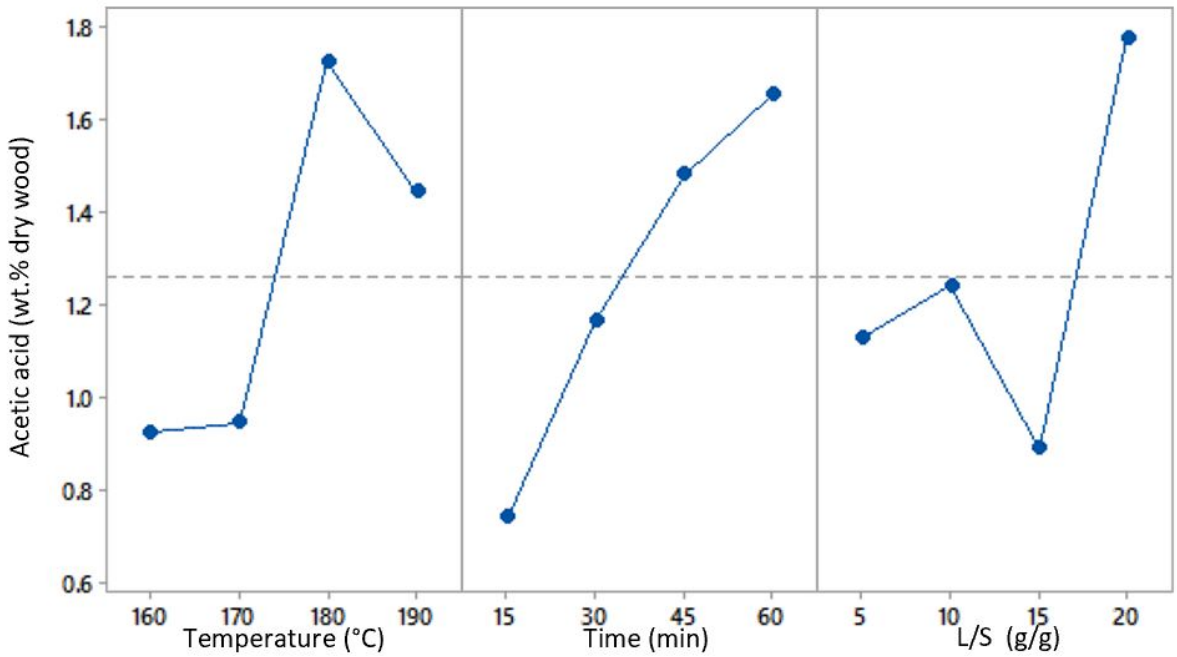

Figure 3.1. Effect of temperature, time, L/S on acetic acid production

3.4.2 Influence of process variables on lignin

It is seen in Table 3.3 that P-values for all variables for lignin production in the hydrolysates were less than 0.05. This indicates that temperature, time and L/S had all statistically significant responses. According to their P-value and F-value, temperature had the greatest impact on the lignin content of hydrolysates. The F-value of temperature is slightly larger than that of time. In Figure 3.2, the main parameters impacting lignin production are shown. Temperature and time were proportional to the lignin content in the hydrolysates. At elevated temperature or extended residence time, more acetic acid was generated in the autohydrolysis. A lower pH of the hydrolysates favors the hydrolysis process (Tarasov et al., 2018). Compared to other variables, L/S ratio had the least impact on lignin. Tunc (2014) stated that in the autohydrolysis of eucalyptus globulus wood meal, lignin extraction increased with increasing L/S ratio. Interestingly, L/S ratio was inversely proportional to the lignin content in this study, which may be caused by the large amount of water diluting the concentration of the acetic acid in a flow through circulation system.

Table 3.3. Statistically analysis for the influence of operating parameters on lignin content of hydrolysates

Source	DF	Adj SS	Adj MS	F-Value	P-Value
Temperature	3	19.406	6.4688	18.20	0.002
Time	3	17.278	5.7595	16.20	0.003
L/S	3	8.944	2.9814	8.39	0.014
Error	6	2.132	0.3554		
Total	15	47.761			

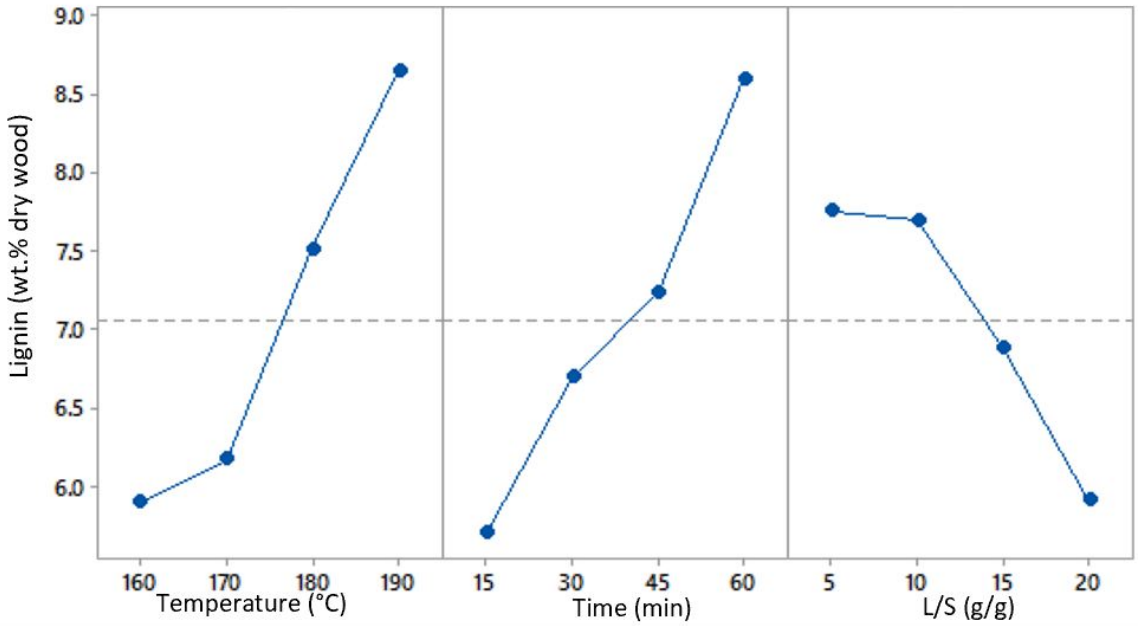

Figure 3.2. Effect of temperature, time, L/S on lignin production

3.4.3 Influence of process variables on hemicellulose

The effect of temperature, residence time and liquid to solid ratio on the production of sugars was shown in Table 3.4. It can be seen that the residence time was the most significant variable although its P-value was slightly larger than 0.05. The extraction of hemicellulose is catalyzed by hydronium ions from water or in-situ produced chemicals, such as acetic acid and phenolic acid (Hou et al., 2014). As the residence time was further extended, more hydronium ions were accumulated in the hydrolysates, which accelerated the dissolution of hemicellulose. Figure 3.3 shows the amounts of hemicelluloses extracted from wood as a function of the process variable.

The increase in temperature from 170 ℃ to 180 ℃ promoted the hemicellulose extraction. This indicated that the majority of the hemicellulose dissolution occurred between 170 ℃ and 180 ℃. These results are in good agreement with the results reported by Garrote et al. (1999), in which 51% of xylan was degraded to xylooligosacharides at 171-185 ℃ in the autohydrolysis of eucalyptus globulus wood. Further temeprature increase to 190 ℃ decreased the sugar content of hydrolysates, which was further converted to furfural. No meaningful conclusion could be made for correlating L/S to hemicellulose content of hydrolysates as its P-value was larger than 0.05.

Table 3.4. Statistically analysis for the influence of operating parameters on sugar concentration of hydrolysates

Source	DF	Adj SS	Adj MS	F-Value	P-Value
Temperature	3	13.4880	4.4960	2.84	0.128
Time	3	21.7714	7.2571	4.59	0.054
L/S	3	0.9172	0.3057	0.19	0.897
Error	6	9.4912	1.5819	-	-
Total	15	45.6678	-	-	-

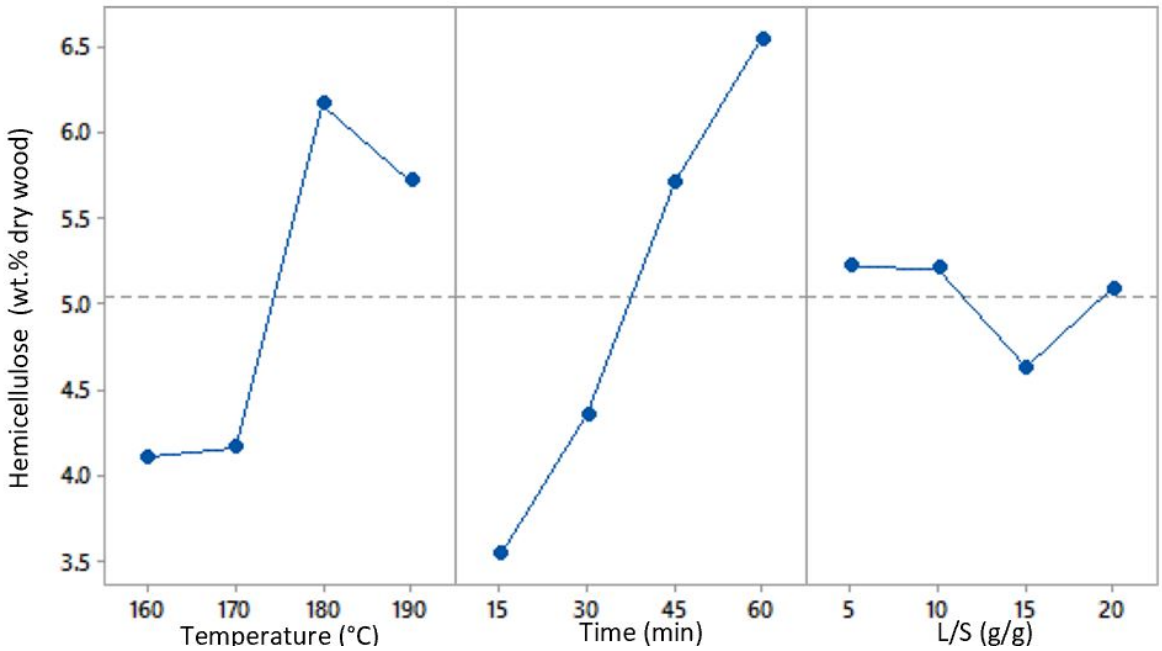

Figure 3.3. Effect of temperature, time, L/S for sugar production

3.4.4 Influence of process variables on furfural

The results in Table 3.5 depicts the statistical significance of the process variables on furfural production. It shows that temperature was the most impactful variable for the furfural production, while residence time and L/S had minor influences. As is well known, the formation of furfural occurs when pentose sugar undergoes dehydration. The impact of process parameters on furfural concentration is shown in Figure 3.4. From 160 to 180 ℃, the furfural content was low, which can be attributed to the degradation of small portion of hemicellulose to monosaccharide in this temperature range. From 180 to 190 ℃, there was a remarkable increase in the furfural production, which is consistent with the reduction in the hemicellulose content in Figure 3.2. This result was consistent with those reported by Khazraie et al. (2017) in that the concentration of furfural dramtically increased from 1.21 to 4.5 g/L when temperature increased from 180 to 190 ℃. In Table 3.1, furfural yield was significantly reduced from 3.44 to 2.15 wt.%, when hydrolysis conditions changed from 190 ℃, residence time of 15, L/S ratio of 5 wt./wt. to 190 ℃, residence time of 30, L/S ratio of 10 wt./wt. This can be due to the reaction of lignin and furfural (Liu et al., 2015). Polysaccharide chains cleaved at a high temperature and hydrolyzed to monosugar, which was further degraded to furfural. With prolonging time, formic acid and levulinic acid would be accumulated in the hydrolysates (Tunc et al., 2014; Galia et al., 2015).

Table 3.5. Statistically analysis for the influence of operating parameter on furfural production from hydrolysate

Source	DF	Adj SS	Adj MS	F-Value	P-Value
Temperature	3	24.8106	8.2702	29.62	0.001
Time	3	1.4033	0.4678	1.68	0.270
L/S	3	0.9610	0.3203	1.15	0.403
Error	6	1.6752	0.2792	-	-
Total	15	28.8501	-	-	-

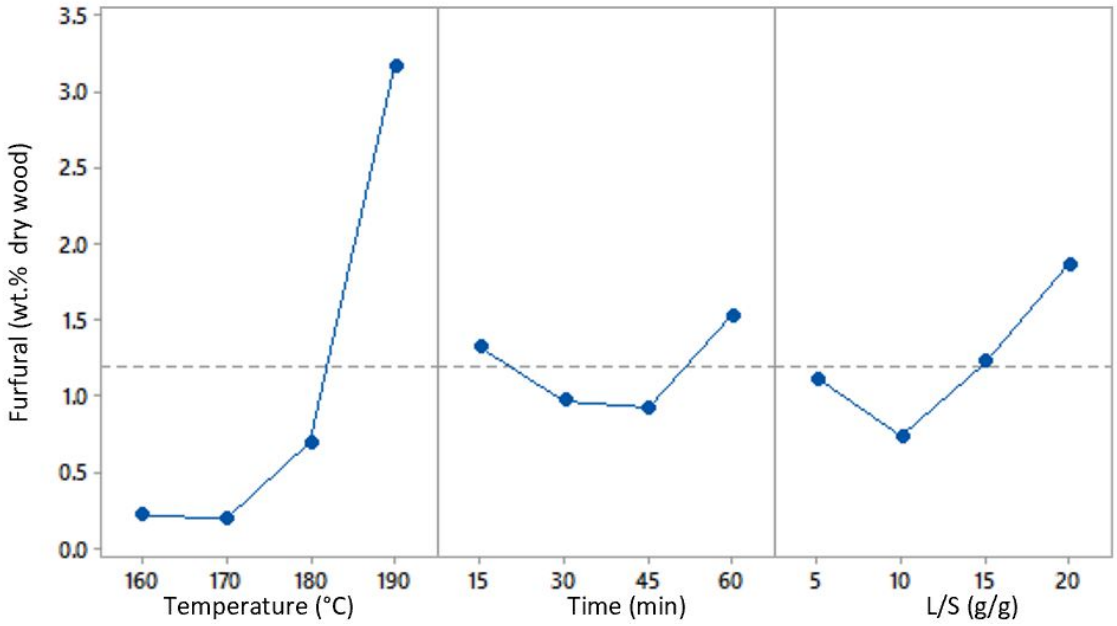

Figure 3.4. Effect of temperature, time, L/S on furfural production

3.4.5 Hydrodynamic size analysis of hydrolysate constituents

Figure 3.5 (a) presents the hydrodynamic size of the hydrolysate constituents as a function of temperature. At room temperature, sample 1 and 2 had the hydrodynamic sizes of 1.3 nm, and 3.3 nm, respectively, although sample 2 had smaller molecular weight than sample 1 as seen in Table 3.6. In general, a polymer with a larger molecular weight tends to have larger hydrodynamic size. However, at low hydrolysis intensity, lignin and hemicellulose moieties of sample 1 may be in lignin-carbohydrate complex (LCC) (Tarasov at al., 2018). At high hydrolysis intentsity, a portion of intermolecular bonds of the LCC in sample 2 was cleaved; therefore, less LCC remained in the hydrolysate (Khazraie et al., 2017). Consequently, sample 1 had smaller hydrodynamic size than sample 2.

The experiments were conducted at 25, 45, 60 and 75 ℃. The results in Figure 3.5 (a) depict that the hydrodynamic size of all samples slightly increased with temperature increase. The hydrodynamic size growth was probably related to the increased Brownian motion of the constituents of hydrolysates at a higher temperature (Azouz et al., 2016). In one study, it was stated that self-assembly of softwood kraft lignin was promoted with increasing temperature from 25 to 75 ℃ (Fritz et al., 2017). In another study, hemiceluloses presented higher degree of self-

association with increasing temperature, where the amphiphilicity of hemicellulose was a driving force for self-association (Patel et al., 2007).

3.4.6 Effect of salt concentration

In Figure 3.5 (b), the effect of potassium chloride salt on the hydrodynamic size of hydrolysate at room temperature was shown. In the absence of salt, samples 1 and 2 had hydrodynamic sizes of 18 nm, and 103.9 nm, respectively. The addition of salt screened the double layer electrostatic interactions between the nanoparticles (Richter et al., 2016). The hydrolysate's constituents yielded from autohydrolysis had very weak charges, thus a small amount of salt stablized the segments in the hydrolysates.

3.4.7 Effect of pH

In order to test the impact of pH on hydrodynamic size of hydrolysate components, the experiments were carried out at room temperature and pH of 2, 3.5 ,5, 7, 9, and 11. The corresponding hydrodynamic size was plotted as a function of pH in Figure 3.5 (c). At pH 2, all the samples had the highest hydrodynamic sizes, which was attributed to the acidification and condensation of hydrolysate components at pH 2 (Wang et al., 2014). In another study, 16-21% of lignin and 16-38% of hemicellulose were extracted when the pH of the solution dropped to 1.5 as a result of association of hydrolysate components (Tarasov et al., 2018). This proves that at low pH, the colloidal stability of the hydrolysate dropped significantly. Since the carboxylate group has a pKa of 4.75, when the pH of hydrolysis is below 4.75, it may mostly protonate and become uncharge. The absence of the electrostatic repulsion force between the subunits on the lignocellulose chains may then result in entanglement of chain and agglomeration of the segments (Salentinig & Schubert, 2017). When the pH increased to 9, the hydrodynamic sizes were agumented, which can be attributed to the screening of charges on the particle surface at higher pH. Meanwhile, significant amount of salt was formed during pH adjustment. When the pH of the hydrolysate approaches 10, which is the pKa of the phenolic group, the functional group is ionized (Shulga et al., 2012). As seen in Figure 3.5c, the hydrodynamic size of all the samples significantly decreased, which was due to the fact that charged particles introduced electrostatic repulsion and stabilized themselves in the system (Chen et al., 2018).

3.4.8 Effect of ultrasonication

Figure 3.5 (d) shows the hydrodynamic size of samples 1 and 2 under different ultrasonic duration. Ultrasonication effectively reduced the hydrodynamic size of the samples in the first 20 min. One study was documented that ultrasonic force could cause the cleavage of agglomerates, hydrophobic interaction and van der Waal's forces (Zhu et al., 2019). The decrease in the hydrodynamic size was attributed to hydrodynamic shear force caused by cavitation (Bi et al., 2015). In the period of 20 min and 40 min, the hydrodynamic size of the samples was stabilized.

3.4.9 Effect of time

Figure 3.5 (e) depicts the self-assembly behavior of hydrolysate constituents over time after ultrasonication. All samples followed very similar trends where their hydrodynamic sizes increased with increasing time. In the first two hours, the hydrodynamic sizes of the samples augmented extremely slow. After 2 h, the components of sample 2 gradually enlarged their sizes to approximately 11.5 nm. At 4 h, sample 1 had a hydrodynamic size of 10 nm. According to literature, without the disruption of chemical or any external force, lignin in the solvent can undergo self-assembly spontaneously through hydrogen bonding, van der Waals force, chain entanglement, and π-π interactions (Mishra & Ekielski, 2019). This was the evidence that the self-assembly and dissociation of polymers in hydrolysates were reversible (Salentinig & Schubert, 2017).

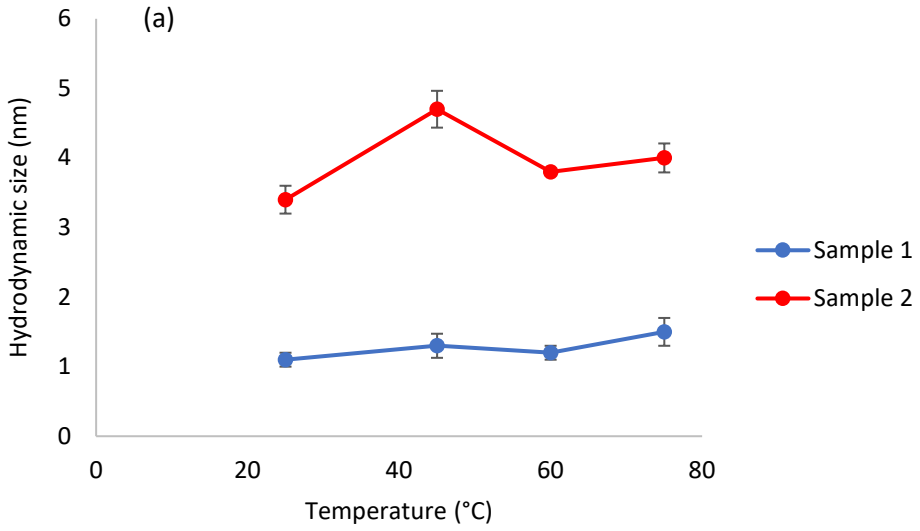

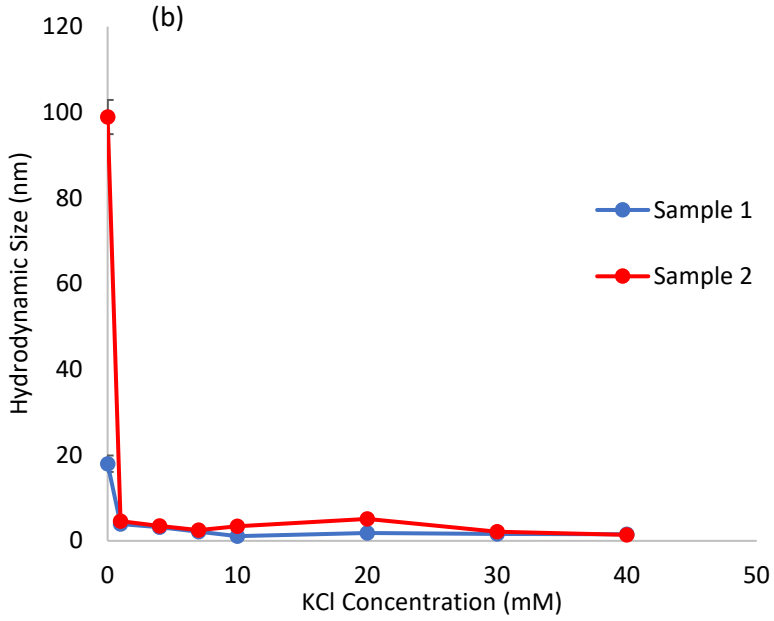
(b)
120
100
80
60
40
20
0
Hydrodynamic Size (nm)
0
10
20
30
40
50
KCl Concentration (mM)
Sample 1
Sample 2

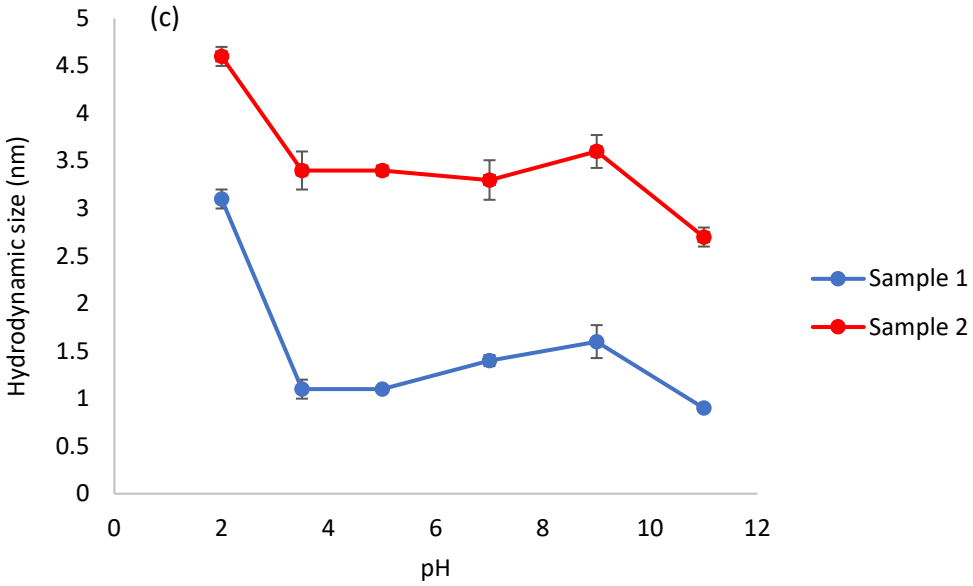
(c)
5
4.5
4
3.5
3
2.5
2
1.5
1
0.5
0
Hydrodynamic size (nm)
0
2
4
6
8
10
12
pH
Sample 1
Sample 2

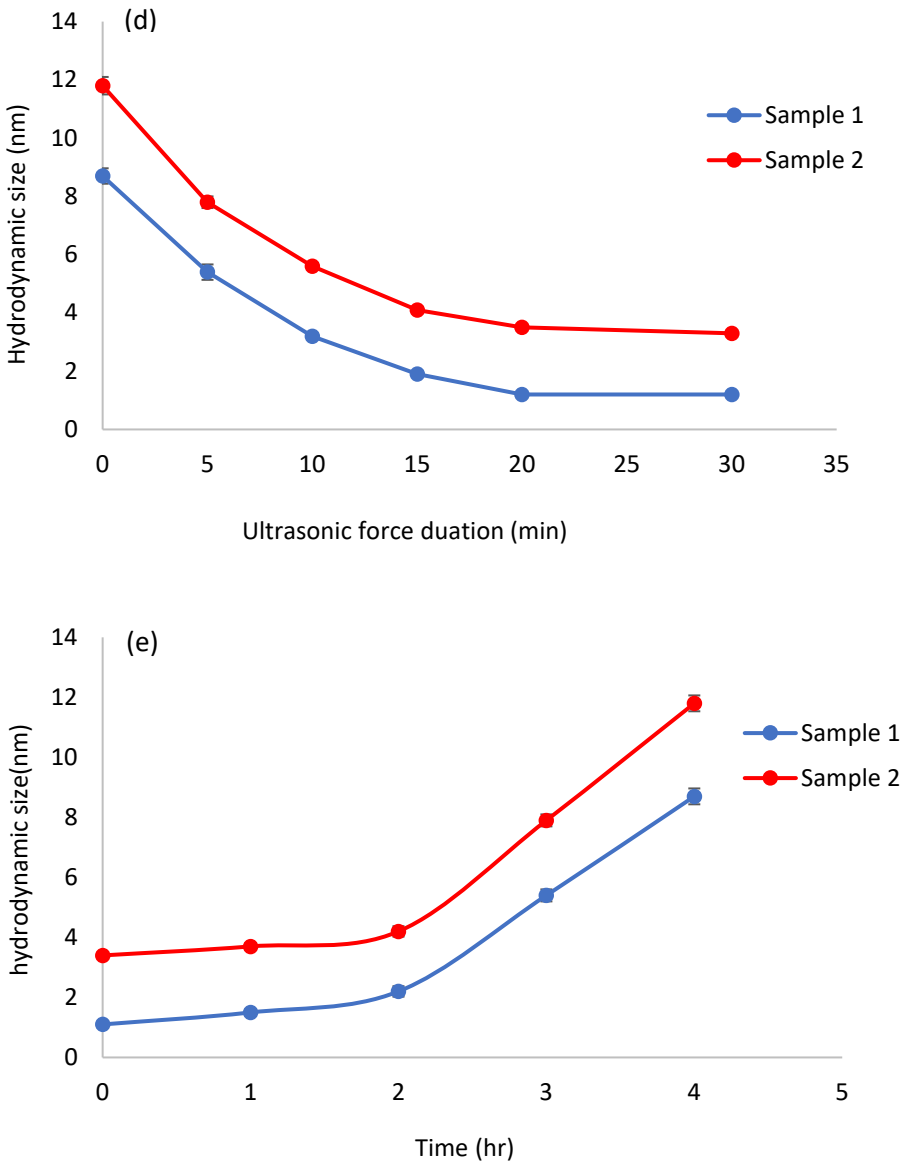

Figure 3.5. Hydrodynamic size of hydrolysate constituents under different experimental conditions: (a)10 mM KCl, 3.5 pH, (b) 25 ºC , 3.5 pH, (c) 25 ºC , 10 mM KCl, (d) 25 ºC , 3.5 pH, 10 mM KCl, (e) 25 ºC , 3.5 pH, 10 mM KCl

3.4.10 Hydrolysis liquor adsorption using HCl as buffer solution

Figure 3.6 (a) shows the adsorbed mass of the hydrolyste of samples 1 and 2 on the QCM sensor as a function of time. At loading stage (0-150 s), the adsorbed mass for both sampels was sharply increased, indicating hydrolysate's constitunents were accumulated on the stainless steel sensor before reaching saturation (Chandrasekaran et al., 2013). At saturation, sample 2 had higher

adsorption affinity than sample 1, as the maximum adsorptions for samples 1 and 2 were 1290 × 10^{-8} kg/m^2 and 3700 × 10^{-8} kg/m^2, respectively.

To better illustrate the adsorption behavior of hydrolysate constituents, their compositions, contact angle, surface tension, and hydrodynamic size were listed in Table 3.6. As can be seen, the contact angles of samples 1 and 2 on the stainless steel sensor were 78.9 and 65.8°, respectively, implying more hydrophilic nature of sample 1. The lignin and hemicellulose contents of sample 1 were 12.5 g/L and 2.4 g/L, respectively, while those of sample 2 were 16.35 g/L and 7 g/L, respectively, which could be due to lower concentration of lignin in sample 1. Owing to its higher concentration and more hydrophilicity, hydrolysate consitutuents could interact more with the stainless steel via hydrophilic-hydrophilic interaction. The less water solubility of lignin would also contribute to its settlement and thus deposition on the sensor. Surface tension between hydrolysate and stainless-steel surface is a measure of energy required to form a layer at the interface (Park & Seo, 2011). In addition, the lower surface tension indicating lower Gibbs free energy allowed the adsorption layer to obtain a more thermodynamically stable state. The surface tension of sample 2 was 47.1 mN/m; whereas, that for sample 1 was 50.0 mN/m. These results also confirmed that sample 2 generated more adsorption layer compared to sample 1 due to its low surface tension. In addition, the mass of adsorbed layer may be influenced by the concentration as sample 1 was diluted more than sample 2.

Evidently, the adsorbed mass for both samples significantly dropped in the buffer rising state. Nearly, all of the mass previously adsorbed on the sensor were washed off from the sensor surface, indicating a high level of reversibility in this adsorption process. Eventually, the adsorbed mass dropped to 180 × 10^{-8} kg/m^2 and 60 × 10^{-8} kg/m^2 after buffer rinsing. The pH of hydrolysate and buffer solutions was between 3 and 4, some negetive charges may be originated from carboxylate groups associated with the components of hydrolysates (Lu et al., 2016). Since the isoelectric point of stainless steel is 3-4, at the isoelectric point, stainless steel carries no electric charges, thus no electrical interaction could be developed between hydrolysate componenets and the sensor surface (Chandrasekaran et al., 2013) Charge neutralization is a strong force favoring adsorption behavior. In the absence of charges at the interface between hydrolysate and stainless steel, hydrolysate cannot develop strong bonding with the surface, and the buffer rinsing results provide evidence for this.

Figures 3.6 (b) and (c) reveal the changes in frequency and dissipation of stainless steel coated sensor as a result of lignocellulose adsoprtion. At the beginning (0-80s) of the test, as the hydrolysate constituents have not reached the sensor, there were no significant changes in frequency and dissipation of the sensor. The frequency dropped rapidly followed by a sharp increase in dissipation from 60 to 225s, indicating the adsoprtion of hydrolysate constituents on the sensor. In addition, as shown in Figure 3.6 (c), the dissipation for sample 2 at equilibrium was around 16.5×10^{-6} while that was only approximately 5.5×10^{-6} for sample 1. It can be interpreted that the adsorbed layer for sample 2 on sensor was much softer and looser than that for sample 1 and more water entrapped in the adsorbed layer for sample 2. In the literature, when the ratio of dissipation/frequency was less than 0.4×10^{-6} Hz, the adsorbed layer was considered to be elastic (Micciulla etl al., 2014). The value of dissipation and frequency for both samples maintained relatively stable at approximately 200s. The ratio of dissipation/frequency at 200 s for samples 1 and 2 were 0.42×10^{-6} Hz, and 0.33×10^{-6} Hz, respectively, implying the formation of elastic adsorbed mass on stainless steel sensor for sample 2 and more compact adsorption layer generated for sample 1. The relatively rigid adsorption layer for sample 1 may be attributed to the larger hydrodynamic size as shown in Table 3.6. Sample 1 has longer chain, causing strong chain entanglement with stainless steel surface favoring the adsorption (Striolo et al., 2005). It was noticed that sample 1 had slightly more irreversible mass adsorption than sample 2 in Figure 3.6 (a). This phenomenon can be corresponded to the compact adsorption layer, leading to more interaction affinity with stainless steel surface.

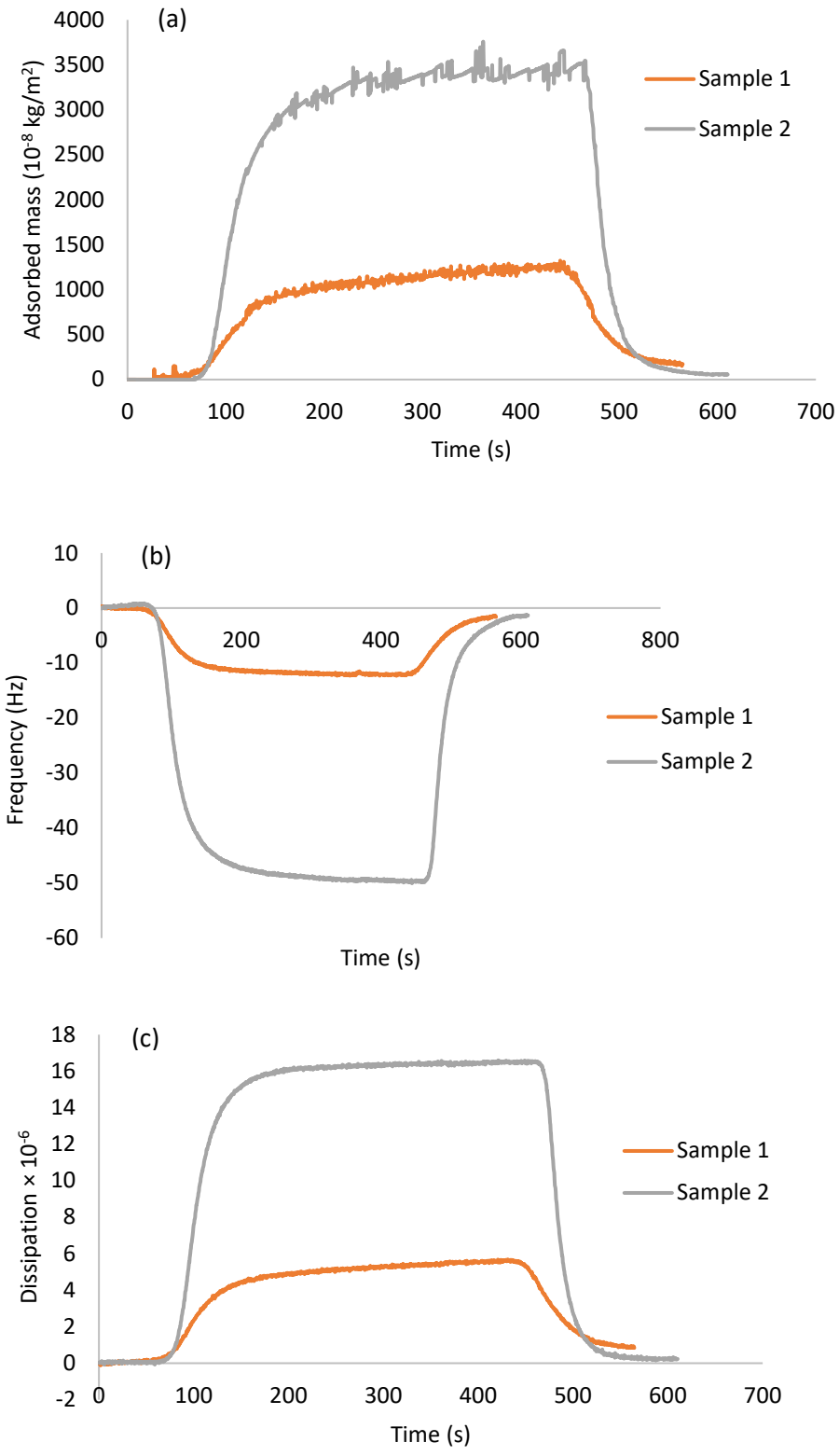

Figure 3.6. QCM results using HCl as buffer solution a) Adsorbed mass change as a function of time, b) frequency change as a function of time, c) dissipation change as a function of time

Table 3.6. Compositions, molecular weight, contact angle, surface tension and hydrodynamic size of samples 1 and 2

	Compositions		Mn	Mw	Mw/Mn	Contact angle	Surface tension (mN/m)	Hydrodynamic size (nm)
	Lignin (g/L)	Sugar (g/L)						
Sample 1	12.5	2.48	4642	8357	1.800	78.9°	50.0	98.9
Sample 2	16.35	7.01	3199	7560	2.363	65.8°	47.2	18.0
Water						56.6°	72.0	

3.4.11 Hydrolysis liquor adsorption using acetic acid as buffer solution

The variations of absorbed mass, frequency and dissipation with respect to time were depicted in Figure 3.7. At equilibrium, adsorbed mass, frequency and dissipation for both samples using acetic acid as buffer solution had good consistency with results using HCL as buffer solution. Due to the low dissipation of sample 1 and high dissipation of sample 2 during oscillation, sample 1 and 2 formed rigid and soft film on the sensor, respectively. The experiment condition differed from the last set of experiments was buffer solution. It was indicated that the buffer chemistry had no impact on adsorption of hydrolysates on stainless steel surface.

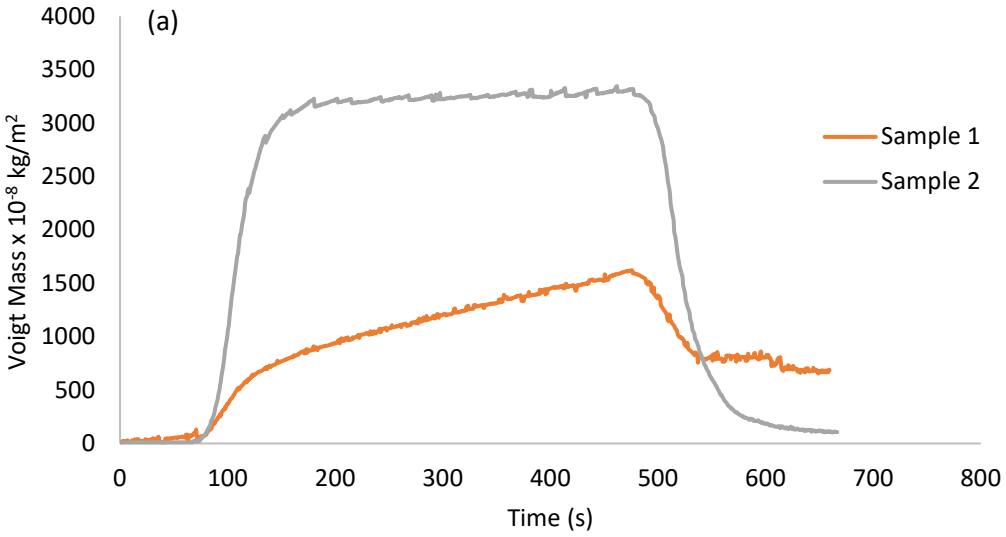

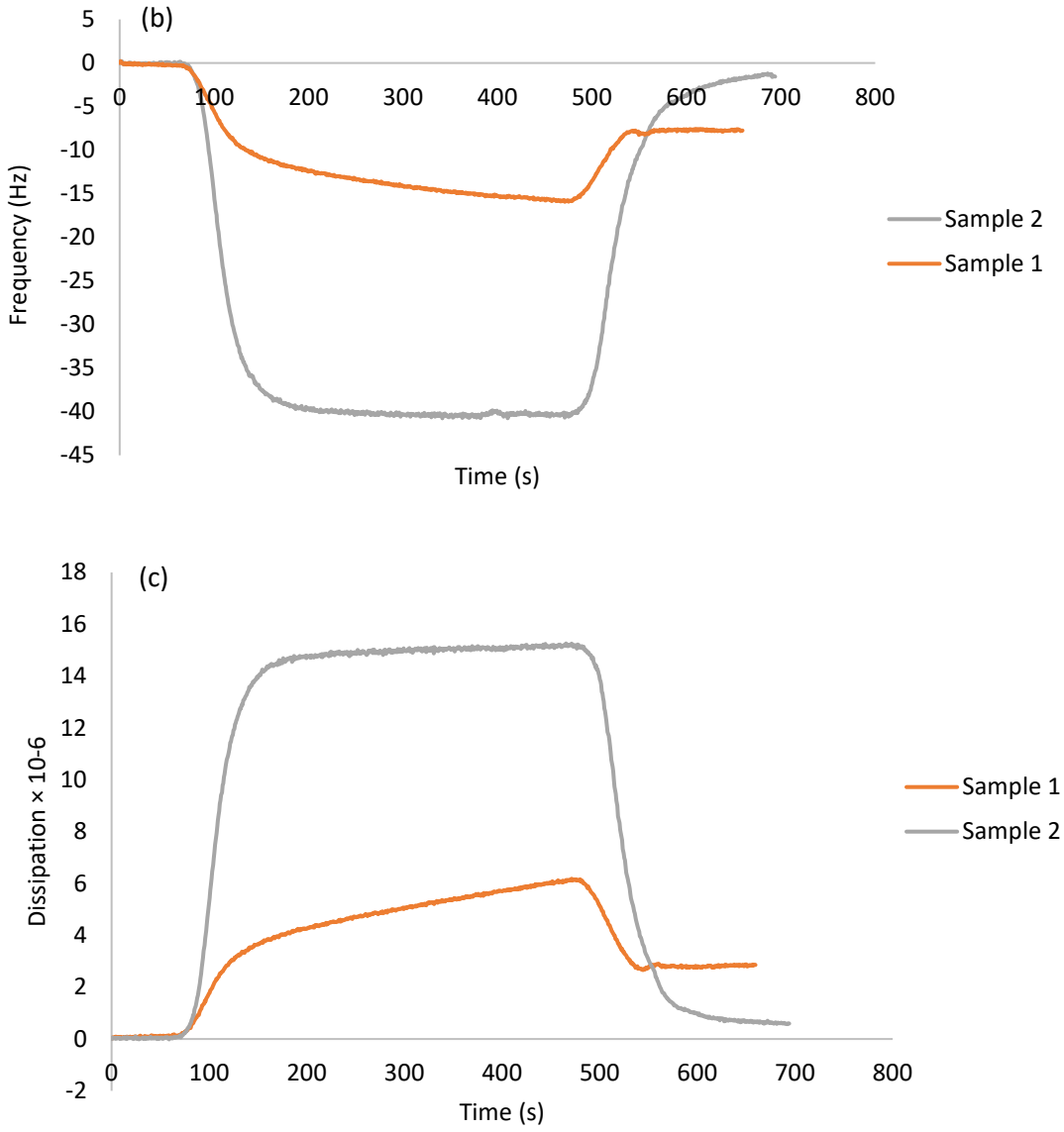

Figure 3.7. QCM results using acetic acid as buffer solution a) adsorbed mass change as a function of time, b) frequency change as a function of time, c) dissipation change as a function time

3.4.12 Scanning electron microscopy (SEM) analysis

The morphology of adsorbed mass for sample 2 on a stainless-steel coated sensor is shown in Figure 3.8 (a), while EDX spectrum is shown in Figure 3.8 (b). The primary elements of carbon and oxygen of hydrolysate constituents were detected. However, carbon and oxygen were not found in spectrum 2 in Figure 3.8 (c). These results confirmed the deposition of hydrolysate constituents on stainless steel coated sensor. As observed, the stainless-steel coated sensor was not fully covered with the components. The adsorbed components tended to form clusters with

different sizes, which were separated from one another. In the cluster, the white particles were connected with some dark/grey particles. As particles were not evenly deposited on the surface, and the surface of the sensor was designed to be flat, it may be concluded that the lignocelluloses were agglomerated initially in the hydrolysates and then the agglomerated particles were deposited on the surface. The dark color between the particles may provide evidence for a bonding effect of lignin for the agglomerated particles to the surface. However, further studies are required to prove this behavior. It was also observed that the morphology of adsorbed layer for sample 2 followed a similar pattern.

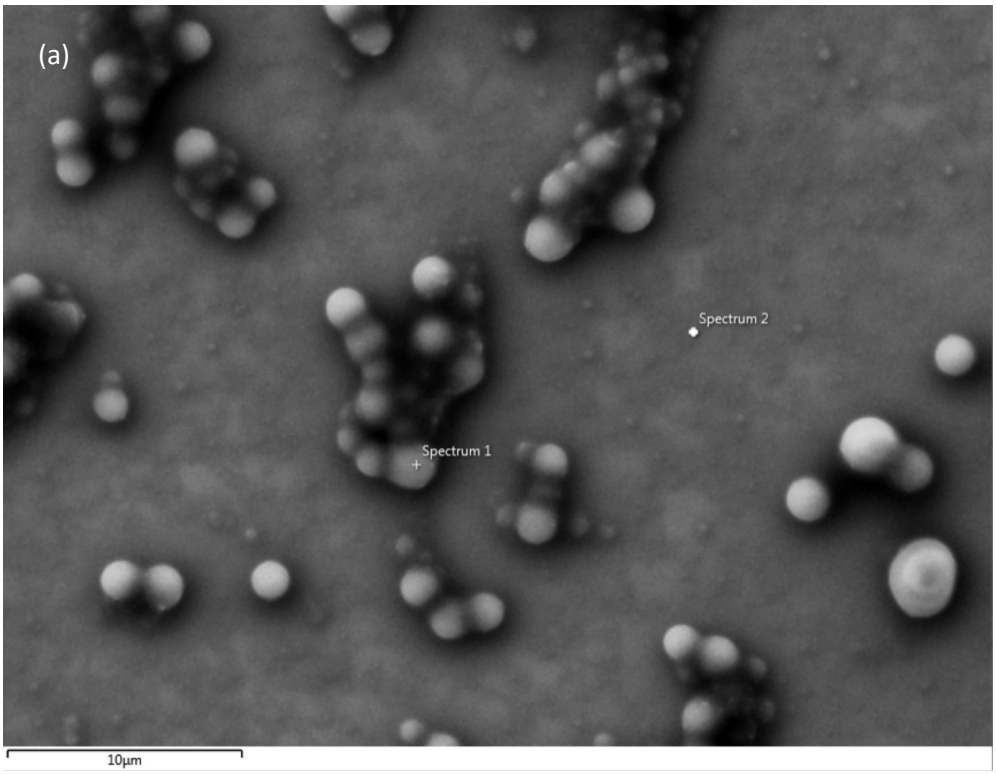

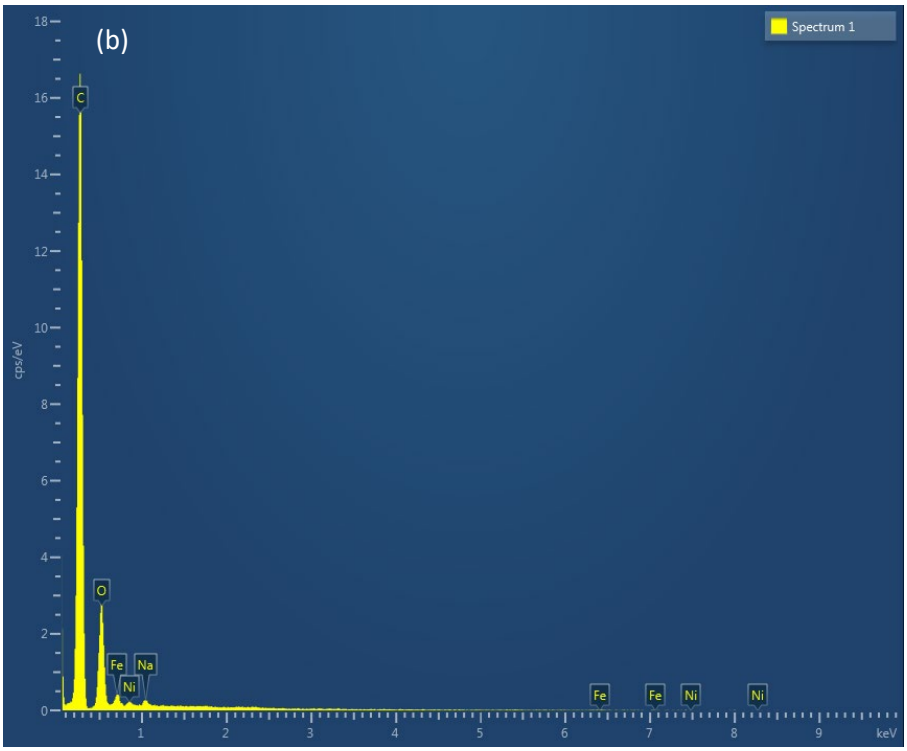

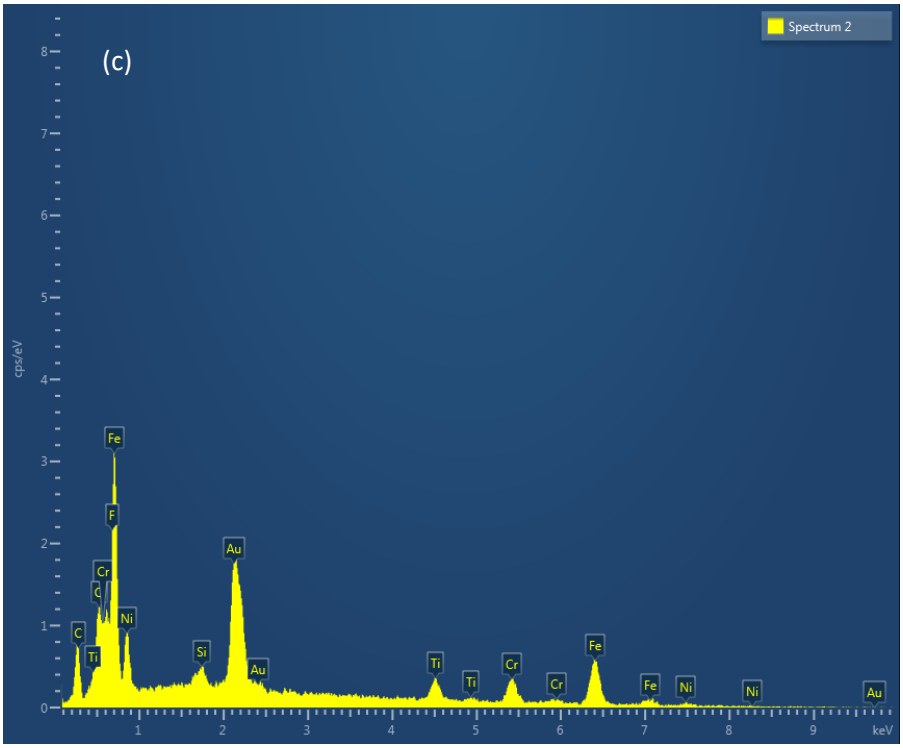

Figure 3. 8. (a) SEM image for the adsorption of hydrolysate components on stainless-steel coated QCM sensor without rinse step using HCL buffer solution, (b) EDX image of adsorbed polymers, (c) EDX image of stainless-steel surface.

3.5 Conclusion

The current study demonstrated that, at higher temperature and longer residence time, the extraction of lignin from softwood increased greatly, while a high liquid to solid ratio hampers the lignin extraction because of lower concentration of acetic acid in the hydrolysate. It was also found that a large portion of sugars were degraded at 170 to 180 ^{0}C. Based on ANOVA analysis, only temperature had a significant impact on furfural production. At the temperature range of 180 and 190 ^{o}C , most of hemicelluloses were presented as monosaccharides, which can be further degraded to furfural. Surprisingly, it was observed that all studied variables had strong impacts on the acetic acid production. Temperature increased the hydrodynamic size of hydrolysate's constituents. The addition of salt was helpful in preventing this agglomeration effectively. The smaller hydrodynamic size of hydrolysate's constituents under alkaline conditions was a sign of their better solubility and lower affinity for agglomeration. The agglomeration of hydrolysate constituents was reversible in hydrolysate. Based on QCM studies, the deposition of hydrolysate components on stainless steel was a reversible process. The greater deposition of components in the sample with higher concentration could be related to their higher hydrophilicity and low surface tension. Larger sized hydrolysate generated rigid structure probably due to long chain entanglement with the surface. The viscoelastic characteristics of adsorbed films did not change at the same pH regardless of strong or weak acid buffer solution. The SEM analysis demonstrated the deposition of agglomerated hydrolysate's components on the stainless-steel surface.

3.6 References

Ajao, O., Rahni, M., Marinova, M., Chadjaa, H., & Savadogo, O. (2017). Study of separation and fouling of reverse osmosis membranes during model hydrolysate solution filtration. *Membranes, 7*(68).

Al-Hamarneha, I., Pedrow, P., Eskhan, A., & Abu-Lail, N. (2012). Hydrophilic property of 316L stainless steel after treatment by atmospheric pressure corona streamer plasma using surface-sensitive analyses. *Applied Surface Science, 259*, 424–432.

Alipoormazandarani, N., & Fatehi, P. (2018). Adsorption characteristics of carboxymethylated lignin on rigid and soft surfaces probed by quartz crystal microbalance. *Langmuir, 34*(50), 15293-15303.

Azouz, K. B., Bekkour, K., & Dupuis, D. (2016). Influence of the temperature on the rheological properties of bentonite suspensions in aqueous polymer solutions. *Applied Clay Science, 123*, 92-98.

Beisl, S., Miltner, A., & Friedl, A. (2017). Lignin from micro- to nanosize: production methods. *International Journal of Molecular Sciences*, 18, 1244; doi:10.3390/ijms18061244.

Bi, X., Hemar, Y., Balaban, M. O., & Liao, X. (2015). The effect of ultrasound on particle size, color, viscosity and polyphenol oxidase activity of diluted avocado puree. *Ultrason. Sonochem., 27*, 567–575.

Carneiro-da-Cunha, M. G., Cerqueira, M. A., Souza, B. W., Teixeira, J. A., & Vicente∗, A. A. (2011). Influence of concentration, ionic strength and pH on zeta potential and mean hydrodynamic diameter of edible polysaccharide solutions envisaged for multinanolayered films production. *Carbohydrate Polymers , 85*, 522–528.

Chandrasekaran, N., Dimartino, S., & Fee, C. J. (2013). Study of the adsorption of proteins on stainless steel surfaces using QCM-D. *Chemical Engineering Research and Design, 91*, 1674–1683.

Chen, L., Zhou, X., Shi, Y., Gao, B., Wu, J., Kirk, T. B., & Jiake Xue, W. X. (2018). Green synthesis of lignin nanoparticle in aqueous hydrotropic solution toward broadening the window for its processing and application. *Chemical Engineering Journal, 346*, 217-225.

Dadi, A. P., Schall, C. A., & Varanasi, S. V. (2007). Mitigation of cellulose recalcitrance to enzymatic hydrolysis by ionic liquid pretreatment. *Applied Biochemistry and Biotechnology, 95*, 904–910.

Delbecq, F., Wang, Y., Muralidhara, A., Ouardi, K. E., Marlair, G., & Len, C. (2018). Hydrolysis of hemicellulose and derivatives—A review of recent advances in the production of furfural. *Frontiers in Chemistry, 6: 146*.

Deng, Y., Feng, X., Zhou, M., Qian, Y., Yu, H., & Qiu, X. (2011). Investigation of aggregation and assembly of alkali lignin using iodine as a probe. *Biomacromolecules, 12*, 1116–1125.

Dommelen, R. v., Fanzio, P., & Sasso, L. (2018). Surface self-assembly ofcolloidal crystals for micro- and nano-patterning. *Advances in Colloid and Interface Science, 251*, 97-114.

Eronena, P., Österberg, M., Heikkinen, S., Tenkanen, M., & Laine, J. (2011). Interactions of structurally different hemicelluloses with nanofibrillar cellulose. *Carbohydrate Polymers, 86*, 1281-1290.

Fatehi, P., Hamdan, F. C., & Ni, Y. (2013). Adsorption of lignocelluloses of pre-hydrolysis liquor on calcium carbonate to induce functional filler. *Carbohydrate Polymers, 94*(1), 531-538.

Fatehi, P., Ryan, J., & Ni, Y. (2013). Adsorption of lignocelluloses of model pre-hydrolysis liquor on activated carbon. *Bioresource Technology, 131*, 308-314.

Fritz, C., Salas, C., Jameel, H., & Rojas, O. J. (2017). Self-association and aggregation of kraft lignins via electrolyte and nonionic surfactant regulation: stabilization of lignin particles and effects on filtration. *Nordic Pulp & Paper Research Journal, 32*(4).

Galia, A., Schiavo, B., Antonetti, C., Galletti, A. M., Interrante, L., Lessi, M., & Valenti, O. S. (2015). Autohydrolysis pretreatment of Arundo donax: a comparison between microwave-assisted batch and fast heating rate flow-through reaction systems. *Biotechnol Biofuels, 8*, 218.

Garrote, G., Dominguez, H., & Parajo, J. C. (1999). Mild autohydrolysis: an environmentally friendly technology for xylooligosaccharide. *Journal of Chemical Technology and Biotechnology, 74*, 1101-1109.

Giummarella, N., Zhang, L., Henriksson, G., & Lawoko, M. (2016). Structural features of mildly fractionated lignin carbohydrate complexes (LCC) from spruce. *RSC Adv., 6*(48), 42120-42131.

Gütsch, J. S., Nousiainen, T., & Sixta, H. (2012). Comparative evaluation of autohydrolysis and acid-catalyzed hydrolysis of Eucalyptus globulus wood. *Bioresource Technology, 109*, 77-85.

Hamaguchi, M., Kautto, J., & Vakkilainen, E. (2013). Effects of hemicellulose extraction on the kraft pulp mill operation and energy use: Review and case study with lignin removal. *Chemical Engineering Research and Design, 91*, 1284–1291.

Hayes, M. H., Mylotte, R., & Swift, R. S. (2017). Chapter Two - Humin: Its Composition and Importance in Soil Organic Matter. In *Advances in Agronomy* (Vol. 143, pp. 47-138).

Hou, Q., Wang, Y., Liu, W., Liu, L., Xu, N., & Li, Y. (2014). An application study of autohydrolysis pretreatment prior to poplar chemi-thermomechanical pulping. *Bioresource Technology, 169*, 155-161.

Jansson, M., Danielsson, S., Saadatmand, S., Edlund, U., & Albertsson, A.-C. (2014). Upgrading of wood pre-hydrolysis liquor for renewablebarrier design: a techno-economic consideration. *Cellulose, 21*, 2045–2062.

Jiang, B., Zhang, Y., Guo, T., Zhao, H., & Jin, Y. (2018). Structural characterization of lignin and lignin-carbohydrate complex (LCC) from ginkgo shells (Ginkgo biloba L.) by comprehensive NMR spectroscopy. *Polymers, 10*(736).

Khazraie, T., Zhang, Y., Tarasov, D., Gao, W., Price, J., DeMartini, N., . . . Fatehi, P. (2017). A process for producing lignin and volatile compounds from hydrolysis liquor. *Biotechnol Biofuels 10:47 DOI 10.1186/s13068-017-0729-9*.

Leschinsky, M., Zuckerstatter, G., Weber, H. K., & Sixta, R. P. (2008). Effect of autohydrolysis of Eucalyptus globulus wood on lignin structure. Part 1: Comparison of different lignin fractions formed during water prehydrolysis. *Holzforschung, 62*, 645-652.

Li, D., Sevastyanova, O., & Ek, M. (2012). Pretreatment of softwood dissolving pulp with ionic liquids. *Holzforschung, 66*, 935–943.

Li, H., Fu, S., Peng, L., & Zhan, H. (2012). Surface modification of cellulose fibers with layer-by-layer self-assembly of lignosulfonate and polyelectrolyte: effects on fibers wetting properties and paper strength. *Cellulose, 19*, 533-546.

Li, M., Pu, Y., & Ragauskas, A. J. (2016). Current understanding of the correlation of lignin structure with biomass recalcitrance. *Frontiers in Chemistry, 4*.

Linder, Å., Bergman, R., Bodin, A., & Gatenholm, P. (2003). Mechanism of assembly of xylan onto cellulose surfaces. *Langmuir 2003, 19*, 5072-5077.

Liu, G., Feng, Q., Ou, L., Lu, Y., & Zhang, G. (2006). Adsorption of polysaccharide onto talc. *Minerals Engineering, 19*(2), 147-153.

Liu, H., Hu, H., Baktash, M. M., Jahan, M. S., Ahsan, L., & Ni, Y. (2014). Kinetics of furfural production from pre-hydrolysis liquor (PHL) of a kraft-based hardwood dissolving. *Biomass and Bioenergy, 66*, 320-327.

Liu, H., Hu, H., Jahan, M. S., & Ni, Y. (2015). Improvement of furfural production from concentrated pre-hydrolysis liquor (PHL) of a kraft-based hardwood dissolving pulp production process. *Journal of Wood Chemistry and Technology, 35*, 260-269.

Liu, H., Hu, H., Nairy, A., Jahan, M. S., Yang, G., & Ni, Y. (2013). Viscosity of prehydrolysis liquor of a hardwood kraft-based dissolving pulp production process. *Ind. Eng. Chem. Res., 52*, 3974−3979.

Liu, L., Chang, H.-m., Jameel, H., & Park, S. (2018). Furfural production from biomass pretreatment hydrolysate using vaporreleasing reactor system. *Bioresource Technology, 252*, 165-171.

Liu, L., Liu, W., Hou, Q., Chen, J., & Xu, N. (2015). Understanding of pH value and its effect on autohydrolysis pretreatment prior to poplar chemi-thermomechanical pulping. *Bioresource Technology, 196*, 662–667.

Liu, S., Lu, H., Hu, R., Shup, A., Lin, L., & Liang, B. (2012). A sustainable woody biomass biorefinery. *Biotechnology Advances, 30*(4), 785-810.

Liu, Z., Fatehi, P., Jahan, M. S., & Ni, Y. (2011). Separation of lignocellulosic materials by combined processes of pre-hydrolysis and ethanol extraction. *Bioresource Technology, 102*(2), 1264-1269.

López, F., García, M., Feria, M., García, J., Diego, C. d., Zamudio, M., & Díaz, M. (2014). Optimization of furfural production by acid hydrolysis of Eucalyptus globulus in two stages. *Chemical Engineering Journal, 240*, 195–201.

Lu, Y., Lu, C., Hu, H.-Q., Xie, F.-J., Wei, X.-Y., & Fan, X. (2017). Structural characterization of lignin and its degradation products with spectroscopic methods. *Journal of Spectroscopy*, 15.

Martinez, C. R., & Iverson, B. L. (2012). Rethinking the term “pi-stacking”. *Chemical Science, 3*, 2191–2201.

Micciulla, S., Dodoo, S., Chevigny, C., Laschewsky, A., & Klitzing, R. v. (2014). Short versus long chain polyelectrolyte multilayers: a direct comparison of self-assembly and structural properties. *Phys. Chem. Chem. Phys.,, 16*, 21988−21998.

Mishra, P. K., & Ekielski, A. (2019). The self-assembly of lignin and its application in nanoparticle synthesis: A short review. *Nanomaterials, 9*(243).

Norgren, M., Edlund, H., & Wågberg, L. (2002). Aggregation of lignin derivatives under alkaline conditions. kinetics and aggregate structure. *Langmuir, 18*, 2859-2865.

Oveissi, F., & Fatehi, P. (2015). Characterization of four different lignins as a first step toward the identification of suitable end-use applications. *J. Appl. Polym. Sci.*

Park, S.-J., & Seo, M.-K. (2011). Chapter 3 - Solid-Liquid Interface. In *Interface Science and Technology* (Vol. 18, pp. 147-252).

Patel, T. R., Harding, S. E., Ebringerova, A., Deszczynski, M., Hromadkova, Z., Togola, A., . . . Rowe, A. J. (2007). Weak self-association in a carbohydrate system. *Biophysical Journal, 93*, 741-749.

Qiu, X., Li, H., Deng, Y., & Ouyang, X. (2014). Influences of hydroxyl groups on the compactness of lignin adsorption layer. *Acta Polymerica Sinica, 9*, 1281-1285.

Ren, H., Dai, X., Huaming Zhai, Z. L., & Omori, S. (2015). Comparison of bamboo native lignin and alkaline lignin modified by phase-separation method. *Cellulose Chem. Technol, 49*((5-6)), 429-438.

Richter, A. P., Bharti, B., Armstrong, H. B., Brown, J. S., Plemmons, D., Paunov, V. N., . . . Velev, O. D. (2016). Synthesis and characterization of biodegradable lignin nanoparticles with tunable surface properties. *Langmuir, 32*, 6468−6477.

Salentinig, S., & Schubert, M. (2017). Softwood lignin self-assembly for nanomaterial design. *Biomacromolecules, 17*, 2649−2653.

Sarip, H., Hossain, M. S., N, M. A., & Allaf, K. (2016). A review of the thermal pretreatment of lignocellulosic biomass towards glucose production: autohydrolysis with DIC technology. *Bioresources, 11*(4).

Seemala, B., Haritos, V., & Tanksale, A. (2016). Levulinic acid as a catalyst for the production of 5-hydroxymethylfurfural and furfural from lignocellulose biomass. *ChemCatChem, 8*, 640 – 647.

Shen, J., Fatehi, P., Soleimani, P., & Ni, Y. (2012). Lime Treatment of prehydrolysis liquor from the kraft-based dissolving pulp production process. *Industrial & Engineering Chemistry Research, 51*(2), 662-667.

Shulga, G., Vitolina, S., Shakels, V., Belkova, L., Cazacu, G., Vasile, C., & Nita, L. (2012). Lignin separated from the hydrolyzate of the hydrothermal treatment of birch wood. *Cellulose Chemistry and Technology, 46*(5-6), 307-318.

Sipponen, M. H., Lange, H., Ago, M., & Crestini, C. (2018). Understanding lignin aggregation processes. A case study: Budesonide entrapment and stimuli controlled release from lignin nanoparrticles. *ACS Sustainable Chem. Eng., 6*, 9342−9351.

Sixta, H., Iakovlev, M., Hummel, M., Testova, L., Roselli, A., Hummel, M., . . . Schottenberger, H. (2013). Novel concepts of dissolving pulp production. *Cellulose, 20*, 1547–1561.

Song, T., Pranovich, A., Sumerskiy, I., & Holmbom, B. (2008). Extraction of galactoglucomannan from spruce wood with pressurised hot water. *Holzforschung, 62*(6), 659–666.

Striolo, A., Jayaraman, A., Genzer, J., & Hall, C. K. (2005). Adsorption of comb copolymers on weakly attractive solid surfaces. *The journal of chemical physics, 064710*.

Tarasov, D., Leitch, M., & Fatehi, P. (2018). Flow through autohydrolysis of spruce wood chips and lignin carbohydrate complex formation. *Cellulose, 25*(2), 1377–1393.

Tarasov, D., Leitch, M., & Fatehi, P. (2018). Lignin–carbohydrate complexes: properties, applications, analyses, and methods of extraction: a review. *Biotechnol Biofuels , 11:269*.

Tunc, M. S. (2014). Effect of liquid to solid ratio on autohydrolysis of eucalyptus globulus wood meal. *BioResources, 2*, 3014-3024.

Tunc, M. S., & Heiningen, A. R. (2009). Autohydrolysis of mixed southern hardwoods: Effect of P-factor. *Nordic Pulp and Paper Research Journal , 24 no. 1*, 42-47.

Tunc, M. S., Chheda, J., Heide, E. v., Morris, J., & Heiningen, A. V. (2014). Pretreatment of hardwood chips via autohydrolysis supported by acetic and formic acid. *Holzforschung, 68*(4), 401-409.

Wang, P., Fu, Y., Shao, Z., Zhang, F., & Qin, M. (2016). Structural changes to aspen wood lignin during autohydrolysis pretreatment. *BioResources, 11*(2), 4086-4103.

Wang, Q., Jahan, M. S., Liu, S., Miao, Q., & Ni, Y. (2014). Lignin removal enhancement from prehydrolysis liquor of kraft-based dissolving pulp production by laccase-induced polymerization. *Bioresource Technology, 164*, 380-385.

Westbye, P., Köhnke, T., Glasser, W., & Gatenholm, P. (2007). The influence of lignin on the self-assembly behaviour of xylan rich fractions from birch (Betula pendula). *Cellulose (2007), 14*(6), 603–613.

Yuan, T.-Q., Sun, S.-N., Xu, F., & Sun, R.-C. (2011). *Jo urnal of Agricultural and Food Chemistry, 59*, 10604–10614.

Zhao, J., Xiuwen, W., Hu, J., Liu, Q., Shen, D., & Xiao, R. (2014). Thermal degradation of softwood lignin and hardwood lignin by TGFTIR and Py-GC/MS. *Polymer Degradation and Stability, 108*, 133-138.

Zhu, L., Zhu, L., Murtaza, A., Liu, Y., Liu, S., Li, J., . . . Hu, W. (2019). Ultrasonic processing induced activity and structural changes of polyphenol oxidase in orange (Citrus sinensis Osbeck). *Molecules , 24*(1922).

Chapter 4: Polymerization of hydrolysate component

4.1 Abstract

In the present study, the hydrolysates generated via autohydrolysis of spruce wood chips were directly used as feedstock for producing coagulant. In-situ polymerization of acrylamide (AM) and lignocellulose (LC) of hydrolysates was successfully conducted, and the reaction was optimized to generate LC-AM with the highest molecular weight and charge density. NMR spectroscopy confirmed the grafting of acrylamide on LC. Other properties of product were characterized by elemental analyzer, zeta potential analyzer, gel permeation chromatography (GPC) and particle charge detector (PCD). To assess its application as a coagulant for dye pigments, LC-AM was combined with cationic polyacrylamide and anionic polyacrylamide in dual-coagulant systems. These results confirmed that the dual system of LC-AM and APAM led to a similar dye removal as the singular system of APAM, which was attributed to the multibranch structure of LC-AM benefitting bridging. However, the dual polymer system of LC-AM/CPAM was ineffective.

4.2 Introduction

Autohydrolysis has been considered as an inexpensive and environmental friendly method to fractionate biomass since it is a chemical-free process (Rigual et al., 2018). The hydrolysates from autohydrolysis treatment include mono-saccharides, oligo-saccharides, lignin, furfural, and acetic acid (Wu, 2016). Generally, autohydrolysis predominantly affects hemicellulose with less impact on the dissolution of lignin due to the recalcitrance nature of lignin. In hydrolysates, lignin is mainly covalent bound to hemicellulose forming a lignin-carbohydrate complex (LCC), which makes hydrolysis difficult (Tarasov et al., 2018; Wang et al., 2019).

Lignin, a renewable biomass composed of methoxylated phenylpropane structures, can be widely used as raw material for polymer production, especially for flocculant productions (Li et al., 2016). It was reporetd that a lignin based flocculant was produced via graft polymerization of dimethyl diallyl ammonium chloride (DMC) or etherification of 2, 3-epoxypropyl trimethyl ammonium chloride (GTA) (Guo et al., 2019). Hemicellulose is the second most abundent polysaccharides in biomass, and it has been regarded as an organic waste of forest industry (Zhang et al., 2014). However, hemicellulose has great potential to be applyed as the raw material for many applications, e.g., drug delivery, pharmaceutical field, plastic industry, waste

water treatment, tannery effluent treatment, and textile industry (Kumar et al., 2017). In the literature, xylan modified with (2-methacryloyloxyethyl) trimethyl ammonium chloride (DMC) was successfully used in flocculation/coagulation process (Chen et al., 2018). Hydrolysate has the potential to produce value-added products since lignin and hemicellulose exist in hydrolysates.

Recently, there is a growing interest in the development of novel flocculants by utilizing industrial and agricultural wastes as eco-friendly raw materials. Based on its functional groups and chemical properties, biopolymers have the potential to be converted to effective coagulants for wastewater treatment (Fang et al., 2010; Liu et al., 2008). Wang et al. (2009) reported a novel cationic chitosan-based flocculant (from fungi biomass) in the wastewater treatment exhibiting an excellent flocculation efficiency. In another work, Cassia obtusifolia seed was proved to be more effeicent than aluminum sulfate in the treatment of high strength agricultural and industrial wastewater (Shak & Wu, 2014).

Dye can be found in wasterwater effulents from various industries such as dye manufacturing, textile, cosmetics, pharmaceuticals, food, rubber, leather, printing, and pulp and paper, and it can cause seriouse environmental problem due to its complex structure and poor biodegradability (Wang et al., 2019). Dual coagulation systems have extensively been used in the wastewater treatment system because they are remarkably efficient, and generate smaller volume of sludge compared with the singular inorganic coagulant (Dotto et al., 2019; Chen et al., 2010). Inorganic-organic dual coagulants have been carried out in treating dye wastewater in the past. In one paper, the use of polyferric-chloride (PFC)- polydimethyldiallylammonium chloride (PDADMAC) resulted in 60.2% and 95.5% of the removal of Yellow k-4G and Yellow RGFL from simulated solutions, respectively (Wei et al., 2009). However, inorganic-organic systems usually require a high dosage and they are effective over a wide pH range. In a previous study, in order to simulate dual polyelectrolyte systems, polydiallyldimethylammonium chloride (polyDADMAC) (low molecular weight) was first introduced into wastewater and served as a destabilizer while polyacrylamide (PAM) (high molecular weight) was used as a bridging component (Ariffin et al., 2012). Moreover, it was reported that the dual system of starch and PAM in manicipal wastewater reduced the PAM dosage without affecting the flocculation kinetic and floc size (Lapointe & Barbeau, 2017). Therefore, the dual polymeric systems may be more promising alternatives to

signular coagulation/flocculantion systems. In this system, the dual polymers of hydrolysate-based polymer, cationic and anionic PAM may work as an effective coagulation system for dye removals.

This study aims at synthesizing the polymerization of lignocellulose (LC) of hydrolysate with acrylamide (AM) and the application of the product in the dye wastewater treatment. The experiments were conducted under different reaction times, temperatures, initiator dosages and AM/LC molar ratios. The properties of produced polymers (LC-AM) under optimal conditions were also characterized. LC-AM was used as a coagulant for the dye wastewater containing ethyl violet (EV) along with commercial polyacrylamides. The main novelties of this study were 1) the in-situ polymerization of hydrolysate constituents with acrylamide and 2) the use of LC-AM as a coagulant for the dye removal in singular and dual coagulant systems.

4.3 Materials and methods

4.3.1 Materials

Hydrolysis liquor was produced via autohydrolysis of spruce wood chips using a 2 L pulping digester (Greenwood Instruments, 2200). Acrylamide (98 wt.%), acrylic acid (99 wt.%), potassium persulfate (KPS), deuterium oxygen (D_2O) and ethyl violet (EV) with the charge density of 2.65 meq/g were obtained from Sigma-Aldrich. Ethanol (95 vol.%), acetone (98 wt.%), sulfuric acid (98 wt.%), and sodium hydroxide powder (97 wt.%) were purchased from Fisher Scientific. Decahydronaphthalene, mixture of cis and trans, cellulose acetate membrane tubes with a molecular weight cut-off of 10,000 g/mol were obtained from Wako Chemicals, Japan. Cationic polyacrylamide (CPAM) and anionic polyacrylamide (APAM) were purchased from Cambrian Solutions. The CPAM had a charge density of 3.31 meq/g and a molecular weight of 1024 kg/mol; whereas, the APAM had a charge density of -2.71 meq/g and a molecular weight of 6090 kg/mol.

4.3.2 Polymerization of hydrolysate's components

Hydrolysate containing 2.0 g of lignocellulosic material (oven dried) was introduced in a 250 mL three neck round bottom flask under stirring at 300 rpm. Once the optimal reaction time, temperature, initiator dosage, and AM/LC molar ratio were determined, the polymerizations of hydrolysate components were conducted using two different hydrolysis liquors. The required amounts of potassium persulfate and acrylamide were added into separate beakers with 10 mL of deionized water, and the products were stirred at 300 rpm. Once all the chemicals were completely dissolved, the solutions were purged under nitrogen for 20 min and the pH of the solutions were

adjusted to 3.5. The flasks were immersed into a water bath. Potassium persulfate solution was then charged into the flasks. When water was heated to the desired temperature, acrylamide was added into the flasks. The total volume of the solutions in the flasks was controlled at 60 mL. The flask was sealed with rubber or glass stoppers. A continuous supply of nitrogen was maintained throughout the reaction to prevent oxygen from the systems.

4.3.3 LC-AM purification

After polymerization, the solutions were cooled down to room temperature by immersing the flasks in tap water for 20 min. The solutions were added into an ethanol/water mixture (80/20 wt./wt.) dropwise using a pipette. After precipitating lignocellulose acrylamide polymer (LC-AM) from the mixtures, the precipitates were collected and washed again with ethanol solution three times to remove impurities. Afterward, the precipitated LC-AM was dissolved in 100 mL of deionized water, and the pH of the system was adjusted to 7. The dialysis was conducted to remove salt and monomer from the LC-AM polymer. The deionized water used for dialysis was changed every 6 hours for 2 days. After dialysis, the solutions were dried at 60 °C and the dried mass was considered as the final product of LC-AM.

4.3.4 Molecular weight analysis

The molecular weight of LC-AM was measured using a gel permeation chromatography (GPC), Malvern GPCmax VE2001 Module+Viscotek TDA305 equipped with multi-detectors and PolyAnalytic PAA206 and PAA203 columns. The solution of LC-AM was prepared by mixing 1 g of dried LC-AM in 20 mL of 0.1mol/L $NaNO_3$. The solution was agitated at 300 rpm for 12 hours. The solution of 0.1 mol/L $NaNO_3$ was utilized as solvent and eluent. In the measurements, column temperature of the GPC was set at 35 °C and the flow rate was set at 0.70 mL/min.

4.3.5 Charge density of LC-AM

About 0.2 g of LC-AM polymer was added to 20 mL of deionized water. In order to dissolve all of the polymers, the solutions were shaken in a water bath shaker (Innova 3100, Brunswick Scientific, Edison, NJ, USA) for 2 h at 30 °C and 150 rpm. A particle charge detector (Mütek PCD 04, Arzbergerstrae, Herrsching, Germany) with 0.005M PDADMAC solution was used to determine the charge density of the prepared solutions.

4.3.6 Characterization of LC-AM

The yield of LC-AM was calculated using Equation 4.1:

$$Y\ (\%) = \frac{W_1}{W_2 + W_3} \times 100\% \quad [4.1]$$

where W_1 is the weight of LC-AM, W_2 is the weight of the dry hydrolysate, W_3 is the weight of the monomer, and Y (%) is the yield (wt.%).

The grafting ratio of acrylamide on LC-AM was determined using Equation [4.2]

$$G\ (\%) = \frac{\frac{n}{19.7}}{1 - \frac{n}{19.7}} \quad [4.2]$$

where n is the nitrogen content (wt.%) of LC-AM, which was obtained using a vario EL cube elemental analyzer (Elementar, Germany), 19.7 is the nitrogen content (wt.%) in acrylamide repeating units attached to the lignin carbohydrate and $G\ (wt\%)$ is the grafting ratio.

4.3.7 Effect of furfural and acetic acid on polymerization

To explore the effect of furfural and acetic acid on the polymerization, 3 additional control experiments were carried out. In the first experiment, 6 g of acrylamide and 0.03 g of KPS were reacted at 80 °C, 3 hours, pH of 3.5 (adjusted using sulfuric acid). In the second experiment, 6 g of acrylamide and 0. 03 g of KPS were reacted at 80 °C, for 3 hours, and at pH of 3.5. In the third experiment, 6 g of acrylamide, 0.03 g of KPS, and 0.4 g of furfural were reacted at 80 °C, 3 hours, pH of 3.5. All the experiments were conducted in oxygen free environment by purging with nitrogen. After the reactions, the unreacted acrylamide and salts in the samples were removed by membrane dialysis. The final samples were dried at 60 °C and the molecular weights of these samples were determined by GPC.

4.3.8 H^1NMR

The spectra of LC-AM and hydrolysate constituents were obtained using a nuclear magnetic resonance (NMR) spectroscopy (Varian Unity Inova 500 MHz) with the pulse angle of 45° and a relaxation time of 1.0 s. The samples were prepared by adding 0.1 g of freeze-dried LC-AM into 1 mL of D_2O in a small vial. The final solution was stirred at 100 rpm for 30 mins and transferred into a 5 mm NMR tube.

4.3.9 Dye removal efficiency

The concentration of ethyl violet dye in the solution was also determined using the UV instrument at a wavelength of 595 nm. The flasks were shaken in an incubator shaker at 150 rpm and 30 °C

for 30 min. The mixtures were centrifuged at 3000 rpm for 10 min. The supernatants of the mixtures were collected in order to determine the concentration of the EV using a UV–vis spectrophotometer at 595 nm wavelength. Color removal efficiency was evaluated by comparing the concentration of EV using a calibration curve using Equation [4.3]

$$R\ (\%) = \frac{C_0 - C_f}{C_o} \times 100 \qquad [4.3]$$

where C_0 is the concentration of EV in original dye solution, C_f is the concentration of EV after the treatment, and $R\ (\%)$ is the dye removal efficiency.

4.3.10 Singular coagulant system

The LC-AM solution was prepared by mixing LC-AM polymers in deionized water (1 g/L). The dye solution was also prepared by adding 250 mg of ethyl violet (EV) powder into 1 L of deionized water. It was stirred at 300 rpm for 6 h. LC-AM solutions with different dosages ranging from 0.06 to 1 g/g dye were added to different Erlenmeyer flasks containing 10 mL of dye solution. The total volume of the mixtures was kept at 25 mL by adding deionized water. The color removal efficiency analysis was conducted for all the LC-AM/dye mixtures. The optimum dosage of LC-AM for singular coagulant system was obtained when highest dye removal was obtained. Using the same procedure, the removal of dye by APAM and CPAM was also analyzed.

4.3.11 Dual coagulants system

Firstly, LC-AM was mixed with 10 mL of dye solution in Erlenmeyer flasks at the optimal dosage achieved for the singular coagulant system. Secondly, different amounts of APAM solution (1 g/L) were added to the flasks that contained LC-AM and dye in different flasks. The total volume of the mixtures was kept at 25 mL by adding deionized water. The optimal dosages of APAM/LC-AM dual coagulant systems were determined based on the dye removal efficiency of the final solution. The optimal dosage of CPAM/LC-AM dual coagulant systems were determined using the same procedure.

4.3.12 Zeta potential analysis

After shaking the dye and coagulant mixtures incubated at 150 rpm and 30 °C for 30 min, the large particles in the final solution were removed by a syringe filter (0.22 μm opening). The filtrates were diluted 10 times with 1mM KCl and transferred into cuvettes. Then, their zeta potential was

characterized by a NanoBrook Zeta PALS (Brookhaven Instruments Corp, USA). The measurements were conducted in triplicates and the mean values were used in this study.

4.4 Results and discussion

4.4.1 Characterizations of hydrolysates

The compositions of two dry hydrolysates are shown in Table 4.1. Sample 1 and sample 2 were produced from autohydrolysis of spruce wood at a high temperature. While sample 1 was rich in lignin and furfural, sample 2 was rich in hemicellulose and acetic acid. Sample 1 was more concentrated than sample 2 because of lower liquid to solid ratio in the autohydrolysis process. Sample 1 was used to determine the optimum polymerization condition with changing variables such as residence time, initiator dosage, temperature, monomer dosage. Afterwards, samples 1 and 2 were applied to investigate the effect of hydrolysates composition on grafting polymerization at the determined optimum conditions.

Table 4.1. Compositions of the hydrolysates used in polymerizing with acrylamide

	Lignin (wt.%)	Polysaccharides (wt.%)	Furfural (wt.%)	Acetic acid (wt.%)	Temperature (°C)	Residence time (min)	Liquid to solid ratio (g/g)
Sample 1	45.13	32.27	19.34	3.26	190	15	5
Sample 2	36.34	45.69	4.36	13.63	180	45	20

4.4.2 Mechanism of polymerization

Figure 4.1 shows the mechanism of graft polymerization of lignocellulose of hydrolysate with acrylamide, which is initiated by potassium persulfate ($K_2S_2O_8$). The sulfate radical is produced from the decomposition of the initiator ($K_2S_2O_8$) when subjected to heat. The sulfate radicals can take the unstable hydrogen from phenol group of both lignin and carbohydrate to form phenoxyl radicals, serving as reaction sites for the polymerization. Then, the active sites attract the acrylamide to propagate a polymeric chain. The grafted monomer works as free radical donors to offer free radicals to neighboring molecules in order to prolong the grafted chain (Ren et al., 2014). In termination stage, lignin/sugar polymer can be further coupled with a propagating acrylamide or another lignin/sugar polymer. The sulfate radicals can initiate side reactions to homopolymerize vinyl monomer (Wang et al., 2016).

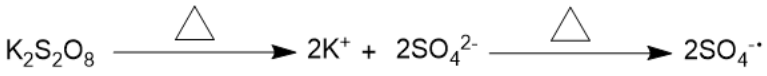
K2S2O8
2K+ + 2SO4 2-
2SO4 -•

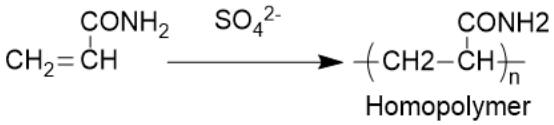
CONH2
CH2=CH
SO4 2-
CONH2
CH2–CH
n
Homopolymer

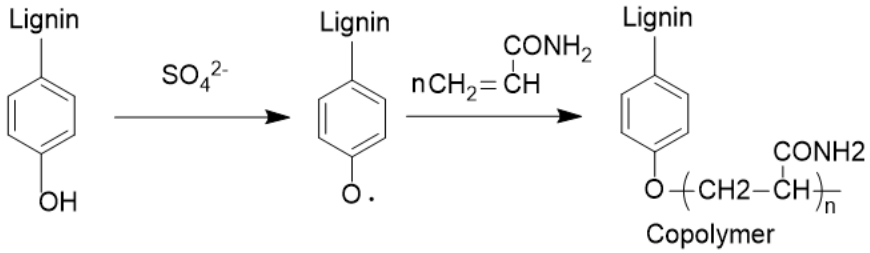
Lignin
OH
SO4 2-
Lignin
O.
nCH2=CH
CONH2
Lignin
O
CH2–CH
CONH2
n
Copolymer

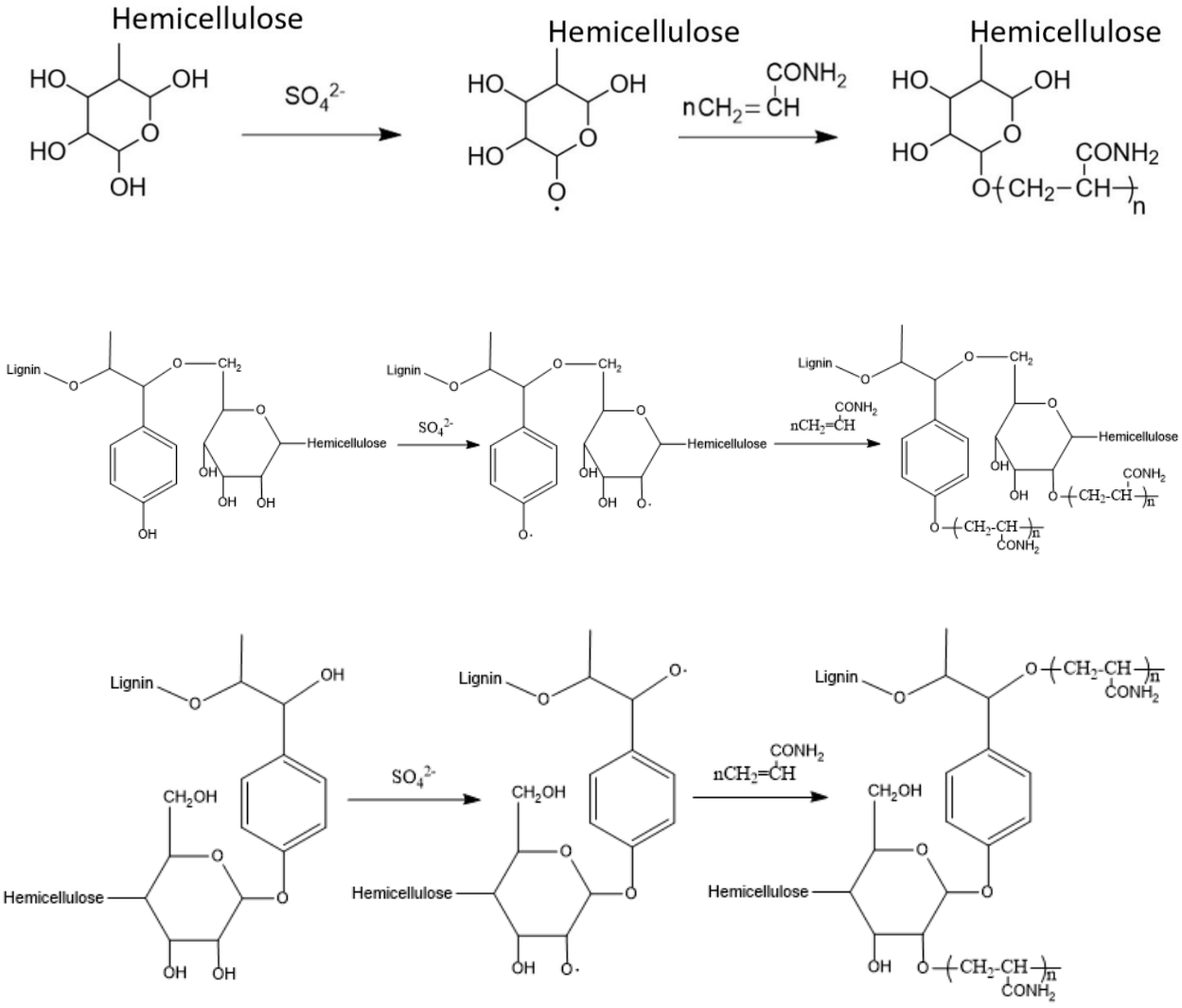

Figure 4.1. Mechansim of polymerization of lignocellulose with acrylamide

4.4.3 Effect of residence time on polymerization

Figure 4.2 (a) shows the impact of process conditions on the yield and grafting ratio of the polymerization reaction. The yield and grafting ratio gradually increased as reaction time was extended to 3 hours. The maximum yield (30.7%) and grafting ratio (358.1%) were achieved for 3 h of reaction. When the reaction time was further prolonged, the yield and grafting ratio barely changed. This indicated that propagation process was completed in 3 hours, as the concentration of acrylamide dropped with elapsing time (Fang et al., 2009). As the reaction time extended to 4

h, the yield and grafting ratio did not significantly increase. The properties of produced polymers are shown in Table 4.2. The molecular weight of polymers produced in 4 hours is only slightly larger than that produced in 3 h. Considering the production yiled, 3 hours was more reasonable to be considered as the optimized residence time.

4.4.4 Effect of initiator dosage on polymerization

The grafting polymerization was carried out at different initiator dosages varying from 1.5 wt. % to 6 wt. % as depicted in Figure 4.2 (b). The yield and grafting ratio increased when the initiator dosage increased from 1.5 wt. % to 4 wt. % based on the dried mass of hydrolysate. The maximum yield was 54.25% while the maximum grafting ratio was 657.69% at the initiator dosage of 4 wt.%. The yield and grafting ratio were leveled off when the initiator dosage was beyond 4 wt. %. This phenomenon could be due to the competition between initiation and termination reactions through chain-transfer reactions and coupling between initiator radicals (Li and Zhou, 2017). Table 4.2 also lists the molecular weight of the polymers produced at different initiator dosages. The largest molecular weight was 36,724 g/mol produced at the initiator dosage of 4 wt. % based on the dried mass of hydrolysate. At a high initiator dosage, the formation of homopolymer (polyacrylamide) was probably favored more than that of polymerization with lignin and carbohydrate (Maia et al., 2012).

4.4.5 Effect of temperature on polymerization

The variations in yield and grafting ratio as functions of the reaction temperature are shown in Figure 4.2 (c). They increased with elevating temperature from 40 to 60 °C. It was reported that the decomposition of the initiator at an elevated temperature was promoted, providing more free radicals that could improve the rate of initiation and propagation of the grafting chain (Mahdavi et al., 2011). The maximum yield and grafting ratio observed at 60 °C were 53.3% and 603.5%, respectively. In the range of 60 to 70 °C, the yield and grafting ratio declined significantly, due to the shorter half-life of the initiator, which caused a higher termination rate and lower polymerization rate (Ibrahim et al., 2014). The maximum molecular weight occurred at 60 °C, thus the optimal temperature for polymerization was considered at 60 °C.

4.4.6 Effect of monomer dosage on polymerization

The trend of yield was consistent with that of grafting ratio when the molar ratio of acrylamide to dried hydrolysates increased from 1.18 to 5.63. This result may be attributed to the higher

concentration of acrylamide leading to higher chance of collision with hydrolysate's constituents, thus improving the polymerization. However, when the molar ratio was greater than 5.63, the grafting ratio significantly decreased. This was probably ascribed to the domination of polyacrylamide formation. Interestingly, when molar ratio was further increased, the polymeric solution transferred from liquid phase to a gel-like phase. It was reported in another article that acrylamide was grafted onto oil palm empty fruit bunch fiber in 90 min, after which the reaction mixture became gel (Ibrahim et al., 2005). It was observed that the grafting ratio was leveled off while the yield increased when the molar ratio was greater than 5.63. At 6.53 AM/LC, the molecular weight of the product was lower in contrast to the product produced at 5.63 AM/LC. These results can prove that, due to the formation of polyacrylamide intensively at high LM/LC molar ratio, less acrylamide was grafted on the hydrolysates' components.

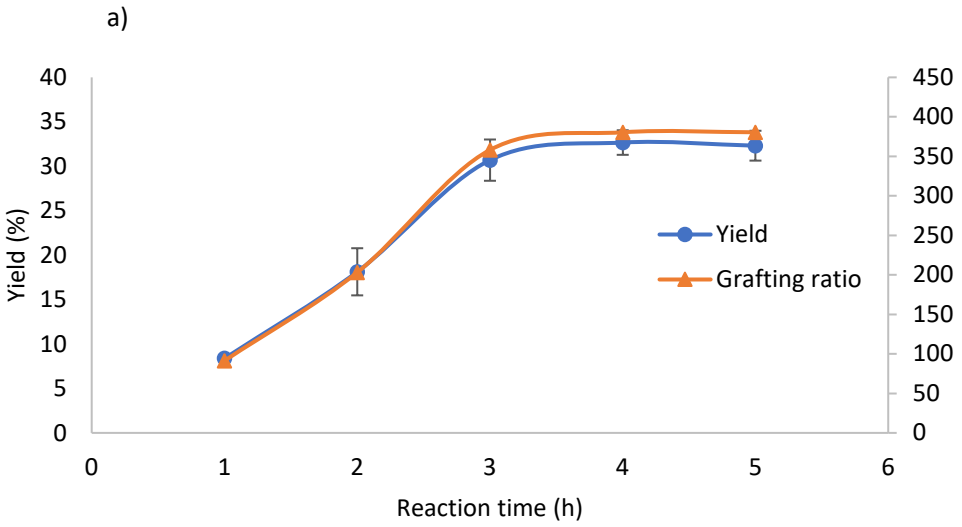

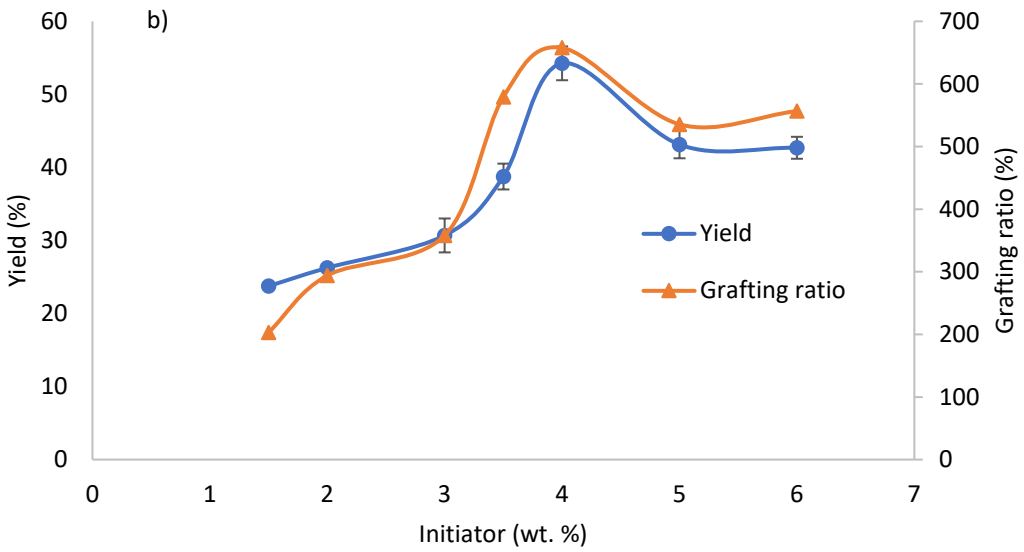
b)
Yield (%)
Grafting ratio (%)
Initiator (wt. %)
Yield
Grafting ratio
0
10
20
30
40
50
60
0
100
200
300
400
500
600
700
0
1
2
3
4
5
6
7

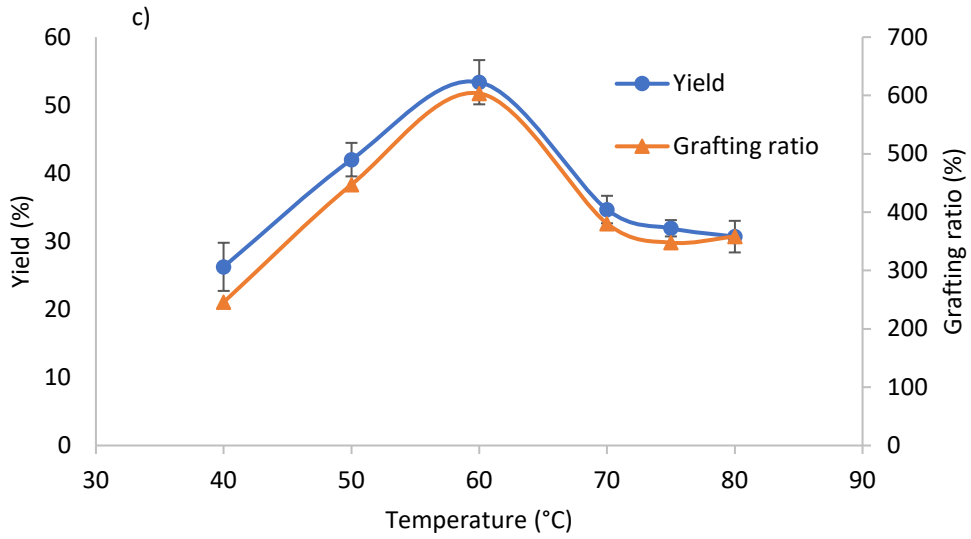
c)
Yield (%)
Grafting ratio (%)
Temperature (°C)
Yield
Grafting ratio
0
10
20
30
40
50
60
0
100
200
300
400
500
600
700
30
40
50
60
70
80
90

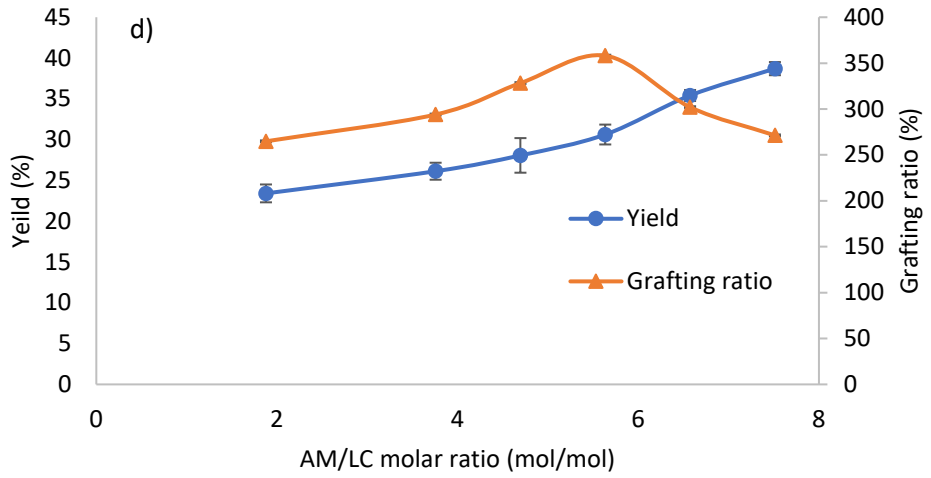

Figure 4.2. a) Effect of reaction time on grafting polymerization (experimental condition: 80 ℃, 3 wt.% initiator based on total mass of hydrolysate, 5.63 AM/LC molar ratio, pH 3.5); b) Effect of initiator dosage on grafting polymerization (experimental condition: 80, 3 hours, 5.63 AM/LC molar ratio, pH 3.5); c) Effect of temperature on grafting polymerization (experimental condition: 3 hours, 3 wt.% initiator based on total mass of hydrolysate, 5.63 AM/HL molar ratio, pH 3.5;) d) Effect of monomer dosage on copolymerization (experimental condition: 80 ℃, 3 wt.% initiator based on total mass of hydrolysate, 3 hours, pH 3.5)

Table 4.2 shows the molecular weight of 12 synthesized polymers at different reaction conditions. The conditions were selected corresponding to the peak point and the adjacent points of each figure in Figure 4.2. The reaction time and AM/LC molar ratio had limited impact on the molecular weight of the polymers. Initiator dosage and temperature effectively influenced grafting polymerization. At the moderate initiator dosage or temperature, the molecular weight of the polymer was increased above 33000 g/mol. The results of Figure 4.2 also indicate that the initiator dosage and temperature were more impactful than other parameters on the polymerization. The higher molecular weight of polymers also validated the effect of the optimum conditions.

Table 4.2 The effects of operating variables on the molecular weight of product

Run	Temperature ºC	Initiator dosage (wt. %)	Residence time (h)	AM/LC molar ratio (mol/mol)	pH	Molecular weight (g/mol)
1	80	3	2	5.63	3.5	22732
2	80	3	3	5.63	3.5	25848
3	80	3	4	5.63	3.5	26359
4	80	3	3	5.63	3.5	25848

5	80	4	3	5.63	3.5	36724
6	80	5	3	5.63	3.5	32913
7	50	3	3	5.63	3.5	27425
8	60	3	3	5.63	3.5	33223
9	70	3	3	5.63	3.5	24821
10	80	3	3	3.75	3.5	20419
11	80	3	3	5.63	3.5	25848
12	80	3	3	6.53	3.5	24573

4.4.7 Optimization

Table 4.3 shows the yield, grafting ratio, molecular weight and charge density of LC-AM prepared at the optimum conditions, which were 3 hours, 60 ºC, 4 wt.% initiator based on dried mass of hydrolysate, an AM/LC molar ratio of 5.63. The maximum yield, grafting ratio and molecular weight were 58%, 670.4% and 41057 g/mol, respectively. The LC-AM1 prepared from sample 1 and LC-AM2 from sample 2 had very weak negative charges. The yield and molecular weight obviously enhanced comparing to molecular weights listed in Table 4.2. Interestingly, the LC-AM1 had a greater yield, grafting ratio and molecular weight than did LC-AM2. These results revealed that the LC-AM1 had longer polymer chains. As explained in the previous section, sulfate radicals removed hydrogen from phenolic hydroxyle group, generating radicals for the interactions with acrylamide polymer chains. However, in one study, acrylic acid was able to graft on aliphatic groups in the presence of phenolic group of lignin (Kong et al., 2015). Hemicellulose contains primarily aliphatic hydroxy group (Ben et al., 2018). Hence, acrylamide has a higher possibilty to be grafted on lignin than on hemicellulose. The higher yield and grafting ratio of LC-AM1 was probably due to the fact that lignin was dominant in LC-AM1 and hemicellulose was dominant in LC-AM2 (Table 4.1).

Table 4.3 shows the molecular weight of polyacrylamide with or without acetic acid and furfural in the reaction of polymerization of acrylamide without hydrolysates. The molecular weight of acrylamide produced under the conditions of 3 hours, 80 °C, and pH of 3.5 was 530485 g/mol. With the interference of acetic acid, the molecular weight of polyacrylamide reduced to 301173 g/mol. Although the polymerization degree was lower in presence of acetic acid, a number of polyacrylamides were still formed in the reaction judging by the its high molecular weight. However, when furfural was added to the reaction, the molecular weight of polyacrylamide was 69392 g/mol, indicating that furfural was effective in inhibiting the formation of acrylamide. As

seen in Table 4.2, when hydrolysates reacted with acrylamide under similar conditions, the molecular weight was much lower (69392 g/mol). This may provide evidence that no homopolymer was produced in the polymerization of hydrolysate with acrylamide. The carboxyl group of the carbohydrate content was the primary reason for the weak negative charge density of LC-AM1 (Ren and Omori, 2014). The yields of polyacrylamide were increased with increasing molecular weight. PAM 1 had a yield of 89.4% indicating the majority of acrylamide was polymerized in the reaction. PAM 3 had a yield of 26.5% confirming the inhibition effect of furfural in the polymerization of acrylamide.

Table 4.3. Properties of LC-AM produced at the optimal conditions and the properties of PAM produced with or without of acetic acid and furfural

	Yield (%)	Grafting ratio (%)	Molecular weight (g/mol)	Charge density (meq/g)
LC-AM1	58.4	670.4	41057	-0.252
LC-AM2	56.7	648.2	38642	-0.237
PAM 1	89.4	N/A	530485	-0.243
PAM 2	67.4	N/A	301173	-0.231
PAM 3	26.5	N/A	69392	-0.238

4.4.8 ^{1}H-NMR of LC-AM

Figure 4.3 shows the ^{1}H-NMR spectra of LC1 and LC-AM1 produced under optimized conditions. In the spectrum of LC1, the peaks in the region of 2.00-2.20 ppm belonged to acetic acid. It was observed that some peaks in the region from 3.0 to 4.5 ppm were attributed to the protons of lignin and hemicellulose (Chiarinia et al., 2004; Saeed et al., 2011). In the spectrum of LC-AM1, the peaks at 3.34 and 3.65 ppm were assigned to protons in the methoxy groups of lignin. The peaks between 4.6 and 5.0 ppm were corresponded to solvent D_2O (Wang et al., 2016). It was observed that the peaks at 1.65, 1.78, 2.22 and 2. 35 ppm labeled as 1, 2, 3 and 4 were not shown in the spectrum of LC1. These peaks were attributed to the protons in the methenyl connected to the amide group of arylamide (Dong et al., 2012). The sepctra for sample 2 (available in Appendix Figure A1) followed a similar pattern to that of sample 1. It was confirmed that acrylamide was successfully grafted on lignocelluloses at the optimum conditions.

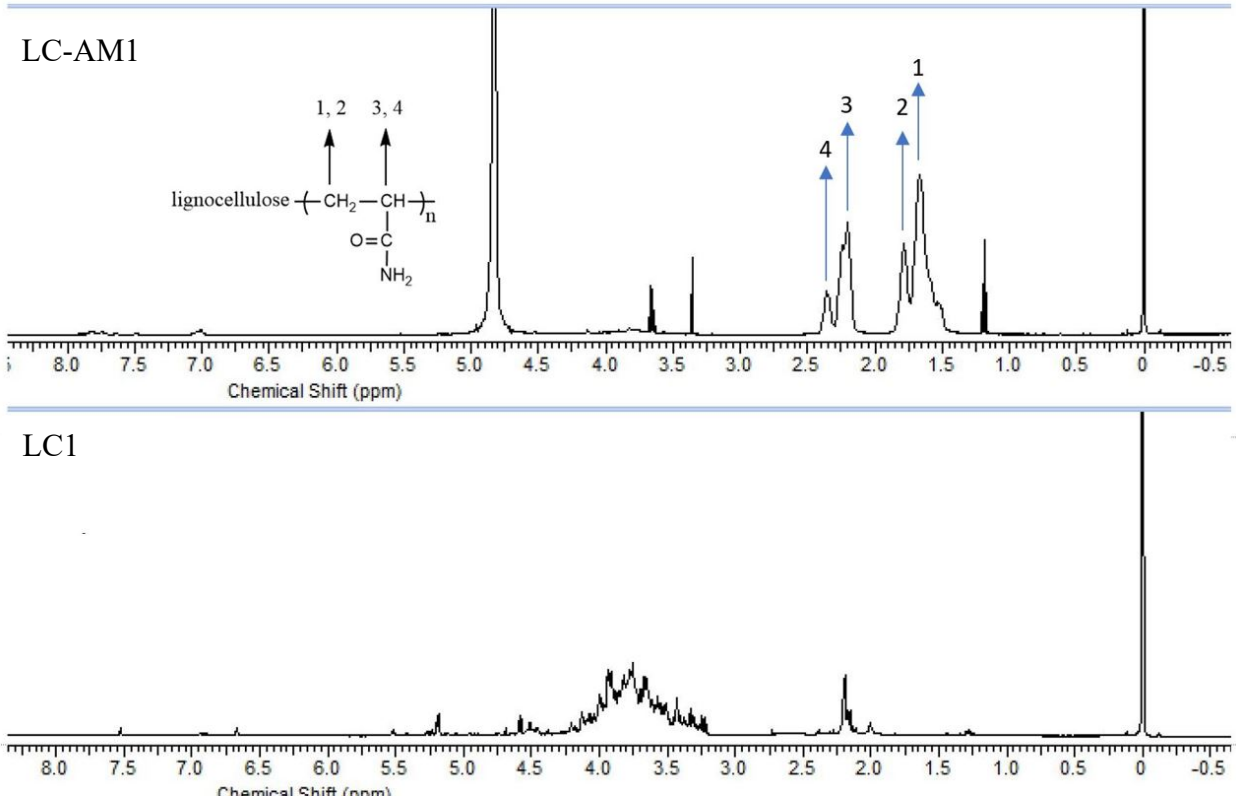

Figure 4.3. ^{1}H-NMR spectra of LC1 and LC-AM1 (generated at 60 ^{0}C, 4 wt.% initiator based on total mass of hydrolysate, 3 hours, 5.63 AM/HL molar ratio, pH 3.5)

4.4.9 Dye removal in singular systems

In Figure 4.4 (a), dye removal and zeta potential of solutions were illustrated as a function of LC-AM dosage. It was observed that the dye removal increased from 20.3% to 47.21% and zeta potential decreased from 25 mV to 6.4 mV when the dosage of LC-AM was increased from 0.06 g/g dye to 0.2 g/g dye. In this case, 0.2 g/g of LC-AM/dye was the optimal dosage achieving the maximum dye removal effciency in the EV solution. The dye solution had the charge density of 2.65 meq/g, while LC-AM had that of -0.252 meq/g. Theoretically, the dosage of LC-AM should be 10.5 g/g dye to naturalize the cationic particles in dye solution. In this set of experiments, only 1 g/g of LC-AM/dye could reduce the zeta potential of dye dispersions to 3.9 mV, implying that LC-AM did not interact with dye particles stoichiometrically. In addition to charge neutralization, bridging between dye and LC-AM may be contributed to the interactions of LC-AM with dye molecules, which was due to the interaction of π-electron originating from the anthraquinone group of EV and hydroxy group of lignocellulose (Zafar et al., 2015). Furthermore,

hydrophobic/hydrophobic interaction with dye particles were developed by the aromatic part and hydroxy group of lignocellulose (Razali et al., 2012).

The effect of CPAM dosage on the dye removal and zeta potential of the EV solution is displayed in Figure 4.4 (b). The zeta potential of the colloidal system as increased from 26mV to 39 mV when the CPAM dosage increased from 0.14 g/g to 1.6 g/g dye. As previously mentioned, CPAM and EV both carried a positive charge. Therefore, no charge neutralization was involved in this test and electrical repulsion force stabilized the system. Furthermore, bridging effect may occur with polyelectrolytes carrying the same amount of charge as the dye molecules (Gregory and Barany, 2011). The maximum dye removal was 29.8% when 0.6 g/g of CPAM/dye was added to the system. As stated in the experimental section, the molecular weight of CPAM was 1024 kg/mol, which was much larger that of LC-AM1. High molecular weight of this polymer favored coagulation of CPAM and EV through bridging mechanism (Hasan and Fatehi, 2018; Lee and Schlautman, 2015). When the zeta potential further increased from 36 to 39 mV, the agglomeration was greatly restricted by electrostatic repulsion force resulting a decrease in dye removal.

Figure 4.4 (c) shows the changes in the dye removal and zeta potential as a function of APAM dosage. The overall dye removal increased as a function of APAM dosage, which was in accordance with the reduction in the zeta potential. It was observed that the dye removal dramatically increased to 63% when the zeta potential approached zero. The alteration of zeta potential to zero could be the result of electrostatic neutralization of dye pigments in the presence of oppositely charged polyelectrolytes (Bouyer et al., 2001). The optimal coagulant dosage was 0.8 g/g dye at the maximum dye removal efficiency of 80%. The maximum dye removal efficiency was not occurred at zeta potential of zero, implying both charge neutralization and bridging were contributed to the removal of dye particles. When the zeta potential further went down below zero, the increment in dye removal was relatively slow. This was due to the overdosed APAM which caused charge reversal and repulsion force to hinder the interactions with dye molecules (López-Maldonado et al., 2014). As stated previously, the high molecular weight polymer would promote bridging effect among the dye particles, which would dominate the slow dye removal regime. As metioned in the experimental section, APAM had a molecular weight of 6090 kg/mol, which was 6 times larger than that of CPAM. This would be one of the reason for high dye removal when applying APAM.

To understand the performance of LC-AM/CPAM dual coagulation system in the EV solution, dye removal and zeta potential were plotted as a function of total coagulant dosage in Figure 4.4 (d). Dye removal efficiency reached its maximum value of 35 mV, which was even lower than that in the singular system of LC-AM1. The zeta potential and coagulant dosage at the maximum dye removal were 32 mV and 0.7 g/g dye (0.2 g LC-AM and 0.5 g CPAM/g dye), respectively. The zeta potential of LC-AM/CPAM dual coagulation system was lower than that for the singular system of CPAM and LC-AM1. Thus, the dye removal efficiency for the dual system lied between the singular coagulant systems. Similarly, the major coagulation mechanism of this experiment was bridging because the zeta potential never approached zero, while the removal was significant. However, this dual system was not very effective in removing EV since only 35% of dye was removed.

Figure 4.4 (e) depicts the dye removal and zeta potential of EV solution in the presence of dual coagulants at different dosages. At dual coagulant dosage of 0.8 g/g and 1 g/g, the dye removal efficiencies were 75.8 and 78.7%, respectively. In general, the bridging effect was more pronounced when the polymer had a high molecule weight and charge density (Wang et al., 2018). Although APAM had a much higher charge density and molecular weight than did LC-AM, dual coagulants obtained similar or slightly lower efficiency than did APAM. As it was proposed that PAM had a linear structure, the flocs formed by PAM and dye particles were probably loosely bridged (Lee et al., 2014). LC-AM had a multibranched structure leading stronger bridging and more compact flocs which weakened re-stabilization effect at high zeta potential of the dye suspensions (Zhou et al., 2019; Duval and Lawoko, 2014). In this case, LC-AM may have prevented APAM in flocculation with the dye, and thus it reduced its efficiency in coagulating the dye particles, as some were coagulated with LC-AM1 instead of APAM, and Figure 4a and 4c show that the coagulation efficiency of LC-AM1 was lower than that of APAM. Therefore, singular coagulant and dual coagulant system had similar dye removal efficiency at 0.8 g/g dye.

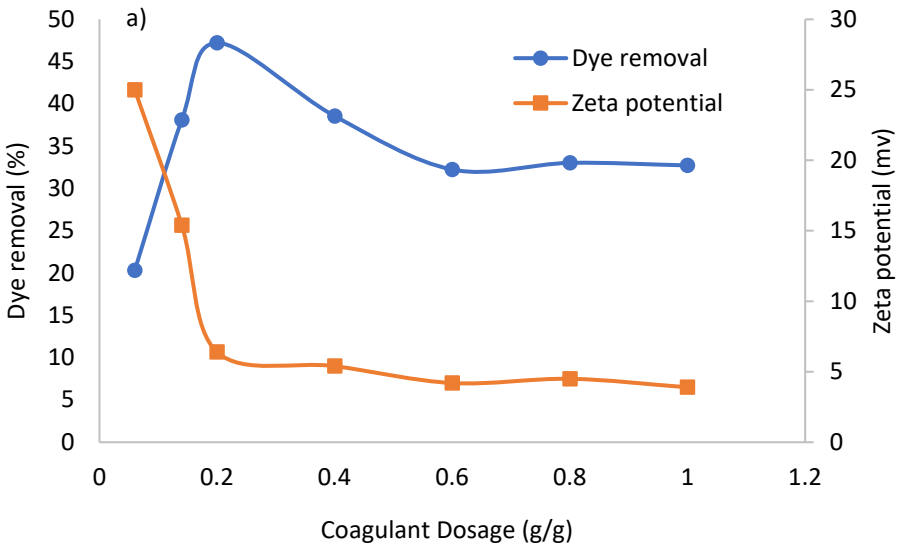
a)
Dye removal
Zeta potential
Dye removal (%)
Zeta potential (mv)
Coagulant Dosage (g/g)
0
5
10
15
20
25
30
35
40
45
50
0
0.2
0.4
0.6
0.8
1
1.2

...

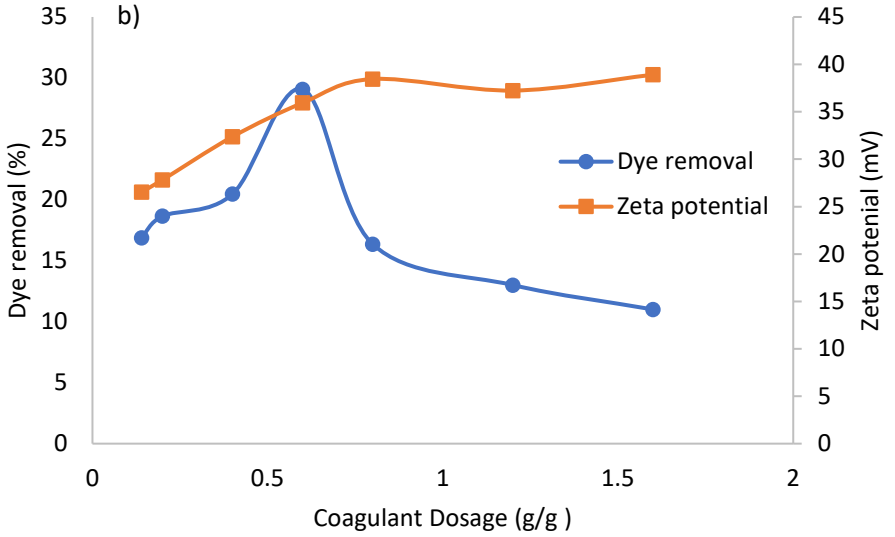
b)
Dye removal
Zeta potential
Dye removal (%)
Zeta potenial (mV)
Coagulant Dosage (g/g)
0
5
10
15
20
25
30
35
40
45
0
0.5
1
1.5
2

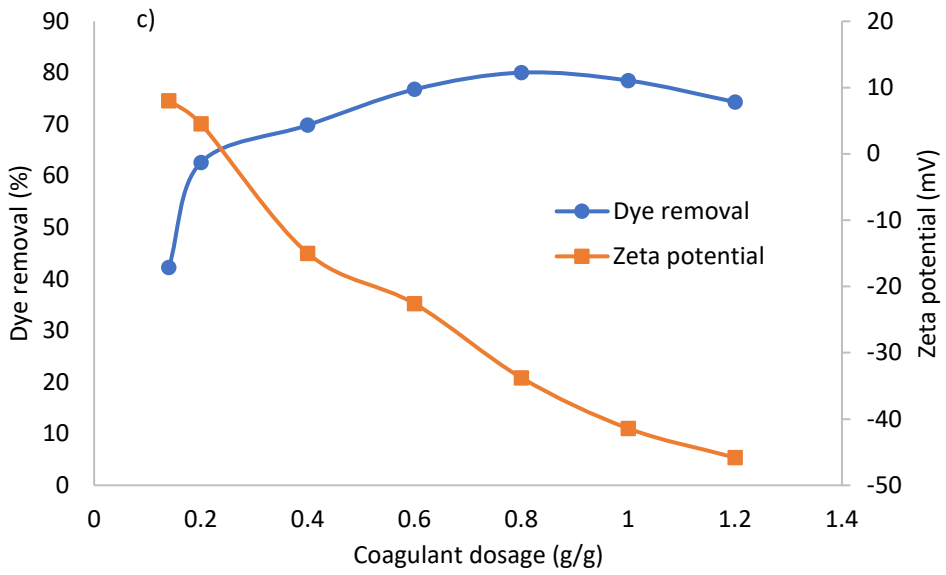
c)
Dye removal (%)
Zeta potential (mV)
Coagulant dosage (g/g)
Dye removal
Zeta potential
0
10
20
30
40
50
60
70
80
90
-50
-40
-30
-20
-10
0
10
20
0
0.2
0.4
0.6
0.8
1
1.2
1.4

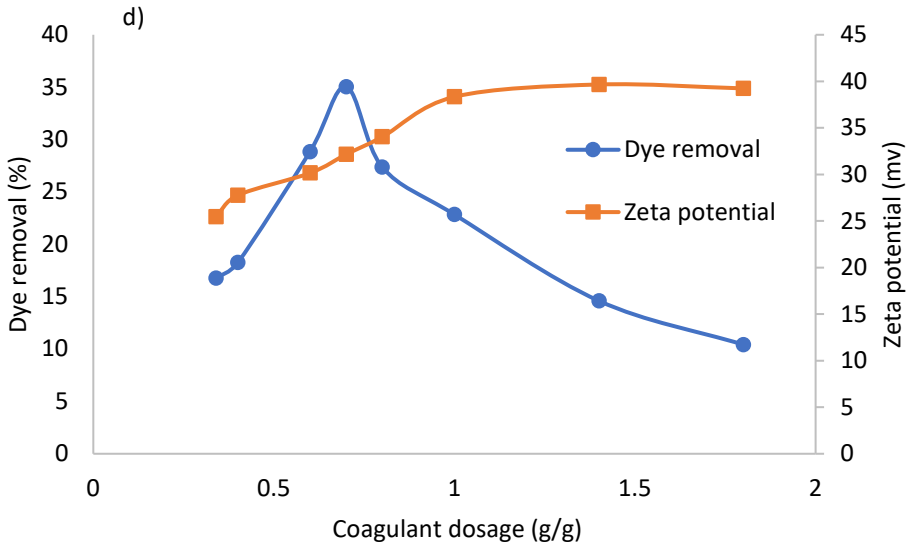
d)
Dye removal (%)
Zeta potential (mv)
Coagulant dosage (g/g)
Dye removal
Zeta potential
0
5
10
15
20
25
30
35
40
0
5
10
15
20
25
30
35
40
45
0
0.5
1
1.5
2

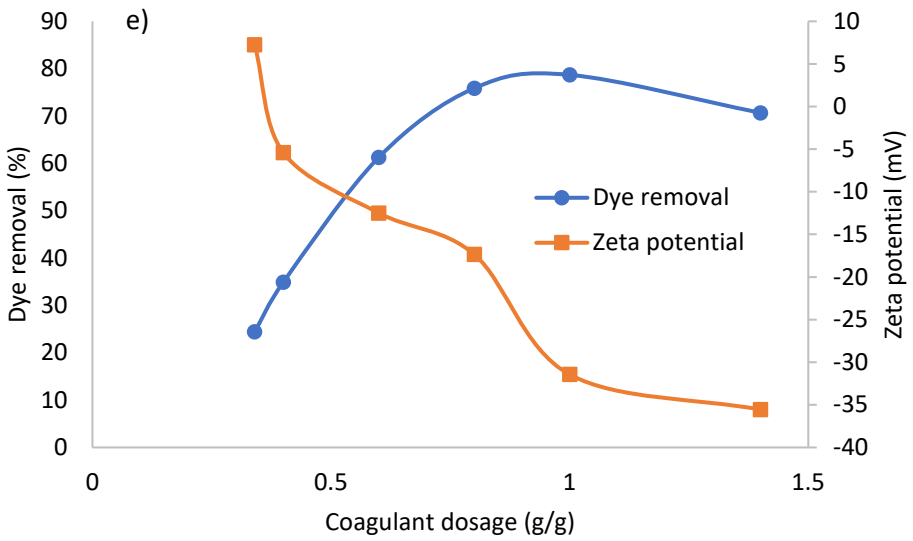

Figure 4.4. a) Effect of LC-AM dosage on dye removal and zeta potential in EV solution, b) Effect of CPAM dosage on dye removal and zeta potential in EV solution, c) Effect of APAM dosage on dye removal and zeta potential in EV solution, d) Effect of LC-AM and CPAM dosage on dye removal and zeta potential in EV solution (0.2 g LC-AM/g dye was fixed throughout the experiment), e) Effect of LC-AM and APAM dosage on dye removal and zeta potential in EV solution (0.2 g LC-AM/g dye was fixed throughout the experiment)

4.5 Conclusions

The in-situ polymerization of acrylamide and hydrolysate constituents was successfully conducted using K_2SO_8 as an initiator in an aqueous system. It was proved that the homopolymerization of AM was inhibited by acetic acid and furfural. Therefore, in the polymerization of acrylamide and hydrolysate, very few polyacrylamide may be generated. The optimum conditions for polymerization were at 3 hours, 60 ^{o}C, 4 wt.% initiator based on total mass of hydrolysate, an AM/LC molar ratio of 5.63. Under the optimal conditions, LC-AM had yield, grafting ratio, molecular weight and charge density of 58%, 670.4%, 41057g/mol and -0.252 meq/g, respectively. It was found that lignin promoted the polymerization of acrylamide at optimal conditions in comparison with two LC-AM from two hydrolysate samples. The dual polymer system of LC-AM and CPAM was proved to be ineffective in removing the dye from solution. The maximum dye removal efficiency was 80 % when APAM at the dosage of 0.8 g/g dye was used in the EV solution. In the LC-AM/APAM dual system, the maximum dye removal efficiency was slightly lower than that in the APAM system.

4.6 References

Ahsan, L., Jahan, M. S., & Ni, Y. (2014). Recovering/concentrating of hemicellulosic sugars and acetic acid by nanofiltration and reverse osmosis from prehydrolysis liquor of kraft. *Bioresource Technology, 155*, 111-115.

Alvarez, C., Reyes-Sosa, F. M., & Diez, B. (2016). Enzymatic hydrolysis of biomass from wood. *Microbial Biotechnology, 6*(2), 149-156.

Ariffin, A., Razali, M., & Ahmad, Z. (2012). PolyDADMAC and polyacrylamide as a hybrid flocculation system in the treatment of pulp and paper mills waste water. *Chemical Engineering Journal, 179*, 107– 111.

Barany, S. (2011). Electrokinetic potential of polystyrene latex particles in polyelectrolyte mixtures. *Material Sciences and Engineering, Miskolc, 36*(2), 11-20.

Ben, H., Chen, X., Han, G., Shao, Y., Jiang, W., Pu, Y., & Ragauskas, A. J. (2018). Characterization of Whole biomasses in pyridine based ionic liquid at low temperature by 31 P nMr: an approach to quantitatively measure hydroxyl groups in biomass as their original structures. *Front. Energy Res., 6:13*.

Bhattacharjee, S. (2016). DLS and zeta potential – What they are and what they are not? *Journal of Controlled Release, 235*, 337–351.

Bouyer, F., Robben, A., Yu, W. L., & Borkovec, M. (2001). Aggregation of colloidal particles in the presence of oppositely charged polyelectrolytes: Effect of surface charge heterogeneities. *Langmuir, 17*, 5225-5231.

Chen, T., Gao, B., & Yue, Q. (2010). Effect of dosing method and pH on color removal performance and floc aggregation of polyferric chloride–polyamine dual-coagulant in synthetic dyeing wastewater treatment. *Colloids and Surfaces A: Physicochem. Eng. Aspects , 355*, 121-129.

Chen, X., Si, C., & Fatehi, P. (2018). Cationic xylan- (2-methacryloyloxyethyl trimethyl ammonium chloride) polymer as a flocculant for pulping wastewater. *Carbohydrate Polymers, 186*, 358–366.

Chiarinia, L., Cescutti, P., Drigo, L., Impallomeni, G., Herasimenka, Y., Bevivino, A., . . . & Rizzo, R. (2004). Exopolysaccharides produced by Burkholderia cenocepacia recA lineages IIIA and IIIB. *Journal of Cystic Fibrosis, 3*, 165–172.

Dong, L., Hu, H., Yang, S., & Cheng, F. (2012). Grafted copolymerization modification of hemicellulose directly in the alkaline peroxide mechanical pulping (APMP) effluent and its surface sizing effects on corrugated paper. *Bioresource Technology, 118*, 204-209.

Dotto, J., Fagundes-Klen, M. R., Veit, M. T., Palácio, S. M., & Bergamasco, R. (2019). Performance of different coagulants in the coagulation/flocculation process of textile wastewater. *Journal of Cleaner Production, 208*, 656-665.

Duval, A., & Lawoko, M. (2014). A review on lignin-based polymeric, micro- and nano-structured materials . *Reactive & Functional Polymers, 85*, 78–96.

Eriksson, L., Alm, B., & Stenius, P. (1993). Formation and structure of polystyrene latex aggregates obtained by flocculation with cationic polyelectrolytes: 1. Adsorption and optimum flocculation concentrations. *Colloids and Surfaces A: Physicochemical and Engineering Aspects, 70*(1), 47-60.

Fang, R., Cheng, X., Fu, J., & Zheng, Z. (2009). Research on the graft copolymerization of EH-lignin with acrylamide. *Natural Science, 1*, 17-22.

Fatehi, P., Catalan, L., & Cave, G. (2014). Simulation analysis of producing xylitol from hemicelluloses of pre-hydrolysis liquor. *Chemical Engineering Research and Design, 92*, 1563–1570.

Gregory, J., & Barany, S. (2011). Adsorption and flocculation by polymers and polymer mixtures. *Advances in Colloid and Interface Science, 169*, 1-12.

Guo, K., Gao, B., Wang, W., Yue, Q., & Xu, X. (2019). Evaluation of molecular weight, chain architectures and charge densities of various lignin-based flocculants for dye wastewater treatment. *Chemosphere, 215*, 214-226.

Gürses, A., Açıkyıldız, M., Güneş, K., & Gürses, M. S. (2016). Dyes and pigments: their structure and properties. In *Dyes and Pigments* (pp. 13-29). Springer International Publishing.

Hasan, A., & Fatehi, P. (2018). Cationic kraft lignin-acrylamide as a flocculant for clay suspensions: 1. Molecular weight effect. *Separation and Purification Technology, 207*, 213–221.

Ibrahim, M. N., Lim, S. L., Ahmed-Haras, M. R., & Fayyadh, F. S. (2014). Preparation and characterization of lignin graft copolymer as a filtrate loss control agent for the hydrocarbon drilling industry. *BioResources, 9*(1), 1472-1487.

Ibrahim, N. A., Abu-Ilaiwi, F., Rahman, M. Z., MansorB.Ahmad, Dahlan, K. Z., & Yunus, W. M. (2005). Graft copolymerization of acrylamide onto oil palm empty fruit bunch (OPEFB) fiber. *Journal of Polymer Research, 12*, 173-179.

Karimi, S., & Karimi, K. (2018). Efficient ethanol production from kitchen and garden wastes and biogas from the residues. *Journal of Cleaner Production, 187*, 37-45.

Kong, F., Wang, S., Price, J. T., Kondurib, M. K., & Fatehi, P. (2015). Water soluble kraft lignin–acrylic acid copolymer: synthesis and characterization. *Green Chem, 17*, 4355–4366.

Kumar, D., Pandey, J., Raj, V., & Kumar, P. (2017). A Review on the modification of polysaccharide through graft copolymerization for various potential applications. *The Open Medicinal Chemistry Journal, 11*, 109-126.

Kumar, H., & Christopher, L. P. (2017). Recent trends and developments in dissolving pulp production and application. *Cellulose, 24*, 2347–2365.

Lapointe, M., & Barbeau, B. (2017). Dual starch-polyacrylamide polymer system for improved flocculation. *Water Research, 124*, 202-209.

Lee, B. J., & Schlautman, M. A. (2015). Effects of Polymer molecular weight on adsorption and flocculation in aqueous kaolinite suspensions dosed with nonionic polyacrylamides. *Water, 7*, 5896-5909.

Lee, C. S., Robinson, J., & Chong, M. F. (2014). A review on application of flocculants in wastewater treatment. *Process Safety and Environmental Protection, 92*, 489-508.

Li, R., Gao, B., Sun, J., Qinyan Yue, Y. W., & Xu, X. (n.d.) (2016). Synthesis, characterization of a novel lignin-based polymer and its behavior as a coagulant aid in

coagulation/ultrafiltration hybrid process. *International Biodeterioration & Biodegradation, 113,* 334-341.

Li, W., & Zhou, X. (2017). Modification of the water-insoluble hemicelluloses via free radical copolymerization in diluted alkali aqueous medium. *Journal of Wood Chemistry and Technology, 37*, 191-200.

López-Maldonado, E. A., Oropeza-Guzmán, M. T., & Ochoa-Terán, A. (2014). Improving the efficiency of a coagulation-flocculation wastewater treatment of the semiconductor industry through zeta potential measurements. *Journal of Chemistry, 3*.

Mahdavi, M., Ahmad, M. B., Haron, M. J., & Fatehi, M. Z. (2011). Optimized conditions for graft copolymerization of poly(acrylamide) onto rubberwood fibre. *BioResources, 6*(4), 5110-5120.

Maia, A. M., Silva, H. V., Curti, P. S., & Balaban, R. C. (2012). Study of the reaction of grafting acrylamide onto xanthan gum. *Carbohydrate Polymers, 90*, 778-783.

Nasser, M., & James, A. (2006). The effect of polyacrylamide charge density and molecular weight on the flocculation and sedimentation behaviour of kaolinite suspensions. *Separation and Purification Technology, 52*, 241-252.

Patel, V. R., & Agrawal, Y. K. (2011). Nanosuspension: An approach to enhance solubility of drugs. *Journal of Advanced Pharmaceutical Technology & Research , 2*(2), 81-87.

Pérez-Bibbins, B., Torrado-Agrasar, A., Salgado, J. M., Mussatto, S. I., & Domínguez, J. M. (2016). Xylitol production in immobilized cultures: a recent review. *Crit Rev Biotechnol, 36*(4), 691–704.

Razali, M. A., Sanusi, N., Ismail, H., Othman, N., & Ariffin, A. (2012). Application of response surface methodology (RSM) for optimization of cassava starch grafted polyDADMAC synthesis for cationic properties. *Starch-Starke, 64*(12), 935-943.

Ren, H., & Omori, S. (2014). Comparison of hemicelluloses isolated from soda cooking black liquor with commercial and bacterial xylan. *Cellulose Chemistry and Technology, 48*(7), 675-681.

Rigual, V., Santos, T. M., Domínguez, J. C., Alonso, M. V., Oliet, M., & Rodriguez, F. (2018). Evaluation of hardwood and softwood fractionation using autohydrolysis and ionic liquid microwave pretreatment. *Biomass and Bioenergy, 117*, 190–197.

Saeed, A., Fatehi, P., Ni, Y., & Heiningen, A. v. (2011). Impact of furfural on the sugar analysis of prehydrolysis liquor of kraft-based dissolving pulp production process using the hpaec technique. *BioResources, 6*(2), 1707-1718.

Sanghi, R., Bhattacharya, B., & Singh, V. (2006). Use of Cassia javahikai seed gum and gum-g-polyacrylamide as coagulant aid for the decolorization of textile dye solutions. *Bioresource Technology, 97*, 1259–1264.

Shak, K. P., & Wu, T. Y. (2014). Coagulation–flocculation treatment of high-strength agro-industrial wastewater using natural Cassia obtusifolia seed gum: Treatment efficiencies and flocs characterization. *Chemical Engineering Journal, 256*, 293–305.

Tarasov, D., Leitch, M., & Fatehi, P. (2018). Flow through autohydrolysis of spruce wood chips and lignin carbohydrate complex formation. *Cellulose, 25*(2), 1377–1393.

Tarasov, D., Leitch, M., & Fatehi, P. (2018). Lignin–carbohydrate complexes: properties, applications, analyses, and methods of extraction: a review. *Biotechnol Biofuels , 11:269*.

Tunc, M. S., & Heiningen, A. R. (2009). Autohydrolysis of mixed southern hardwoods: Effect of P-factor. *Nordic Pulp and Paper Research Journal , 24 no. 1*, 42-47.

Ur-Rehman, S., Mushtaq, Z., Zahoor, T., Jamil, A., & Murtaza, M. A. (2015). Xylitol: a review on bioproduction, application, health benefits, and related safety issues. *Critical Reviews in Food Science and Nutrition, 55*, 1514–1528.

Vallejos, M. E., Chade, M., Mereles, E. B., Bengoechea, D. I., Brizuela, J. G., Felissia, F. E., & Area, M. C. (2016). Strategies of detoxification and fermentation for biotechnological production of xylitol from sugarcane bagasse. *Industrial Crops and Products, 91*, 161–169.

Wang, H., Pu, Y., Ragauskas, A., & Yang, B. (2019). From lignin to valuable products–strategies, challenges, and prospects. *Bioresource Technology, 271*, 449–461.

Wang, J.-P., Chen, Y.-Z., Yuan, S.-J., Sheng, G.-P., & Yu, H.-Q. (2009). Synthesis and characterization of a novel cationic chitosan-based flocculant with a high water-solubility. *Water Research, 43*, 5267-5275.

Wang, Q., Tian, D., Hu, J., Shen, F., Yang, G., Zhang, Y., . . . Hu, Y. (2018). Fates of hemicellulose, lignin and cellulose in concentrated phosphoric acid with hydrogen peroxide (PHP) pretreatment. *RSC Adv., 8*, 12714–12723.

Wang, S., Kong, F., Fatehi, P., & Hou, Q. (2018). Cationic high molecular weight lignin polymer: a flocculant for the removal of anionic azo-dyes from simulated wastewater. *Molecules, 23*(2005).

Wang, S., Kong, F., Fatehi, P., & Hou, Q. (2019). Cationic high molecular weight lignin polymer: a flocculant for the removal of anionic azo-dyes from simulated wastewater. *Molecules, 23*(2005).

Wang, S., Sun, Y., Kong, F., Yang, G., & Fatehi, P. (2016). Preparation and characterization of lignin-acrylamide copolymer as a paper strength additive. *BioResources, 11*(1), 1765-1783.

Wang, W., Chen, X., Tan, X., Wang, Q., Liu, Y., He, M., . . . Yuan, Z. (2017). Feasibility of reusing the black liquor for enzymatic hydrolysis and ethanol fermentation. *Bioresource Technology, 228*, 235–240.

Wei, J., Gao, B., Yue, Q., & Wang, Y. (2009). Effect of dosing method on color removal performance and flocculation dynamics of polyferric-organic polymer dual-coagulant in synthetic dyeing solution. *Chemical Engineering Journal, 151*, 176–182.

Wu, C. (2016). The Potential of pre-hydrolysis liquor from the dissolving pulp process as recovery source of xylooligosaccharide - A Mini-Review. *BioResources 11(3)*, 7917-7927.

Zafar, M. S., Tausif, M., Mohsin, M., Ahmad, S. W., & Zia-ul-Haq, M. (2015). Potato starch as a coagulant for dye removal from textile wastewater. *Water Air Soil Pollut*, 226: 244.

Zhang, S., Guan, Y., Fu, G.-Q., Chen, B.-Y., Peng, F., Yao, C.-L., & Sun, R.-C. (2014). Organic/inorganic superabsorbent hydrogels based on xylan and montmorillonite. *Journal of Nanomaterials,* 11.

Zhou, L., Zhou, H., & Yang, X. (2019). Preparation and performance of a novel starch-based inorganic/organic composite coagulant for textile wastewater treatment. *Separation and Purification Technology, 210*, 93-99.

Chapter 5: Conclusions and recommendations for future work

5.1 Conclusion

The scope of this work was to produce hydrolysates from autohydrolysis of spruce in order to 1) study the interaction of their components under different conditions in solutions and the adsorption of these components on stainless steel surfaces and 2) to generate hydrolysate-based flocculants for dye wastewater treatment. It was observed that the isolation of lignin and hemicellulose from softwood was enhanced in autohydrolysis at higher temperature and longer residence time compared to other hydrolysis conditions. However, a high liquid to solid ratio hampered the lignin extraction due to the dilution of the system. The production of other hydrolysis components was not significantly affected by Liquid to solid ratio. Temperature favored the furfural production significantly as most of hemicelluloses were degraded to monosaccharides and then to furfural by elevating temperature. In terms of acetic acid, the studied hydrolysis variables strongly impacted its production. In analyzing the self-agglomeration of hydrolysate components, it was found that temperature increased the hydrodynamic size of hydrolysate components due to intensified Brownian Motion. The effective strategy to prevent the agglomeration of dissolved components was to add salt to screen the double layer of dissolved particles in the hydrolysates. At pH 2, the hydrodynamic size of hydrolysate constituents was relatively large, which was attributed to insolubility of lignin under acidic condition and condensation of hydrolysate components. Due to the ionization of their functional groups, the dissolved components tended to have smaller hydrodynamic size under alkaline conditions in the hydrolysate. Ultrasonication could dissociate the hydrolysates but without ultrasonication, the hydrolysate could undergo self-assembly and agglomeration. Therefore, the agglomeration of hydrolysate was a reversible process. In the QCM analysis, the hydrolysate sample that had higher hydrophilicity had a better deposition on the stainless-steel sensor. The sample that had larger molecular weight generated more compact adsorbed layer on the sensor probably due to the chain entanglement of the segments on the surface. The viscoelastic characteristics of adsorbed layers remained the same at different pH. The adsorption performance of hydrolysates followed the same trend when using acetic acid and hydrogen chloride as buffer solution. The SEM and EDX analysis confirmed the deposition of agglomerated hydrolysate segments on the stainless-steel surface after rinsing. This study clarified that the composition and hydrodynamic size of hydrolysates from the hydrolysis of spruce could be controlled by various operating variables.

In addition, the in-situ polymerization of acrylamide, AM, onto hydrolysate constituents was successful in an aqueous system. Both acetic acid and furfural inhibited the polymerization of AM on the components. The H^1-NMR spectra confirmed the polyacrylamide was grafted on hydrolysate component successfully. In order to generate the coagulant with a high molecular weight, the grafting polymerization reaction had been conducted under different conditions. The optimum conditions for the polymerization were 3 hours, 60 ℃, 4 wt.% initiator based on total mass of hydrolysate, an AM/LC molar ratio of 5.63. Under the optimal conditions, hydrolysates grafted with acrylamide had the yield, grafting ratio, molecular weight and charge density of 58%, 670.4%, 41057 g/mol and -0.25 meq/g, respectively. Based on the results from the optimization of the reaction, lignin present in the hydrolysates of spruce presented a better grafting efficiency under optimal conditions. The application of LC-AM as a coagulant was also studied in singular and dual polymer systems in this work. In a LC-AM singular system, at optimal dosage of 0.2 g/g dye, 47.32% of dye removal was obtained. The results showed that both charge neutralization and bridging effects were involved in the suspension system. The maximum dye removal efficiency was 80 % when APAM at the dosage of 0.8 g/g dye was used alone in the EV solution. The performance of CPAM in both singular and dual coagulant systems was around 29% and 35%, respectively because CPAM had a high charge density leading electrostatic repulsion. In the LC-AM/APAM dual system, the maximum dye removal efficiency of this system was similar with that of the APAM system. The main advantages of LC-AM were its biodegradable, environmentally friendliness, and inexpensive production costs compared with other oil-based coagulants used in industry.

5.2 Future work

To gain better understanding of aggregation and adsorption of hydrolysate components on various surfaces, DLS and QCM experiments can be carried out using lignin and hemicellulose isolated from hydrolysates. The efficiency of the isolated lignin and hemicelluloses in polymerizing with various monomers may be examined in order to induce highly efficiency flocculants. Furthermore, the self-assembly of lignocellulose-based polymers can be investigated using QCM. The self-assembly of polymers play an important role in the efficiency of flocculants and dispersants in colloidal systems. To further develop the application of hydrolysate-based polymers, the use of the generated polymers in various colloidal systems should be studied.

Appendix

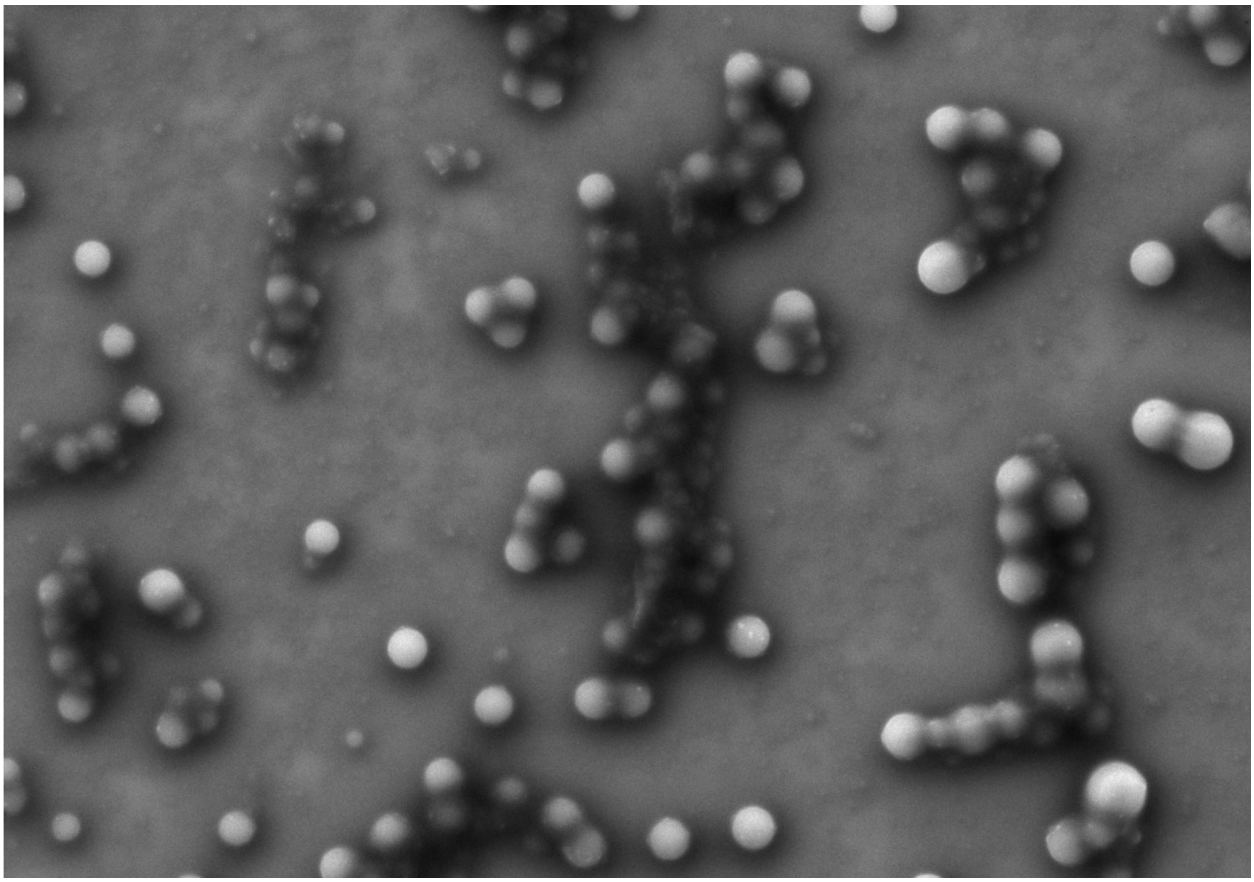

Figure A.1 Morphology of adsorbed layer for sample 2 using HCL buffer solution

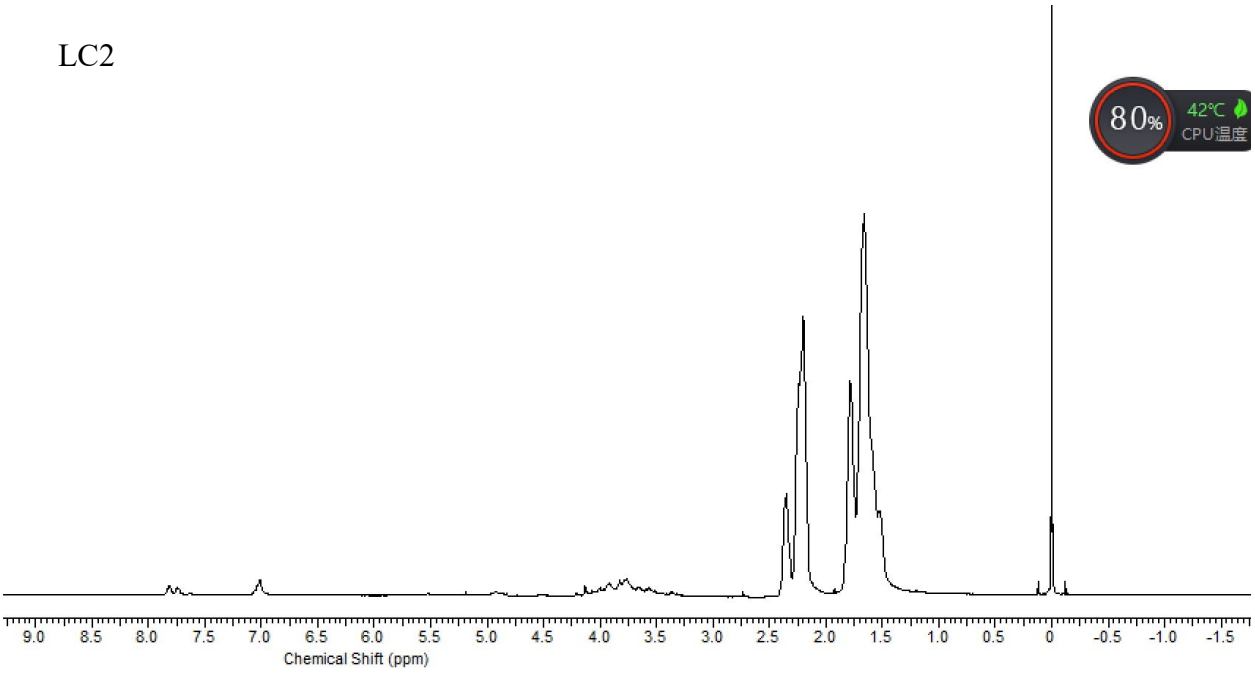

Figure A.2. ^{1}H-NMR spectra of hydrolysates from sample 2